Information bounds the robustness of self-organized systems

Nicolas Romeo,[1, 2] David G. Martin,[3, 1] Mattia Scandolo,[1] Michel
Fruchart,[4] Edwin M. Munro,[2, 5, 6] and Vincenzo Vitelli[1, 2, 5, 7, *]

[1]*Department of Physics, University of Chicago, Chicago, Illinois 60637, USA*
[2]*Center for Living Systems, University of Chicago, Chicago, Illinois 60637, USA*
[3]*LPTMC, CNRS UMR 7600, Université Pierre et Marie Curie, 75252 Paris, France*
[4]*Gulliver, ESPCI Paris, Université PSL, CNRS, 75005 Paris, France*
[5]*Institute for Biophysical Dynamics, University of Chicago, Chicago, Illinois 60637, USA*
[6]*Department of Molecular Genetics and Cell Biology,
University of Chicago, Chicago, Illinois 60637, USA*
[7]*Leinweber Center for Theoretical Physics, University of Chicago, Chicago, Illinois 60637, USA*
(Dated: November 4, 2025)

Self-assembled systems, from synthetic nanostructures to developing organisms, are composed of fluctuating units capable of forming robust functional structures despite noise. In this Letter we ask: are there fundamental bounds on the robustness of self-organized nano-systems? By viewing self-organization as noisy encoding, we prove that the positional information capacity of short-range classical systems with discrete states obeys a bound reminiscent of area laws for quantum information. This universal bound can be saturated by fine-tuning transport coefficients. When long-range correlations are present, global constraints reduce the need for fine-tuning by providing effective integral feedback. Our work identifies bio-mimetic principles for the self-assembly of synthetic nanosystems and rationalizes, on purely information-theoretic grounds, why scale separation and hierarchical structures are common motifs in biology.

The self-organization of nano- or microscale subunits to assemble engineered structures [1–4] (Fig. 1a) or the organization of sub-cellular and cellular components to form cells and tissues [5–7] (Fig. 1b) rely on a complex balance of component interactions [8–16], material transport [3, 17–20], and the processing of external signals [21, 22] to reliably form functional structures. A key challenge for robust spatial self-organization of both synthetic and living systems is the presence of noise, either thermal [23] or due to intrinsically stochastic molecular processes or other forms of disorder [24–26].

Despite the noise, biological signals are known to precisely generate target patterns that encode information about cellular positioning [21, 27–30], enabling development but also intra- and inter-cellular communication at large [31, 32]. Take, for example, the determination of the body plan of the fruit fly embryo: Maternal gradients provide an initial signal that activates a set of interacting gap genes whose resulting expression profile is tightly controlled and enables precise localization of body parts [21, 33]. More generally, biological pattern formation is enabled by both integrating external signals (sometimes called positional information [22, 27]) and various nonlinear self-organizing regulation schemes [29, 34–38], which feature recurring ingredients such as negative feedback [10] and the combination of short- and long-range interactions [20].

Abstracting away from the specific nature of the interactions, we would like to identify general design principles for synthetic systems by isolating the properties of spatial processes enabling robust patterning. To this end,

we view self-organization in these complex systems in terms of information processing, with information from external sources encoded into a downstream spatially-patterned signal field (Fig. 1c) [5]. In this perspective, robust self-organization is equivalent to a faithful encoding of the source signal. Here we ask: Are there general limits on the ability of self-organizing processes to faithfully encode spatial information?

Quantifying robustness in terms of information-theoretic quantities measuring the statistical relationship between location and final state [39–41], we investigate how different spatial processes reliably establish functional order, here defined as reproducible patterned states. We find a fundamental limitation to robust self-organization in systems with short-ranged interactions, reminiscent of area laws for quantum information [42, 43]. Finally, we show that mixing short- and long-range interactions, generically known to lead to pattern formation, also promotes their robustness.

QUANTIFYING ROBUSTNESS IN A MINIMAL MODEL OF SELF-ORGANIZED PATTERNING

We study minimal models of self-organized patterning, using as our main illustration the prototypical example of cell fate patterning on a one-dimensional ring (Fig. 1d). In such systems, directly relevant to biological development [7, 35], cell division [44], or regeneration and wound repair [45], signals–known in this context as morphogens–are emitted by external or spontaneously generated sources. These signals then diffuse and interact, either directly or via state-dependent expression or degradation by the host cell. This class of
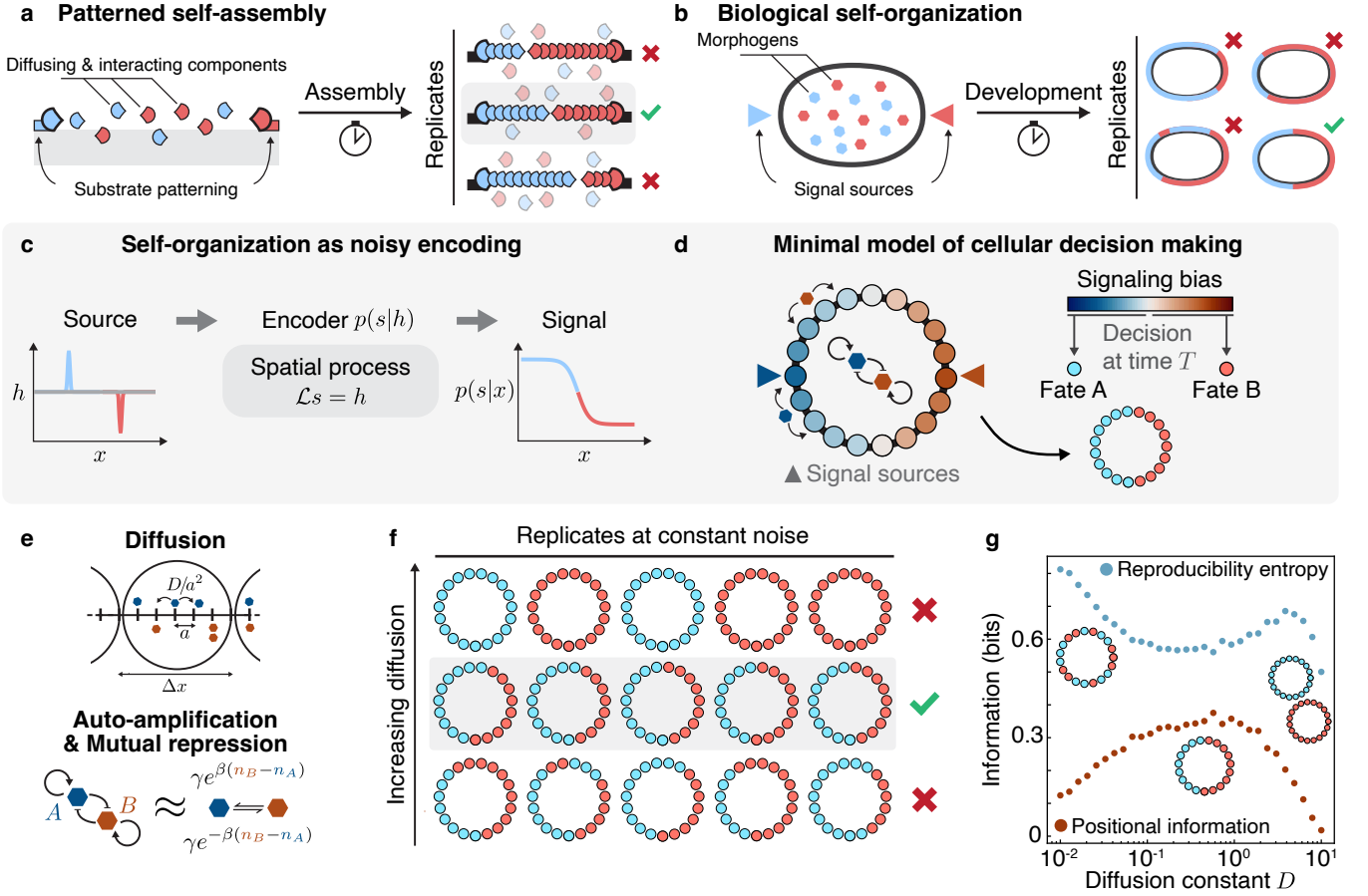
* vitelli@uchicago.edu

FIG. 1. Reproducible self-assembly from the balance between transport and interactions. **a.** Synthetic self-assembled systems with prescribed boundaries are subject to noise, which can limit yield and functionality. **b.** Viable biological self-organization requires precise establishment of chemical gradients in response to pre-existing or external symmetry breaking. **c.** The self-organizing process can be understood as a noisy encoding process. Are there limits on the quality of the encoder depending on the nature of the spatial process, represented here by a nonlinear differential operator $\mathcal{L}$? **d.** We focus on a minimal model of cellular decision-making, where two interacting species of particles diffuse around and carry opposing signals generated at diametrically opposed signaling sources. At a specified time T, the sign of the local difference in signal concentration sets the cell fates. **e.** This system is mapped onto a diffusive Ising model, where particles diffuse at a set rate and change type according to local concentrations. **f.** At fixed particle numbers, we find that cell fates are most reproducible at intermediate diffusion. **g.** This reproducibility is quantified by information-theoretic quantities. While the outcomes are most reproducible at large D, the most informative patterns require intermediate diffusion. Simulation in **g** are done with $\Delta x = L/8$, $a = L/48$, $T = 500$, $\gamma = 1$, $\beta = 2\beta_c$, $h_0 = 2\beta$, where $\beta_c = \ln(1 + \sqrt{2})$; distributions are estimated from 500 replicates.

systems is commonly modeled in the reaction-diffusion framework [22, 46], which can be adapted to incorporate mechanical effects such as coupling to flows or elasticity [36, 47].

In addition to diffusion, our minimal cell fate model includes mutually repressing and autoamplifying morphogens, a common motif leading to bistability in cell decision. To model cellular decision, at a time T cells pick a fate (color) based on the morphogen that is the most present.

To study these systems up to large noise regimes, we consider a minimal microscopic model of morphogen dynamics which combines these elements of diffusion, interactions, and external signal. In this model, sometimes

known as the diffusive Ising model (DIM) [48–50], the ring of cells, each of size Δx, is abstracted into a one-dimensional lattice on which morphogens can hop between N_s sites of width a with an average rate D/a^2. The number of morphogens is taken to be constant such that on average we have one morphogen per site; there are $\Delta x/a$ sites per cell. Morphogens come in two species A and B, which mutually suppress each other by changing their type according to the local concentrations n_A and n_B: If there are more A than B, then morphogens of type B are likely to turn into A, and vice versa (Fig. 1e). In this model, a detailed field-theoretic analysis shows that the noise variance is proportional to a, or equivalently scales with $1/N_{\Delta x} = a/\Delta x$ the average number

of particles per cell [49–51]. This is essentially a restatement of the central limit theorem: as the number of particles considered grows, the importance of fluctuations diminishes. More details on microscopic dynamics and field-theoretical analyses are provided in Methods, Fig. E1; additional results in SI Sec. I, derivations in SI Sec. VI-VII.

We create a symmetric pattern by introducing localized sources at opposing locations, implemented by introducing a biasing signal $h_i = h_0(\delta_{i,0} - \delta_{i,N_s/2})$ at site i that strongly favors particles of type A at one end and of type B at the other. Simulating this random process at constant noise levels for a duration T, we find that the distribution of resulting configurations for different realizations displays variable reproducibility and functionality. At large diffusion, we have reproducible, but non-patterned outcomes; at low diffusion, we obtain patterned but variable outcomes. At intermediate diffusion, we find an optimal regime of patterned and reproducible outcomes, which is characteristic of *robust* patterning. (Fig. 1f). This observation can be intuitively understood: In systems where $D = 0$, there is no neighbor-to-neighbor communication. The signal is then localized at the source points, and sites away from the source have little information to work with. If $D \to \infty$, the system becomes homogeneous and all spatial information is destroyed.

This qualitative interpretation in terms of information can be made quantitative by using information-theoretic tools to define reproducibility and pattern robustness. For a system of N cells and Z possible states, we can consider the joint distribution $p(z_1, \ldots, z_N) \equiv p(\{z_i\})$ that encodes the probability of finding together cell 1 at state z_1, cell 2 at state z_2 and so on [39–41]. Introducing the marginal probability $p_i(z)$ of finding the i-th cell in state z, which can be expressed in terms of $p(\{z_i\})$, we consider the positional information (PI) defined as

$$\text{PI} = \frac{1}{N} \sum_{i=1}^{N} \sum_{z=1}^{Z} p_i(z) \log_2 \left(\frac{p_i(z)}{P_z} \right) \leq \log_2 Z = 1 \text{ bit}$$

(1)

where P_z is the probability of finding any cell in the state z, reflecting the average fraction of cells of each type. The PI can be understood as the mutual information between position and state, that is, the information gained on the location of a particle by knowing its fate, and vice versa. If every cell is equally likely to take any of the Z possible fates, then PI = 0. In this definition, the PI formalizes early insights by Wolpert, who suggested that morphogen gradients could encode spatial information, and has been shown to be an experimentally-relevant quantity defining the optimality of cellular position encoding schemes [27, 52, 53]. We note that we find similar results using other probabilistic measures to quantify robustness [54, 55]. We discuss the relative merits of these measures in SI Sec. II, Fig. S1, and focus on PI for the remainder.

Returning to our minimal model, we see that positional information peaks at intermediate diffusion

D^*, indicating an optimal robustness of the pattern (Fig 1f). In accordance with our previous observation, we note that we can also quantify the reproducibility of outcomes by the reproducibility entropy $S_{\text{rep}} = -\sum_{\{z_i\}} p(\{z_i\}) \log_2 p(\{z_i\})$, which does not account for the presence of a pattern: as expected, S_{rep} has a minimum at D^*, but also displays a second extremum at large diffusion when the system is uniform (Fig. 1g).

POSITIONAL INFORMATION IS LIMITED IN SHORT-RANGE SYSTEMS

To obtain a more mechanistic insight into the origin of an optimal diffusivity D^*, we use a hydrodynamic expansion of our microscopic model to obtain partial differential equations (PDE) describing the evolution of the total density $\rho = n_A + n_B$ and the signal bias $m = n_A - n_B$ [50, 56, 57]. For small enough lattice sizes a, the resulting model has the same phenomenology as the following Landau-Ginzburg-type model with Brownian noise $\zeta_1(x,t)$ and positive coefficients r_1, u_1, Θ, with dynamics for m reading as

$$\partial_t m = D\partial_x^2 m + r_1 m - u_1 m^3 + h(x) + \sqrt{a\Theta}\zeta_1(t,x), \quad (2)$$

where the term $h(x) = ah_0 (\delta(x) - \delta(x - L))$ accounts for the presence of the external signal at $x = 0$ and $x = L$ with strength $\pm h_0$. The coefficients r_1, u_1 reflect the timescale of the reactions and the amplitude of the steady state, while Θ reflects the reaction noise; the noise variance is scaled by the lattice size a (More details in Methods; see SI Sec. IV, Fig. S5 for comparison between the phenomenology of continuum simulations and microscopic dynamics).

Eq. 2 allows for homogeneous solutions $M_0 = \pm\sqrt{r_1/u_1}$, but also supports the emergence of our desired pattern as a domain wall centered at a position $X(t)$, with morphogens of different types segregating on either side of the wall. Mathematically, such solutions of the continuum version of this model are approximately given by hyperbolic tangents $m(x) = M_0 \tanh [(x - X(t))/\sqrt{2}\ell]$ with a width ℓ set by the diffusion constant as $\ell = \sqrt{D/r_1}$. When there are no boundaries or external signals, the presence of noise induces a Brownian diffusion of the wall position with diffusivity $D_f \propto a\sqrt{rD}$ [58–60] (SI Section III). In the presence of boundaries, but without noise, by symmetry the domain wall localizes in the middle. By examining the spatial profiles of concentrations for variable diffusion, we observe that to maximize the PI, configurations require domain wall widths $\ell \approx L$, where L is the distance between sources, such that the entire system has size $2L$. If $\ell \ll L$, the domain walls can be anywhere in between the signaling loci. If ℓ is too large ($\ell \gg L$), then the domain wall solutions are unstable (Fig. 2a).

These conclusions suggest a qualitative picture where the position $X(t)$ in the presence of external signals does
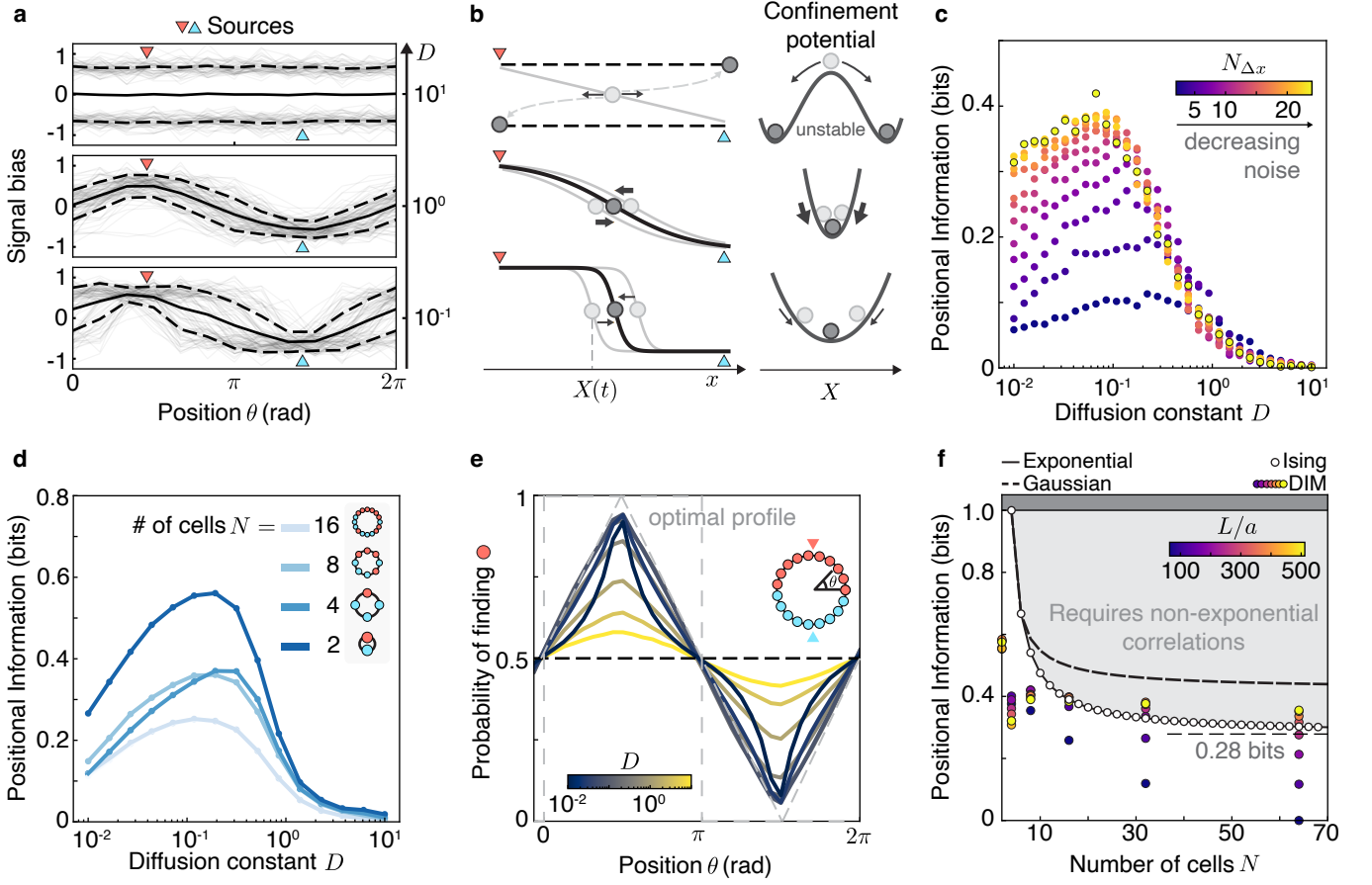
FIG. 2. A universal bound on positional information in short-ranged correlated systems. **a.** Variance in domain position is minimal when domains walls have a width $\ell \approx L$. If ℓ is too large, then domain wall solutions are unstable. Signal bias is here normalized by average total density. Full black line indicates mean signal, dashed lines one standard deviation, lighter lines are replicates. **b.** This optimum in variance can be understood through the energetic cost of shifting the domain wall: if $\ell \ll L$, then translating the domain wall changes very little the value of the signal at the boundary $\Delta m \approx 0$. If $\ell > L$ then the front solution is unstable. These effects materialize as a sharply peaked confinement stiffness. **c.** Positional information is maximal at intermediate diffusion, and saturate as the particle number density $N_{\Delta x}$ increases. Here, we have $N = 16$ cells. **d.** The maximal value of PI at constant particle density $a = L/96$ depends on the number of cells $N = L/\Delta x$. **e.** This saturation can be explained by considering the relationship between positional information and the marginal probability $p(\theta)$ of finding a red region at θ: in short-ranged correlated systems, PI is maximal when $p(\theta)$ is piecewise linear; in diffusive systems, a different optimum exists. **f.** This constraint leads to a system-size dependent bound on PI for systems with short-ranged correlations. All simulations have $h_0 = 3\beta, \beta = 3\beta_c/2, \gamma = 1$ and are averaged over 500 replicates.

not simply diffuse but has a variance set by the competition between the tendency of the system to conform to the external cue and the strength of the noise. To approximately describe this competition, in SI Sec. III.C we compute perturbatively the restoring force acting on the domain when shifted away from its average middle position X_0. This model predicts a confining force $f_c(X) = -k_c(X - X_0)$ resulting in an Ornstein-Uhlenbeck equation [61]

$$\frac{dX}{dt} = f_c(X) + \sqrt{2D_f}\zeta(t) \qquad (3)$$

where $\zeta(t)$ follows a standard Brownian noise. Hence, the larger k_c, the more confined the domain wall. Our geometric model predicts that the stiffness k_c is propor-

tional to the curvature of the signal profile at the sources: it peaks sharply at intermediate ℓ/L and decays exponentially as D is reduced, but does not vanish as $a \to 0$ (Fig. 2b, Methods, SI Sec III). In practice, in direct simulations of the reduced continuum model we find that there is a weaker scaling of the variance of the front position with D, likely due to the front shape deviating from hyperbolic tangent (Fig. S4). These results indicate that accurate domain wall positioning requires fine-tuned values of the diffusivity D such that $\ell \sim L$, an undesirable property given that diffusion constants can span orders of magnitude depending on the molecular environment [62].

This fine-tuning requirement does not diminish in the DIM as we reduce the noise intensity by increasing the particle numbers. In fact, we find numerically that the

maximum value of the PI saturates as the noise amplitude decreases ($N_{\Delta x} \to \infty$) at a value smaller than its theoretically maximum value of $\log_2 Z = 1$ bit for our two-state system (Fig. 2c).

AREA LAWS FOR CLASSICAL SYSTEMS

The saturation of positional information is also visible in other systems, e.g., an Ising magnet with external fields, a prototypical model of systems with short-range interaction for which marginal probabilities can be exactly computed (Methods, Fig. E2), and also appears in generalizations of the Ising model with $Z > 2$ (Supplement Sec. II, Fig. S3). The saturating value for the optimal diffusion depends on the number of coarse-grained states N, which set the resolution of spatial patterns. A larger N implies a larger possible state space, and the patterns must be more precise to obtain a similar PI (Fig. 2d).

How can we understand this information saturation? This situation in which the existence of a finite correlation length limits the information content of a system is reminiscent of area laws in quantum information theory [42, 43], an analogy we discuss in more detail in the Methods.

More directly, we examine the marginal probability $p_i = p_i(z = A)$ of finding the cell at position i in state A and find that PI is maximized in this system when it takes on a sawtooth profile, which does not saturate the 1-bit bound (Fig 2e). However, this sawtooth profile maximizes the positional information under a convexity constraint. In fact, in Methods we prove the following theorem.

Theorem. *For* 2*-state systems (per unit cell) with short-range correlation, such that there exists a length ξ for which $\langle z_i z_{i+k} \rangle \leq e^{-|k|/\xi}$, where z_i is the signal at cell i, then the* PI *for a system of size N is bounded by the positional information Π_N of the sawtooth profile and*

$$\Pi_N \xrightarrow[N \to \infty]{} 1 - \frac{1}{2 \ln 2} \approx 0.28 \ bits. \tag{4}$$

We generalize this result to systems with Z discrete states with $Z > 2$ and provide a different bound for diffusive systems with Gaussian correlations in the supplement (SI Sec. II, Fig. S2). We find that this bound is tight for the Ising model presented in the Methods, as expected from its exponential correlation structure, while the DIM — which violates the exponential correlation structure assumption due to conserved noise (Methods) — is slightly above the exponential bound and sits below the bound for its limiting diffusive regime (Fig. 2f).

NON-LOCALITY ENABLES ROBUST PATTERNING

Our results show that short-range correlated models have a maximal positional information capacity, which is reached for fine-tuned parameter values. This is undesirable in a biological scenario: Cells in developing embryos have positional information that corresponds to errors in position of the order of a single cell size [21, 28], and biological transport coefficients vary strongly depending on the chemistry of the local environment [18, 62]. Are there simple ways to make the system maximally robust, which, by definition, here means PI = 1 bit?

PI in our previous model is limited by the short-range correlation structure of the diffusive Ising model. In contrast, most self-organizing models of pattern formation develop long-ranged correlations by a combination of long-range diffusion [5, 20] or the presence of higher spatial derivatives [63]. For our purposes, the short-range correlations limit positional information by providing only weak confining forces on the domain wall position. A well-studied way to impose tighter control on the domain wall position is wave-pinning [64, 65], which has been identified as a biologically relevant mechanism in the anterior-posterior patterning of the *Caenorhabditis elegans* embryo [7, 66], and other instances of cell polarization [37, 67–69] (see SI Sec. V for a more detailed comparison with *C. elegans*).

In wave-pinning systems, signaling molecules of a given kind bind to a membrane with a rate proportional to the number of molecules available in a homogeneous reservoir and unbind with a rate that depends on the local bound concentration of signals, giving two possible locally stable states on the membrane, with zero or a finite bound concentration state. The assumption that the reservoir is homogeneous captures the empirical fact that bulk diffusion is often much faster than membrane-bound diffusion. Importantly, the conservation of molecular number implies that the binding rate depends on the state of the entire system.

We simulate a microscopic lattice model of wave-pinning with two competing signals A and B, which, like the DIM, is amenable to path-integral-based coarse-graining (Fig. 3a). We thus obtain an equation for the bound signal density $m = n_A - n_B$, which, for simplicity of presentation, we write here neglecting density dynamics [64, 67]

$$\partial_t m = D \partial_x^2 m + rm - km^3 - \frac{r}{a} \int_0^L \mathrm{d}x\, m(x) + h(x) + \sqrt{a}\zeta \tag{5}$$

with r, k positive constants and ζ Gaussian noise. (See Methods for the full equations and SI Sec. V,VI for the derivation). This equation still admits homogeneous and domain wall solutions, whose stability now depends on the entire state of the system. Because the number of particles of each kind obeys a conservation law, Eq. 5
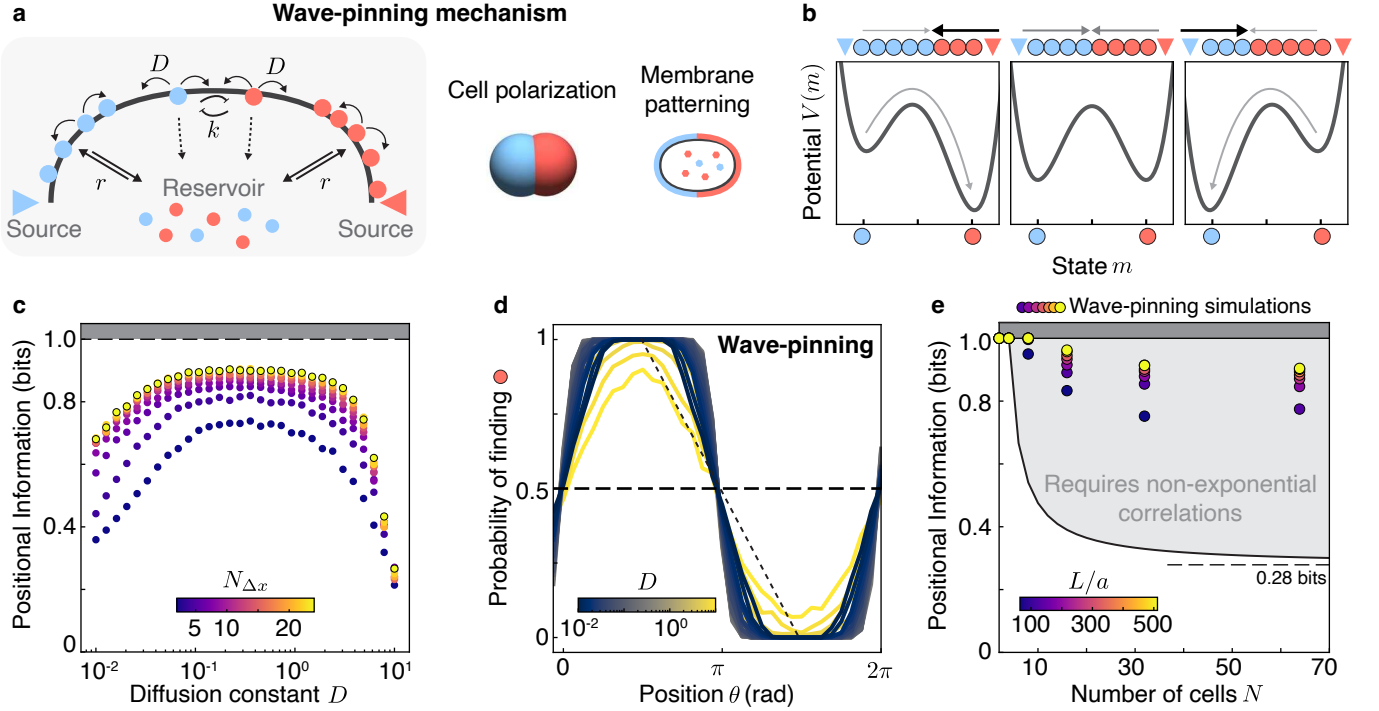
FIG. 3. Long-ranged interactions can stabilize patterns, allowing for increased robustness. **a.** A conserved number of molecules of two types bind to a membrane with a rate proportional to their concentration in the reservoir. Once on the membrane, the molecules diffuse with constant D and unbind at a rate r in the absence of molecules of the other type in the vicinity. When the other molecule type is present, the unbinding rate increase nonlinearly, leading to bistable surface concentration dynamics. **b.** The dependence of the binding rate on the reservoir particle number leads to global coupling which stabilizes the front position: if there are more A (blue) than B (red) bound, then binding of B is favored, and vice versa. **c.** The positional information as a function of D for variable noise is now much higher, and stays at its maximal value for a wider range of D. **d.** The marginal probability of finding B at position θ can now be non-convex. Here we keep $a = L/96$. **e.** The maximal PI can now reach the theoretical maximum, beating the bound for short-ranged systems, with increasing particle numbers L/a (lower noise) leading to better PI. In all simulations $r = 1, k = 4/3, N_0^{A,B} = 6(L/a), T = 5 \cdot 10^3/D, L = 4, \alpha = 30$, and results are averaged over 1000 replicates.

is a nonlocal integro-differential equation: The dynamics of $m(x)$ depend not only on the value of $m(x)$ and its derivatives, but also on the global state of the system via the integral term. Nonlocality commonly appears in systems where fast spatial degrees of freedom are integrated out [70, 71], where topological constraints lead to global couplings [72], or in the presence of quantum entanglement, which allows 'volume law' scaling [42, 43].

With this additional feedback term, the dynamics of the domain wall position $X(t)$ are now subject to an additional force [64, 65]

$$\frac{\mathrm{d}X}{\mathrm{d}t} = f_c(X) + f_{\mathrm{wp}}(X) + \sqrt{2D_f}\zeta(t) \qquad (6)$$

where f_c is again the confinement force induced by the external signal, but now $f_{\mathrm{wp}}(X) = -k_{\mathrm{wp}}(X - X_0)$ is the additional confinement from the wave-pinning feedback. In particular, while k_c decays exponentially when $D \to 0$, this wave-pinning-induced stiffness k_{wp} only decays as $\sqrt{D}$. The presence of an additional global conservation constraint thus realizes a form of spatial integral feed-back, allowing for precise localization of the domain wall with much weaker dependence on the diffusion constant: effectively, the energetic cost of being in the minority state is lowered, and the domain wall moves to expand the minority region (Fig. 3b). We note that wave-pinning does not remedy the instability of front solutions for large D, and therefore this effect only helps to maintain the pattern at small D [66].

Including this mechanism, microscopic simulations show much higher PI, with a flat maximum region achieved for values of D that span an order of magnitude (Fig. 3c). As expected, due to the nonlocal coupling via the reservoir, the marginal probabilities p_i can now have saturating profiles, allowing the PI to beat the bound imposed by exponential or Gaussian correlations (Fig. 3d-e).

DISCUSSION

Small systems that integrate information from their surroundings in time are fundamentally limited in their error rate by the Berg-Purcell limit as their sensing range diminishes [8, 73–75]. In spatially-extended systems that have no memory, our information-theoretic quantification of robustness shows a similar limitation to the information capacity of spatial patterns depending on the nature of their spatial correlations at steady state.

We note that outside of stationary regimes, whether this limitation is important depends on context: If the noise amplitude is small and the observation timescale short, a 'good enough' initial condition might still lead to an acceptable final state for practical purposes (Fig. E4).

Long-range interactions are known to help induce and stabilize pattern formation [20, 38, 76]. Although the patterns we considered here were linearly stable even in the absence of nonlocal correlations, we show that long-range phenomena greatly extend the stability regions of these patterns. In light of this, incorporating long-range interactions in synthetic self-organized systems might be a productive strategy for increasing yield and functionality.

The necessity of building long-range correlations for accurate spatial information processing might explain the evolutionary advantage of hierarchical organizations and scale separations in biological systems. For example, fast information transport has been found to be essential for wound healing [45], and averaging signals over large numbers of cells distributed in space can allow for more precise sensory readouts [77]. Since mechanical responses can be long-ranged, mechano-chemical interactions can enable long-range communication and help complement molecular signaling mechanisms in contexts from development to inflammation [29, 36, 78, 79]. In Fig. E3 we list some examples of engineered and living systems where long-range interactions could or are known to help generate spatial organization.

Finally, other ways to have long-range communication are possible in non-equilibrium physical systems. Systems with conserved degrees of freedom can display non-exponential correlations, as we saw in the DIM [80] and a hallmark of self-organized criticality is the persistence of long-ranged correlations in complex systems, although criticality is also associated with larger sensitivity to noise [81, 82]. It is also known that in active matter, boundary effects can be long-ranged [83, 84]. Designing long-range couplings could thus provide an alternative path to internal information processing and memory to enable robust spatial patterning.

ACKNOWLEDGMENTS

CODE AVAILABILITY

Code is available at `https://github.com/NicoRomeo/RobustPatterns`.

METHODS

Diffusive Ising model

To model the transport and interaction of particles, or morphogens, interacting at a finite range a and with a finite average density ρ_0/a, we consider a microscopic lattice model in which particles of type A and B hop between sites at rate D/a^2 and change type with rate depending on the relative abundance of each species [48–50]. The microscopic evolution rules are the following:

D1 Particles hop with equal probability to a neighboring site with rate D/a^2,

D2 A particles turn into B with rate $\gamma e^{\beta(n_B - n_A)}$,

D3 B particles turn into A with rate $\gamma e^{-\beta(n_B - n_A)}$.

We consider an average number of $\rho_0 = 1$ particle per site. Additionally, if a particle is on a source site with source intensity h_0, the transition rates in **D2-3** are modified to $\gamma e^{\pm\beta(n_B - n_A)\pm h_0}$. These rules lead to Markovian dynamics expressed in terms of a master equation. We use a tau-leaping scheme implemented in `julia` to simulate these stochastic dynamics, as described in [48, 50].

In SI Sec. VI, we use path-integral techniques to reduce these dynamics to a set of nonlinear reaction-diffusion equations for the shifted density $\delta\rho = n_A + n_B - \rho_0$ and the signal $m = n_A - n_B$. If $\sinh\beta \lesssim 2$, then we can approximate these equations by

$$\partial_t \delta\rho = D\partial_{xx}^2 \delta\rho + \partial_x \eta_1, \tag{E1a}$$

$$\begin{aligned}\partial_t m = D\partial_{xx}^2 m - (r + \mu\delta\rho)m - um^3 \\ + h(x) + \partial_x \eta_2 + \eta_3. \end{aligned} \tag{E1b}$$

with a source field $h(x) = \bar{h}[\delta(x) - \delta(x - L)]$ for the symmetric source setup with microscopic source intensity $\pm h_0$ and noise fields η_1, η_2, η_3. The complete nonlinear equations, valid for all values of β, are provided in SI Sec. I. Defining $\hat{\gamma} = 2\gamma e^{-\beta + (\cosh\beta - 1)\rho_0}$, we can write the coefficients and source strength in terms of the micro-

scopic parameters

$$r = \hat{\gamma}(1 - \rho_0 \sinh \beta) \tag{E2a}$$
$$u = \hat{\gamma} \sinh \beta / 3 \tag{E2b}$$
$$\mu = (\cosh \beta - 1)r - 3u. \tag{E2c}$$
$$\bar{h} = arh_0 / \beta \tag{E2d}$$

and the noise correlations are then given by $\langle \eta_n(x,t)\eta_{n'}(x',t') \rangle = M_{n,n'}\delta(x-x')\delta(t-t')$

$$M_{nn'} = \begin{pmatrix} 2aD\rho_0 & & \\ & 2aD\rho_0 & \\ & & 2a\rho_0\hat{\gamma} \end{pmatrix}. \tag{E3}$$

If $r > 0$, that is $\beta < \beta_c = \ln(1 + \sqrt{2})$, then the equations only have a stable homogeneous solution at $m = 0$. If $\beta > \beta_c$, then the equation has two non-zero homogeneous solutions.

The density equation for $\delta\rho$ mostly contributes to additional noise since the average $\langle \delta\rho \rangle$ vanishes and is important for quantitative analysis, but does not change the phenomenological picture presented in Eq. 2. Importantly the system is diffusive at short time scales which induces some non-exponential correlation behavior: the correlation function in Fourier space is not a Lorentzian and reads

$$\langle m_q m_{q'} \rangle = \delta_{q,q'} a\rho_0 \frac{Dq^2 + \hat{\gamma}}{Dq^2 + r} \tag{E4}$$

in the limit $\rho_0(\gamma a^2/D) \ll 1$ discussed below. The diffusive effects effectively lead the DIM to be weakly non-local, and it does not have perfectly exponentially-decaying correlation functions, and as such is not strictly subject to the theorem. In the supplement we derive a different bound for purely diffusive systems with Gaussian spatial correlations (SI Sec. II.C, Fig. S2).

To compute the PI in the diffusive Ising model, we partition the spatial domain into N bins of equal width ("cells") and binarize the signal field as $b_i = \text{sgn}(m_i)$. We estimate the marginal probability P_i^+ of finding $b_i = 1$ by its observed frequency, along with the pooled probability P_+ to find $b = 1$, irrespective of position. This allows us to compute the PI following Eq. 1

$$\text{PI} = \frac{1}{N} \sum_{i=1}^{N} \left[P_i^+ \log_2 \left(\frac{P_i^+}{P_+} \right) + P_i^- \log_2 \left(\frac{P_i^-}{P_-} \right) \right] \tag{E5}$$

with $P_- = 1 - P_+, P_i^- = 1 - P_i^+$.

Coarse-graining small microscopic models

To understand the emergent collective behavior of our spatially-extended assemblies of interacting particles, we build a fluctuating hydrodynamic model which focuses on the large-scale dynamics of this stochastic system. At long wavelengths, the lowest-order contributions from the noise are Gaussian. Starting from diffusive microscopic dynamics described by a master equation, we use exact coarse-graining methods to obtain a fluctuating hydrodynamic description in terms of a Stochastic Partial Differential Equation (SPDE). Spatio-temporal averaging of fluctuating dynamics then gives an effective deterministic reaction-diffusion hydrodynamic model [85, 86]. (Fig. E1) To estimate the validity range of this approach, we perform a self-consistent verification based on estimating the effective deterministic response using Dynamical Renormalization Group (DRG) methods [87](Fig. E1a-b). The DRG calculations are presented in SI Sec. VII. We find that the fluctuating hydrodynamics are valid when $g = \rho_0(\gamma a^2/D) \ll 1$. In statistical physics terms, this validity criterion is a kind of Ginzburg criterion, delineating the regime in which the mean-field approximation holds by quantifying the crossover regime between Gaussian and non-Gaussian fixed points [88]. However, unlike the standard Ginzburg criterion, which states that deviation from mean-field behavior depends on the dimension d of the space, the criterion $g \ll 1$ is dimension-independent.

In practice, we find that the fluctuating hydrodynamic formalism recovers the deterministic limit (Fig. E1c-d) when $D \to \infty$ and $a \to 0$, and that the effective hydrodynamics derived from the fluctuating model is predictive even with systems with around 10 particles per coarse-grained unit length, indicating the validity of the fluctuating hydrodynamic picture as a basis for understanding the collective dynamics of these systems (Fig. E1e).

Alternative model of short-range patterning

To show that the saturation of PI with decreasing noise is a feature of short-range correlated models, we consider the Ising model with an external but localized magnetic field. We consider a periodic lattice with $N = 2M$ sites, with Hamiltonian H given by [89]

$$H(\{s_i\}) = -\sum_{i=1}^{N} Js_i s_{i+1} + h_i s_i \tag{E6}$$

with the convention that $s_{N+1} \equiv s_1$. We take $h_i = h(\delta_{i,1} - \delta_{i,M})$, where $\delta_{i,j}$ is the Kronecker symbol, equal to 1 if $i = j$ and 0 otherwise. The steady-state probability distribution $p(\{s_i\}) = e^{-H(\{s_i\})}/\mathcal{Z}$ where $\mathcal{Z} = \sum_{\{s_i\}} e^{-H(\{s_i\})}$, is computable using the transfer matrix formalism, which allows us to efficiently compute all probabilities and information-theoretic quantities of interest (Fig. E2, see SI Sec. II.B for details of the computation). In SI Sec. II.D, Fig. S3, we also extend this model to the Potts model with more than 2 states and find a similar phenomenology.
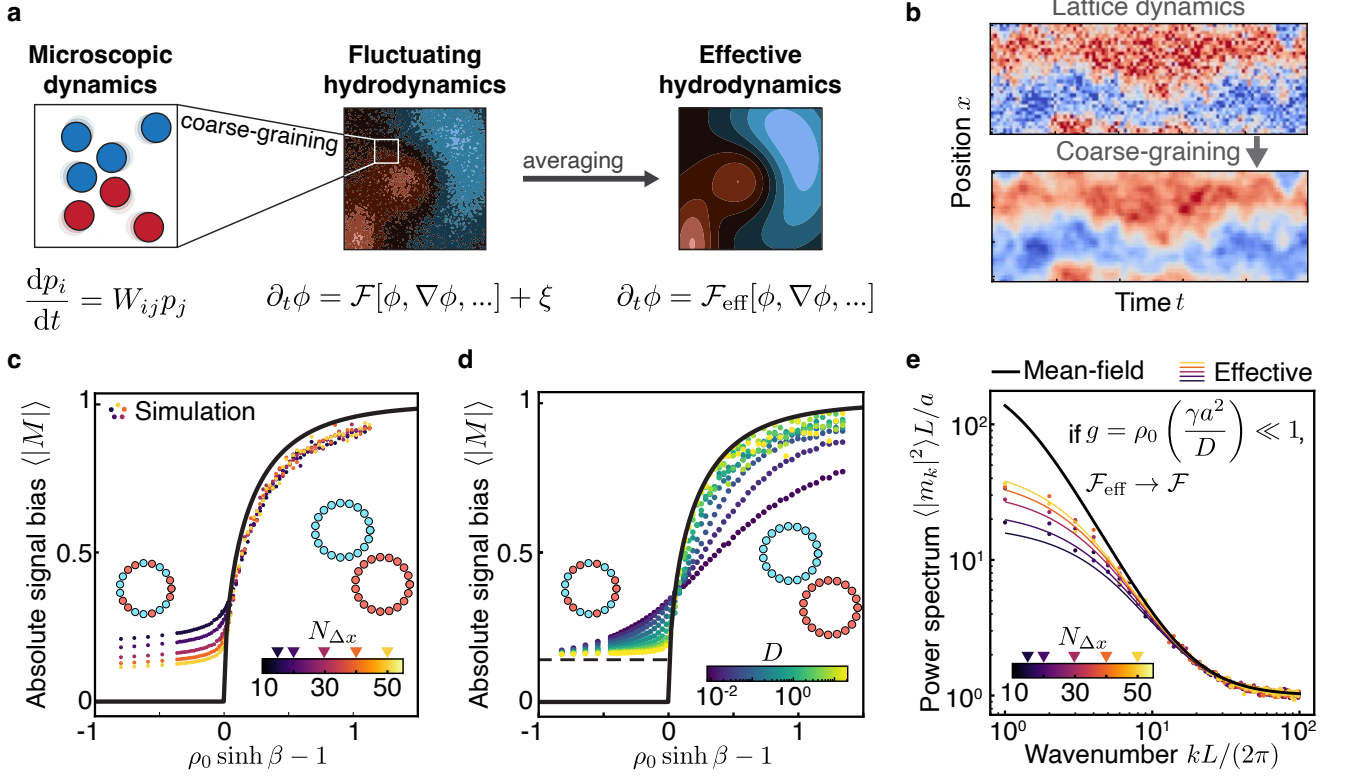
FIG. E1. Understanding the emergence of collective behavior in finite systems. **a.** Starting from diffusive microscopic dynamics described by a master equation, we use exact coarse-graining methods to obtain a fluctuating hydrodynamics description in terms of a SPDE. Spatio-temporal averaging of fluctuating dynamics gives an effective deterministic hydrodynamic model. **b.** This process allows us to understand the emergent collective dynamics and use continuum modeling tools even in small discrete systems. **c-d.** We find that the collective response from microscopic simulations rapidly converge to their continuum predictions (black lines) with increasing particle numbers (**c**) and diffusivity (**d**). Dashed lines indicates expected absolute signal bias for a finite coarse-grained domain size Δx. **e.** The linear response in Fourier domain from simulations is well-described by the renormalization predictions, validating that the fluctuating hydrodynamic picture is accurate even in small systems with less than tens of particles per coarse-graining domain.

Effects of spatial correlations on positional information

In SI Sec. II, we show that the PI can be rewritten in terms of the patterning entropy $S_{\mathrm{pat}} \equiv S(P_z)$ as

$$\mathrm{PI} = S_{\mathrm{pat}} - \frac{1}{N}\sum_{i=1}^{N} S(p_i) \qquad (E7)$$

where $S(p) = -\sum_k p_k \log_2 p_k$ is the Shannon entropy of the distribution p. The maximal value of the PI is achieved for symmetric systems for which $S_{\mathrm{pat}} = \log_2 Z$ and which have deterministic marginals, such that all entropies $S(X_i)$ are vanishing. If the system is stochastic, then we can examine the influence of correlations on the maximal value of PI by using the inequality $0 \le I(X_i : X_j) \le S(X_i)$ for any $j \in \{1, \ldots, N\}$ [90]. Inserting this inequality in Eq. (E7) we find

$$\mathrm{PI} \le S_{\mathrm{pat}} - \frac{1}{N}\sum_i I(X_i : X_j) \qquad (E8)$$

which can be itself bounded using the connected correlation function $C(A, B) = \langle AB \rangle - \langle A \rangle \langle B \rangle$

$$\mathrm{PI} \le S_{\mathrm{pat}} - \frac{1}{N}\sum_i \frac{1}{2Z^2} C(X_i, X_j)^2 \qquad (E9)$$

The inequality (E9) follows from Pinsker's inequality [90] which captures that the mutual information is larger than $C(A, B)$ as it accounts for all correlations between two random variables, including those that are invisible to two-point correlation functions [42]

$$I(A, B) \ge \frac{1}{2}\frac{(\langle fg \rangle - \langle f \rangle \langle g \rangle)^2}{||f||_\infty ||g||_\infty} \qquad (E10)$$

In particular, for $f = g = \mathrm{id}$ and X_i taking values in $\{1, \ldots, Z\}$, we have $I(X_i : X_j) \ge C(X_i, X_j)^2/(2Z^2)$.

Summing the inequalities (E8-E9) for all values of j and dividing by N, we find a symmetrized version of these inequalities showing that the PI is reduced from its maximal value by at least the average pairwise informa-
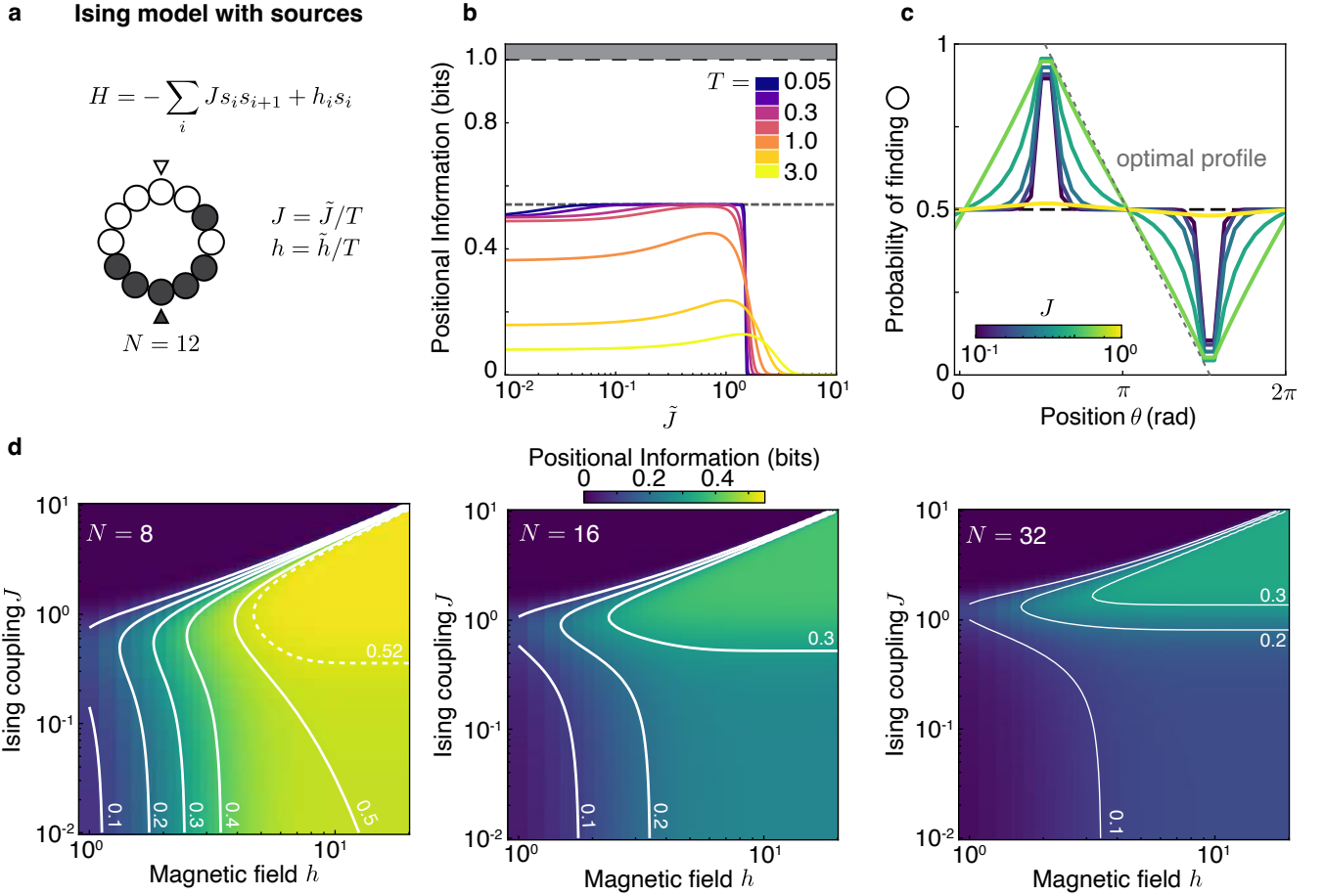
FIG. E2. The Ising model with external sources displays saturating positional information **a.** We consider a 1D Ising chain with broken translational symmetry by having non-zero opposing magnetic field $\pm h$ at two diametrically-opposed points. J is related to the correlation length in this model by $\ell \sim 1/\ln J$. Here states are represented as white and black dots. **b.** As we vary the coupling strength for a given magnetic field strength $h = 3$ for variable temperature T, we find a similar optimal coupling $\tilde{J}^*$ as in the DIM. Interestingly, as we reduce temperature (noise amplitude), the optimal range of $\tilde{J}$ expands but the PI stays bounded. Here, $N = 8$. Dashed line indicates theoretical prediction for the bound. **c.** Marginal probability profiles are similar to the ones in the DIM case: Small J lead to exponentially-peaked probabilities around source points, while large J homogenize the system. Optimal values of J lead to a sawtooth profile. **d.** Parameter search of J and h for variable N show that the optimal region of J, h and optimal value of PI both become smaller with increasing N.

tion

$$\mathrm{PI} \leq S_{\mathrm{pat}} - \frac{1}{N^2} \sum_{i,j} I(X_i : X_j) \qquad (E11)$$

$$\leq S_{\mathrm{pat}} - \frac{1}{2N^2 Z^2} \sum_{i,j} C(X_i, X_j)^2. \qquad (E12)$$

The presence of spatial correlations in a stochastic system can thus counter-intuitively decrease positional information. Informally, to have high PI, one needs signals that are as distinct as possible in every place, which is difficult to achieve in strongly spatially-correlated systems: uniform systems have maximal spatial correlations, but have PI = 0. It is difficult to say more without more constraints on the structure of spatial correlations: increasing spatial correlations without an overall reduction in uncertainty in the marginals $p(X_i)$ reduces PI. However, if spatial correlations have the additional effect of reducing overall entropy by, for instance, averaging signals in space or imposing feedback control, then the PI can reach its maximal value. This latter scenario is similar to results in field theory which state that systems with many neighbors or long-range interactions suppress fluctuations and thus behave closer to mean-field [89].

In what follows, we show that locally interacting systems with a finite correlation range bound the PI below its maximal value. As mentioned in the main text, this is reminiscent of area laws in quantum systems, which generically appear in locally-interacting systems with finite correlation lengths [42, 43]. In the same way that quantum entanglement can 'break the area law', classical long-range correlations can lead to volume-law scaling as we demonstrated in Main Fig. 3. The 'area law' (bound on PI) can also be broken in presence of conservation

laws which introduce non-localities, which we observe in the Diffusive Ising model subject to conserved noise (Figs. 2f, S2, see also SI Sec. II.C), or in continuum systems derived from real-valued fields where no constraint from microscopic models exists to relate noise and spatial correlations (SI Sec. IV, Fig. S5).

Bound on PI in locally-coupled two-species systems

We now prove the theorem stated in the main text by examining the case of locally interacting systems corresponding to our set-up from the main text. In this case, the structure of spatial correlations limits PI. Here we consider $Z = 2$: we extend to the multi-species situation where $Z > 2$ in the SI Sec. II.D.

Consider a periodic system of $N = 2M$ cells. To maximize S_{pat}, as in the main text we consider a situation where $h_i = 0$ except at two diametrically opposite points where $h_1 = h = -h_M$, such that the system is fully symmetric $P_+ = P_- = 1/2$. In this case, we can write

$$\text{PI} = S_{\text{pat}} - S_{\text{cf}} = 1 - \frac{1}{N}\sum_i S_i \qquad \text{(E13)}$$

where $S_i = -p_i \log(p_i) - (1-p_i)\log(1-p_i) \geq 0$ is the binary entropy of the i-th marginal, with equality if $p_i = 0$ or 1. Since $S_i \geq 0$, we have PI ≤ 1 bit for all situations where $Z = 2$. Without loss of generality, we consider here that the system can take values $s_i \in \{0,1\}$. For systems with local couplings such that correlations are short ranged $\langle s_i s_j \rangle \sim e^{-d(i,j)/\xi}$ where $d(i,j)$ is the distance between cells i and j, we can go further and prove a tighter bound. Consider a system of $N = 2M$ cells: we notice that if p_i is maximal at $i = 1$ and minimal at $i = M$, the maximal contributions to the PI are achieved for $p_1 = 1$ and $p_M = 0$. By symmetry, $p_{M/2} = p_{3M/2} = 1/2$, and we will restrict our attention to the sector between 1 and $M/2$. Since $p_1 = 1$, we have $\langle s_1 s_i \rangle = p_i$: Since the correlations are exponentially decaying, p_i is convex and monotonically decreasing between p_1 and $p_{M/2}$. Maximizing PI is now equivalent to minimizing the entropy for $(p_i)_{1 \leq i \leq M/2}$. In this sector $p_i \geq 1/2$: As the entropy is a decreasing function of p_i above $1/2$, minimizing PI is equivalent to maximizing p_i. Since p_i is decreasing and convex, by definition we have the bound $p_i \leq Ai + B$, where A and B are set by the two constraints $p_1 = 1, p_{M/2} = 1/2$. This gives a maximum bound $p_i \leq 1 - (i-1)/M$, which is tight.

The maximum PI is achieved thus when the marginal probability is linear in the position $p_i = 1 - (i-1)/M$ between 0 and M. This implies that the PI is bounded by

$$\text{PI} \leq 1 + 2 \times \frac{1}{2M}\sum_{i=1}^{M}\left[\frac{i-1}{M}\log_2\frac{i-1}{M}\right.$$
$$\left. + \left(1 - \frac{i-1}{M}\right)\log_2\left(1 - \frac{i-1}{M}\right)\right]$$
$$= 1 + \frac{2}{M}\sum_{i=0}^{M-1}\frac{i}{M}\log_2\left(\frac{i}{M}\right) \qquad \text{(E14)}$$

where we switch the indexing in the last sum from 0 to $M-1$ and use the symmetry of the terms. When $N \to \infty$, this sum is a Riemann sum of negative terms and the PI is thus bounded by

$$\text{PI}(N \to \infty) \leq \Pi_\infty = 1 + 2\int_0^1 \mathrm{d}x\, x \log_2(x)$$
$$= 1 - \frac{1}{2\ln(2)} \approx 0.28 \text{ bit} \qquad \text{(E15)}$$

For finite N, the corrections to the integral from the finite sum lead to a less constraining bound on the PI, which is then bounded by a larger value $\Pi_N \geq \Pi_\infty$. The computed value is consistent with the numerically obtained value for the Ising model and close to the saturating value of the DIM (Figs. 2f, E2d).

Domain wall dynamics and positional information

A Landau-Ginzburg type theory can sustain domain walls. The wall centered at position $X(t)$ has a hyperbolic tangent profile $m_{X(t)}(x) = -\tanh\left(\frac{x-X(t)}{\sqrt{2}\ell}\right)$ with $\ell = \sqrt{D/r}$. To understand the effect of external signals, we use techniques from nonlinear front propagation theory [60, 91] to compute the restoring or confinement force f_c acting on the domain wall as a function of the ratio ℓ/L (Details in SI Sec. III). For weak noise, we find that f_c is linear in the deviation away from the average position $\Delta(t) = X(t) - X_0$, and is proportional to the curvature to the front at the sources, giving

$$f_c = -k_c\Delta(t), \quad k_c = \frac{3h_0}{\sqrt{2}\ell}\frac{\sinh\left(L/(2\sqrt{2}\ell)\right)}{\cosh\left(L/(2\sqrt{2}\ell)\right)^3} \qquad \text{(E16)}$$

which has a geometric stiffness k_c proportional to the strength of the source field h_0 and has a maximal value $k_c^* \approx 1.9h_0/L$ for $\ell \approx 0.35L$. In the presence of external sources, the Langevin equation governing the time-evolution of the front position now takes the form

$$\mathrm{d}X = f_c(X)\mathrm{d}t + \sqrt{2D_f}\mathrm{d}W \qquad \text{(E17)}$$

with D_f the front diffusivity and W a standard Brownian process. Counterintuitively, the front diffusivity D_f scales as $\sqrt{D}$. This can be understood as $D_f \sim D/N_{\text{int}}$,

where $N_{\text{int}} \sim \sqrt{D}$ is the number of particles within interaction range between reactions [58, 59]. By equipartition, the domain wall is distributed around its average position with a standard deviation given by the confinement length $\sigma = \sqrt{D_f/k_c}$. If σ is of the order of the system size L, then the front is unstable.

We compare these theoretical results to direct numerical simulations of the continuum theory in SI Sec. III, Fig. S4. While this calculation is approximate, we obtain reasonable qualitative agreement around the optimal diffusion value.

Here, we remark that for the DIM, since both h_0 and D_f scale linearly with the noise amplitude a, σ is independent of a, leading to a non-vanishing optimal confinement length. In non-equilibrium models where this microscopic constraint is not present it is possible to control D and noise amplitude separately. Such systems can have $\sigma \to 0$ for any fixed value of D, leading to arbitrarily strong domain wall confinement and large positional information (SI Sec. IV, Fig. S5).

Wave-pinning dynamics

We here write down a minimal microscopic model of wave-pinning, which we dub the wave-pinning Ising model in comparison with the Diffusive Ising model discussed above. Particles move according to the following rules:

W1 Particles on the surface hop with equal probability to the left or right neighboring site, at rate D/a^2

W2 Particles of type A (resp. B) unbind from the surface into the reservoir with rate $R_A = r + kn_B(n_B - 1)$ (resp. $R_B = r + kn_A(n_A - 1)$).

W3 Particles in the reservoir leave it at a rate $(M + \alpha)r$, with M the number of sites and α the strength of the bias to bind to the source point. Particles which leave the reservoir then bind to a non-source site with probability $1/(M + \alpha)$, and bind to the source site with probability $(1 + \alpha)/(M + \alpha)$.

We again use a tau-leaping scheme to simulate these stochastic dynamics. After coarse-graining (SI Sec. VI), we find the integro-differential equations

$$\partial_t n_A = D\partial_x^2 n_A - rn_A - kn_B^2 n_A + rN_A^c + h_A(x) \tag{E18a}$$

$$\partial_t n_B = D\partial_x^2 n_B - rn_B - kn_A^2 n_B + rN_B^c + h_B(x) \tag{E18b}$$

with the cytoplasmic concentrations given by the conservation laws

$$N_X^c = N_X^0 - \frac{1}{a}\int_0^L \mathrm{d}x\, n_X(x) \tag{E19a}$$

with $X = A$ or B. This system has bistable dynamics, where the state of the system can be either mostly A or mostly B. From the domain wall dynamics point of view, the effect of the integral term can be understood as shifting the potential $V(m)$ of being in state A or B, which sets the domain wall moving towards the state of higher potential (SI Sec. V). Effectively, the integral feedback leads to a wave-pinning force $f_{\text{wp}} = -k_{\text{wp}}(X(t) - X_0)$ with a stiffness given by (SI Sec. V)

$$k_{\text{wp}} = \frac{6\sqrt{2}\,r}{k}\sqrt{r_2 D} \tag{E20}$$

where $r_2 = k(N_A^0 + N_B^0)^2/(4 + 2/a)^2 - r$. As mentioned in the main text, k_{wp} scales as $\sqrt{D}$ and is therefore less sensitive than the boundary confinement force on the diffusivity.

Finally, to confirm that the integral term leads to non-exponentially correlated systems, we compute the two-point correlation function of this system and find that it does not decay at infinity: if we consider $m(x) = m_0(x) + \phi(x)$, with $\phi(x)$ a small perturbation, then there are constants A and B such that $\langle \phi(x)\phi(y)\rangle = A + Be^{-|x-y|/\ell}$ which does not vanish as x and y are taken far apart, violating the conditions for the bound to apply (SI Sec. V).

[1] M. F. Hagan and G. M. Grason, Equilibrium mechanisms of self-limiting assembly, Reviews of Modern Physics **93**, 025008 (2021).

[2] M. Mastrangeli, S. Abbasi, C. Varel, C. Van Hoof, J.-P. Celis, and K. F. Böhringer, Self-assembly from milli- to nanoscales: methods and applications, Journal of Micromechanics and Microengineering **19**, 083001 (2009).

[3] D. Lee, S. Cho, C. Park, K. R. Park, J. Lee, J. Nam, K. Ahn, C. Park, K. Jeon, H. Yuh, W. Choi, C. H. Lim, T. Kwon, Y. H. Min, M. Joo, Y.-H. Choi, J. S. Lee, C. Kim, and S. Kwon, Fluidic self-assembly for MicroLED displays by controlled viscosity, Nature **619**, 755 (2023).

[4] M. Z. Miskin, A. J. Cortese, K. Dorsey, E. P. Esposito, M. F. Reynolds, Q. Liu, M. Cao, D. A. Muller, P. L. McEuen, and I. Cohen, Electronically integrated, mass-manufactured, microscopic robots, Nature **584**, 557 (2020).

[5] F. Schweisguth and F. Corson, Self-Organization in Pattern Formation, Developmental Cell **49**, 659 (2019).

[6] C. Collinet and T. Lecuit, Programmed and self-organized flow of information during morphogenesis, Nature Reviews Molecular Cell Biology **22**, 245 (2021).

[7] N. W. Goehring, P. K. Trong, J. S. Bois, D. Chowdhury, E. M. Nicola, A. A. Hyman, and S. W. Grill, Polarization of PAR Proteins by Advective Triggering of a Pattern-
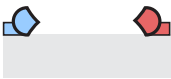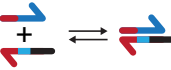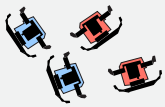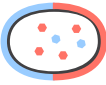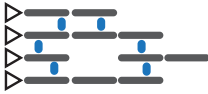
System		Process	Non-local mechanism
Self-assembled electronics		Self assembly on substrate	Fast bulk diffusion, hydrodynamic interactions
Colloidal nanocrystals		Super-crystal assembly	Electrostatic properties of solvent
DNA-based reaction networks		Spatially-patterned reactions	Fast diffusion
Microrobotics		Collective dynamics	Wireless communication Hydrodynamic interactions
C. elegans embryo		Cell polarization	Fast bulk diffusion
Avian skin		Feather follicle morphogenesis	Visco-elastic mechanics
Fish stripes		Turing instability	Long-range inhibition
Cyanobacteria filaments		Heterocyst differentiation	Lateral inhibition
Cytoskeletal assembly		Filament length self-regulation	Cross-linking within bundle
Genome organization		DNA regulation	Chromatin physical organization
Plant growth		Flat leaf growth	Auxin-mediated growth feedback

FIG. E3. Illustrations of self-organized systems where long-range interactions can enable robust patterning. Self-assembly of electronic components could benefit from hydrodynamic interactions [3]. Colloidal nanocrystals self-assembly can be controlled by tuning long-range interactions through the dielectric properties of the solvent [76]. DNA toolkit reactions can benefit from engineering molecular mobility to establish reliable spatial patterns [16], while microrobotic systems [4] can benefit from long-range wireless communication. In biology, *C. elegans* embryo patterning is stabilized by wave-pinning [7], avian skin morphogenesis benefits from long-range mechanical effects [36], and Turing patterning (or lateral inhibition) is a common motif to describe the emergence of fish stripes and other self-organized systems such as cyanobacteria heterocyst differentiation [5, 35, 92]. Nonlocal coupling can also help regulate filament length in cytoskeletal assembly [93]. Physical organization of the genome allows distant regions in the genome to be in physical proximity, effectively creating long-range interactions, a feature that is evolutionarily conserved [94, 95]. Growing flat surfaces such as leaves requires long-range feedback to be stable [38].
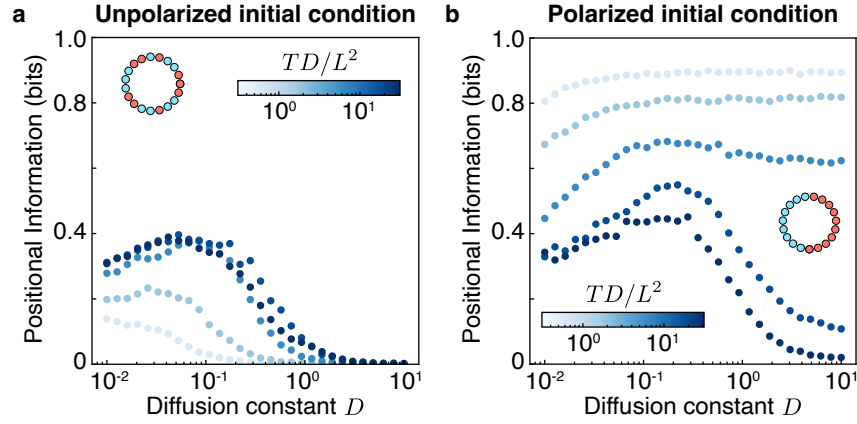
FIG. E4. Initial condition dependence of outcomes with finite decision times in the DIM. **a.** The positional information starting from unpolarized (random) initial conditions increases with decision time T as the system reaches steady state. The color scheme reflects T normalized by the time scale of dynamics with diffusion D. **b.** Conversely, when the system is initialized in a polarized state for which PI = 1 bit, PI decreases to its steady-state value as the decision time T increases. Here $a = L/384, \gamma = 1, \beta = 3\beta_c/2, h_0 = 3\beta, L = 4, N = 32$, and results are averaged over 500 replicates.

Forming System, Science **334**, 1137 (2011).

[8] G. Tkačik and P. R. T. Wolde, Information Processing in Biochemical Networks, Annual Review of Biophysics **54**, 249 (2025).

[9] W. M. Jacobs and D. Frenkel, Self-Assembly of Structures with Addressable Complexity, Journal of the American Chemical Society **138**, 2457 (2016).

[10] M. Freeman, Feedback control of intercellular signalling in development, Nature **408**, 313 (2000).

[11] R. Veneziano, S. Ratanalert, K. Zhang, F. Zhang, H. Yan, W. Chiu, and M. Bathe, Designer nanoscale DNA assemblies programmed from the top down, Science **352**, 1534 (2016).

[12] Q.-Y. Lin, J. A. Mason, Z. Li, W. Zhou, M. N. O'Brien, K. A. Brown, M. R. Jones, S. Butun, B. Lee, V. P. Dravid, K. Aydin, and C. A. Mirkin, Building superlattices from individual nanoparticles via template-confined DNA-mediated assembly, Science **359**, 669 (2018).

[13] J. F. Woods, L. Gallego, P. Pfister, M. Maaloum, A. Vargas Jentzsch, and M. Rickhaus, Shape-assisted self-assembly, Nature Communications **13**, 3681 (2022).

[14] H. Kim, D. J. Skinner, D. S. Glass, A. E. Hamby, B. A. R. Stuart, J. Dunkel, and I. H. Riedel-Kruse, 4-bit adhesion logic enables universal multicellular interface patterning, Nature **608**, 324 (2022).

[15] S. Toda, L. R. Blauch, S. K. Y. Tang, L. Morsut, and W. A. Lim, Programming self-organizing multicellular structures with synthetic cell-cell signaling, Science **361**, 156 (2018).

[16] A. S. Zadorin, Y. Rondelez, G. Gines, V. Dilhas, G. Urtel, A. Zambrano, J.-C. Galas, and A. Estevez-Torres, Synthesis and materialization of a reaction–diffusion French flag pattern, Nature Chemistry **9**, 990 (2017).

[17] P. Li, J. S. Markson, S. Wang, S. Chen, V. Vachharajani, and M. B. Elowitz, Morphogen gradient reconstitution reveals Hedgehog pathway design principles, Science **360**, 543 (2018).

[18] G. Schlissel, M. Meziane, D. Narducci, A. S. Hansen, and P. Li, Diffusion barriers imposed by tissue topology

shape Hedgehog morphogen gradients, Proceedings of the National Academy of Sciences **121**, e2400677121 (2024).

[19] R. Zhu, L. A. Santat, J. S. Markson, N. Nandagopal, J. Gregrowicz, and M. B. Elowitz, Reconstitution of morphogen shuttling circuits, Science Advances **9**, eadf9336 (2023).

[20] A. Gierer and H. Meinhardt, A theory of biological pattern formation, Kybernetik **12**, 30 (1972).

[21] T. Gregor, D. W. Tank, E. F. Wieschaus, and W. Bialek, Probing the Limits to Positional Information, Cell **130**, 153 (2007).

[22] J. B. A. Green and J. Sharpe, Positional information and reaction-diffusion: two big ideas in developmental biology combine, Development **142**, 1203 (2015).

[23] M. Li, M. Liu, F. Qi, F. R. Lin, and A. K.-Y. Jen, Self-Assembled Monolayers for Interfacial Engineering in Solution-Processed Thin-Film Electronic Devices: Design, Fabrication, and Applications, Chemical Reviews **124**, 2138 (2024).

[24] C. L. Bassani, G. Van Anders, U. Banin, D. Baranov, Q. Chen, M. Dijkstra, M. S. Dimitriyev, E. Efrati, J. Faraudo, O. Gang, N. Gaston, R. Golestanian, G. I. Guerrero-Garcia, M. Gruenwald, A. Haji-Akbari, M. Ibáñez, M. Karg, T. Kraus, B. Lee, R. C. Van Lehn, R. J. Macfarlane, B. M. Mognetti, A. Nikoubashman, S. Osat, O. V. Prezhdo, G. M. Rotskoff, L. Saiz, A.-C. Shi, S. Skrabalak, I. I. Smalyukh, M. Tagliazucchi, D. V. Talapin, A. V. Tkachenko, S. Tretiak, D. Vaknin, A. Widmer-Cooper, G. C. L. Wong, X. Ye, S. Zhou, E. Rabani, M. Engel, and A. Travesset, Nanocrystal Assemblies: Current Advances and Open Problems, ACS Nano **18**, 14791 (2024).

[25] M. B. Elowitz, A. J. Levine, E. D. Siggia, and P. S. Swain, Stochastic Gene Expression in a Single Cell, Science **297**, 1183 (2002).

[26] N. Battich, T. Stoeger, and L. Pelkmans, Control of Transcript Variability in Single Mammalian Cells, Cell **163**, 1596 (2015).

[27] L. Wolpert, Positional information and the spatial pat-

tern of cellular differentiation, Journal of Theoretical Biology **25**, 1 (1969).

[28] M. Merle, L. Friedman, C. Chureau, A. Shoushtarizadeh, and T. Gregor, Precise and scalable self-organization in mammalian pseudo-embryos, Nature Structural & Molecular Biology **31**, 896 (2024).

[29] P. Moghe, E. Hannezo, and T. Hiiragi, Optimality as a framework for understanding developmental robustness, Trends in Cell Biology , S0962892425002041 (2025).

[30] Y. T. Loo, J. Chen, R. Harrison, T. Rito, S. Theis, G. Charras, J. Briscoe, and T. E. Saunders, Boundary constraints can determine pattern emergence, bioRxiv 10.1101/2025.07.21.665949 (2025).

[31] S. J. Bryant and B. B. Machta, Physical Constraints in Intracellular Signaling: The Cost of Sending a Bit, Physical Review Letters **131**, 068401 (2023).

[32] N. Hino, L. Rossetti, A. Marín-Llauradó, K. Aoki, X. Trepat, M. Matsuda, and T. Hirashima, ERK-Mediated Mechanochemical Waves Direct Collective Cell Polarization, Developmental Cell **53**, 646 (2020).

[33] S. C. Little, M. Tikhonov, and T. Gregor, Precise Developmental Gene Expression Arises from Globally Stochastic Transcriptional Activity, Cell **154**, 789 (2013).

[34] J. Stelling, U. Sauer, Z. Szallasi, F. J. Doyle, and J. Doyle, Robustness of Cellular Functions, Cell **118**, 675 (2004).

[35] F. Corson, L. Couturier, H. Rouault, K. Mazouni, and F. Schweisguth, Self-organized Notch dynamics generate stereotyped sensory organ patterns in *Drosophila*, Science **356**, eaai7407 (2017).

[36] S. Yang, K. H. Palmquist, L. Nathan, C. R. Pfeifer, P. J. Schultheiss, A. Sharma, L. C. Kam, P. W. Miller, A. E. Shyer, and A. R. Rodrigues, Morphogens enable interacting supracellular phases that generate organ architecture, Science **382**, eadg5579 (2023).

[37] A. B. Goryachev and A. V. Pokhilko, Dynamics of Cdc42 network embodies a Turing-type mechanism of yeast cell polarity, FEBS Letters **582**, 1437 (2008).

[38] S. al Mosleh and L. Mahadevan, How to Grow a Flat Leaf, Physical Review Letters **131**, 098401 (2023).

[39] G. Tkačik and T. Gregor, The many bits of positional information, Development **148**, dev176065 (2021).

[40] J. O. Dubuis, G. Tkačik, E. F. Wieschaus, T. Gregor, and W. Bialek, Positional information, in bits, Proceedings of the National Academy of Sciences **110**, 16301 (2013).

[41] D. B. Brückner and G. Tkačik, Information content and optimization of self-organized developmental systems, Proceedings of the National Academy of Sciences **121**, e2322326121 (2024).

[42] M. M. Wolf, F. Verstraete, M. B. Hastings, and J. I. Cirac, Area Laws in Quantum Systems: Mutual Information and Correlations, Physical Review Letters **100**, 070502 (2008).

[43] J. Eisert, M. Cramer, and M. B. Plenio, *Colloquium* : Area laws for the entanglement entropy, Reviews of Modern Physics **82**, 277 (2010).

[44] G. R. Walther, A. F. M. Marée, L. Edelstein-Keshet, and V. A. Grieneisen, Deterministic Versus Stochastic Cell Polarisation Through Wave-Pinning, Bulletin of Mathematical Biology 10.1007/s11538-012-9766-5 (2012).

[45] Y. Fan, C. Chai, P. Li, X. Zou, J. E. Ferrell, and B. Wang, Ultrafast distant wound response is essential for whole-body regeneration, Cell **186**, 3606 (2023).

[46] S. Kondo and T. Miura, Reaction-Diffusion Model as a Framework for Understanding Biological Pattern Formation, Science **329**, 1616 (2010).

[47] A. Mietke, F. Jülicher, and I. F. Sbalzarini, Self-organized shape dynamics of active surfaces, Proceedings of the National Academy of Sciences **116**, 29 (2019).

[48] A. P. Solon and J. Tailleur, Flocking with discrete symmetry: The two-dimensional active Ising model, Physical Review E **92**, 042119 (2015).

[49] M. Scandolo, J. Pausch, and M. E. Cates, Active Ising Models of flocking: a field-theoretic approach, The European Physical Journal E **46**, 103 (2023).

[50] D. Martin, D. Seara, Y. Avni, M. Fruchart, and V. Vitelli, The transition to collective motion in nonreciprocal active matter: coarse graining agent-based models into fluctuating hydrodynamics (2024), arXiv:2307.08251 [cond-mat].

[51] M. F. Weber and E. Frey, Master equations and the theory of stochastic path integrals, Reports on Progress in Physics **80**, 046601 (2017).

[52] M. D. Petkova, G. Tkačik, W. Bialek, E. F. Wieschaus, and T. Gregor, Optimal Decoding of Cellular Identities in a Genetic Network, Cell **176**, 844 (2019).

[53] T. R. Sokolowski, T. Gregor, W. Bialek, and G. Tkačik, Deriving a genetic regulatory network from an optimization principle, Proceedings of the National Academy of Sciences **122**, e2402925121 (2025).

[54] G. Peyré and M. Cuturi, Computational Optimal Transport 10.48550/arxiv.1803.00567 (2018).

[55] J. Lin, Divergence measures based on the Shannon entropy, IEEE Transactions on Information Theory **37**, 145 (1991).

[56] A. Andreanov, G. Biroli, J.-P. Bouchaud, and A. Lefèvre, Field theories and exact stochastic equations for interacting particle systems, Physical Review E **74**, 030101 (2006).

[57] M. Kourbane-Houssene, C. Erignoux, T. Bodineau, and J. Tailleur, Exact Hydrodynamic Description of Active Lattice Gases, Physical Review Letters **120**, 268003 (2018).

[58] B. Meerson, P. V. Sasorov, and Y. Kaplan, Velocity fluctuations of population fronts propagating into metastable states, Physical Review E **84**, 011147 (2011).

[59] E. Khain and B. Meerson, Velocity fluctuations of noisy reaction fronts propagating into a metastable state, Journal of Physics A: Mathematical and Theoretical **46**, 125002 (2013).

[60] G. Birzu, O. Hallatschek, and K. S. Korolev, Fluctuations uncover a distinct class of traveling waves, Proceedings of the National Academy of Sciences **115**, 10.1073/pnas.1715737115 (2018).

[61] C. W. Gardiner, *Handbook of stochastic methods: for physics, chemistry and the natural sciences*, 2nd ed., Springer series in synergetics No. 13 (Springer, Berlin Heidelberg, 1994).

[62] R. Milo and R. Phillips, *Cell Biology by the Numbers*, 0th ed. (Garland Science, 2015).

[63] J. Swift and P. C. Hohenberg, Hydrodynamic fluctuations at the convective instability, Physical Review A **15**, 319 (1977).

[64] Y. Mori, A. Jilkine, and L. Edelstein-Keshet, Wave-Pinning and Cell Polarity from a Bistable Reaction-Diffusion System, Biophysical Journal **94**, 3684 (2008).

[65] Y. Mori, A. Jilkine, and L. Edelstein-Keshet, Asymptotic and Bifurcation Analysis of Wave-Pinning in a Reaction-

Diffusion Model for Cell Polarization, SIAM Journal on Applied Mathematics **71**, 1401 (2011).

[66] L. Hubatsch, F. Peglion, J. D. Reich, N. T. L. Rodrigues, N. Hirani, R. Illukkumbura, and N. W. Goehring, A cell-size threshold limits cell polarity and asymmetric division potential, Nature Physics **15**, 1078 (2019).

[67] P. W. Miller, D. Fortunato, C. Muratov, L. Greengard, and S. Shvartsman, Forced and spontaneous symmetry breaking in cell polarization, Nature Computational Science **2**, 504 (2022), publisher: Springer Science and Business Media LLC.

[68] M. Zhu, J. Cornwall-Scoones, P. Wang, C. E. Handford, J. Na, M. Thomson, and M. Zernicka-Goetz, Developmental clock and mechanism of de novo polarization of the mouse embryo, Science **370**, eabd2703 (2020).

[69] M. Otsuji, S. Ishihara, C. Co, K. Kaibuchi, A. Mochizuki, and S. Kuroda, A Mass Conserved Reaction–Diffusion System Captures Properties of Cell Polarity, PLoS Computational Biology **3**, e108 (2007).

[70] Y. Couder and E. Fort, Single-Particle Diffraction and Interference at a Macroscopic Scale, Physical Review Letters **97**, 154101 (2006).

[71] W. Chen, A. Izzet, R. Zakine, E. Clément, E. Vanden-Eijnden, and J. Brujic, Evolving Motility of Active Droplets Is Captured by a Self-Repelling Random Walk Model, Physical Review Letters **134**, 018301 (2025).

[72] J. D. Moroz and P. Nelson, Entropic Elasticity of Twist-Storing Polymers, Macromolecules **31**, 6333 (1998).

[73] H. Berg and E. Purcell, Physics of chemoreception, Biophysical Journal **20**, 193 (1977).

[74] M. Vergassola, E. Villermaux, and B. I. Shraiman, 'Infotaxis' as a strategy for searching without gradients, Nature **445**, 406 (2007).

[75] A. Tripathi, J. Dunkel, and D. J. Skinner, Collective is different: Information exchange and speed-accuracy trade-offs in self-organized patterning (2025), version Number: 1.

[76] I. Coropceanu, E. M. Janke, J. Portner, D. Haubold, T. D. Nguyen, A. Das, C. P. N. Tanner, J. K. Utterback, S. W. Teitelbaum, M. H. Hudson, N. A. Sarma, A. M. Hinkle, C. J. Tassone, A. Eychmüller, D. T. Limmer, M. Olvera De La Cruz, N. S. Ginsberg, and D. V. Talapin, Self-assembly of nanocrystals into strongly electronically coupled all-inorganic supercrystals, Science **375**, 1422 (2022).

[77] I. R. Graf and B. B. Machta, A bifurcation integrates information from many noisy ion channels and allows for milli-Kelvin thermal sensitivity in the snake pit organ, Proceedings of the National Academy of Sciences **121**, e2308215121 (2024).

[78] P. Gross, K. V. Kumar, N. W. Goehring, J. S. Bois, C. Hoege, F. Jülicher, and S. W. Grill, Guiding self-organized pattern formation in cell polarity establishment, Nature Physics **15**, 293 (2019).

[79] D. Boocock, N. Hino, N. Ruzickova, T. Hirashima, and E. Hannezo, Theory of mechanochemical patterning and optimal migration in cell monolayers, Nature Physics **17**, 267 (2021).

[80] P. L. Garrido, J. L. Lebowitz, C. Maes, and H. Spohn, Long-range correlations for conservative dynamics, Physical Review A **42**, 1954 (1990).

[81] P. Bak, C. Tang, and K. Wiesenfeld, Self-organized criticality, Physical Review A **38**, 364 (1988).

[82] T. Mora and W. Bialek, Are Biological Systems Poised at Criticality?, Journal of Statistical Physics **144**, 268 (2011).

[83] Y. Baek, A. P. Solon, X. Xu, N. Nikola, and Y. Kafri, Generic Long-Range Interactions Between Passive Bodies in an Active Fluid, Physical Review Letters **120**, 058002 (2018).

[84] Y. Ben Dor, S. Ro, Y. Kafri, M. Kardar, and J. Tailleur, Disordered boundaries destroy bulk phase separation in scalar active matter, Physical Review E **105**, 044603 (2022).

[85] A. De Masi, P. A. Ferrari, and J. L. Lebowitz, Rigorous Derivation of Reaction-Diffusion Equations with Fluctuations, Physical Review Letters **55**, 1947 (1985).

[86] A. De Masi, P. A. Ferrari, and J. L. Lebowitz, Reaction-diffusion equations for interacting particle systems, Journal of Statistical Physics **44**, 589 (1986).

[87] U. C. Täuber, *Critical Dynamics: A Field Theory Approach to Equilibrium and Non-Equilibrium Scaling Behavior*, 1st ed. (Cambridge University Press, 2014).

[88] J. L. Cardy, *Scaling and renormalization in statistical physics*, Cambridge lecture notes in physics No. 5 (Cambridge University Press, Cambridge ; New York, 1996).

[89] M. Kardar, *Statistical Physics of Fields*, 1st ed. (Cambridge University Press, 2007).

[90] T. M. Cover and J. A. Thomas, *Elements of Information Theory*, 1st ed. (Wiley, 2005).

[91] A. Rocco, J. Casademunt, U. Ebert, and W. Van Saarloos, Diffusion coefficient of propagating fronts with multiplicative noise, Physical Review E **65**, 012102 (2001).

[92] A. M. Turing, The chemical basis of morphogenesis, Philosophical Transactions of the Royal Society of London. Series B, Biological Sciences **237**, 37 (1952).

[93] S. G. McInally, A. J. B. Reading, A. Rosario, P. R. Jelenkovic, B. L. Goode, and J. Kondev, Length control emerges from cytoskeletal network geometry, Proceedings of the National Academy of Sciences **121**, e2401816121 (2024).

[94] J. Dekker, M. A. Marti-Renom, and L. A. Mirny, Exploring the three-dimensional organization of genomes: interpreting chromatin interaction data, Nature Reviews Genetics **14**, 390 (2013).

[95] I. V. Kim, C. Navarrete, X. Grau-Bové, M. Iglesias, A. Elek, G. Zolotarov, N. S. Bykov, S. A. Montgomery, E. Ksiezopolska, D. Cañas-Armenteros, J. J. Soto-Angel, S. P. Leys, P. Burkhardt, H. Suga, A. De Mendoza, M. A. Marti-Renom, and A. Sebé-Pedrós, Chromatin loops are an ancestral hallmark of the animal regulatory genome, Nature **642**, 1097 (2025).

Supplement to: Information bounds the robustness of self-organized systems

Nicolas Romeo,[1,2] David G. Martin,[3,1] Mattia Scandolo,[1] Michel Fruchart,[4] Edwin M. Munro,[2,5,6] and Vincenzo Vitelli[1,2,5,7,*]

[1]*Department of Physics, University of Chicago, Chicago, Illinois 60637, USA*
[2]*Center for Living Systems, University of Chicago, Chicago, Illinois 60637, USA*
[3]*LPTMC, CNRS UMR 7600, Université Pierre et Marie Curie, 75252 Paris, France*
[4]*Gulliver, ESPCI Paris, Université PSL, CNRS, 75005 Paris, France*
[5]*Institute for Biophysical Dynamics, University of Chicago, Chicago, Illinois 60637, USA*
[6]*Department of Molecular Genetics and Cell Biology,*
University of Chicago, Chicago, Illinois 60637, USA
[7]*Leinweber Center for Theoretical Physics, University of Chicago, Chicago, Illinois 60637, USA*

CONTENTS

---

* vitelli@uchicago.edu

I. MAIN RESULTS OF THE DIFFUSIVE ISING MODEL ANALYSIS

To model the transport and interaction of particles interacting at a finite range a and with a finite average density ρ_0/a, In the main text we considered a microscopic lattice model in which particles hop between sites at rate D/a^2 and change type $s = \pm$ to align with the locally more common species with a rate r dependent on the number of particles of each type in the vicinity. [1–3].

In the main text we considered $r = \gamma \exp\left(-s(\beta m_i + h_i)\right)$, where $m_i = n_i^+ - n_i^-$ is the population difference in $+$ and $-$ particles at site i, and h_i is the local external source field biasing towards a specific species. In accordance with the statistical mechanics literature, in the supplement we will call the particles 'spins' and will call m the *magnetization*, while $\rho = n_+ + n_-$ is the (unitless) number density, or simply density.

We use a coarse-graining method developed in [4–6] and applied in [3] for the more complex case of two non-reciprocally interacting species. Calculations are detailed in Section VI for the case of finite-ranged interactions.

This method is exact in the limit of short-interaction range $a \to 0$, where the dynamics are dominated by diffusion and the master equation solved by a Poissonian distributions. With finite a, we can use this Poissonian ansatz to to compute higher-order correlations and derive a closed fluctuating hydrodynamic equation. To understand the limits of validity of this procedure, we use renormalization group theory (RG) to derive the effective finite-a response and compare it to our numerical solutions. The RG analysis also provides an analytical criterion of validity for the fluctuating hydrodynamics: the perturbative corrections are valid as long as the coupling constant $g = \rho_0 \left(\hat{\gamma} a^2/D\right)$ of the RG is small, meaning that $g \ll 1$ (Details and derivation in Section VII).

To this order and including the the full dynamics are given by

$$\partial_t \delta\rho = D\partial_{xx}^2 \delta\rho + \sqrt{a}\partial_x \eta_1 \tag{S1a}$$

$$\partial_t m = D\partial_{xx}^2 m - g(\delta\rho, m + h(x)) + \sqrt{a}\partial_x \eta_2 + \sqrt{a\bar{g}(\delta\rho, m + h(x))}\eta_3 \tag{S1b}$$

with the functions

$$g(\delta\rho, m) = 2\gamma e^{-\beta + (\cosh\beta - 1)(\rho_0 + \delta\rho)}\left(\cosh\left(\sinh(\beta)m\right)m - \sinh\left(\sinh(\beta)m\right)(\rho_0 + \delta\rho)\right) \tag{S2a}$$

$$\bar{g}(\delta\rho, m) = 2\gamma e^{-\beta + (\cosh\beta - 1)(\rho_0 + \delta\rho)} \tag{S2b}$$

The noises η_n are correlated by the matrix $\langle \eta_n(x, t)\eta_{n'}(x', t')\rangle = M_{n,n'}\delta(x - x')\delta(t - t')$, with

$$M_{nn'} = \begin{pmatrix} 2D(\rho_0 + \delta\rho) & 2Dm & 0 \\ 2Dm & 2D(\rho_0 + \delta\rho) & 0 \\ 0 & 0 & 2S_f \end{pmatrix} \tag{S3}$$

with $S_f = [\rho\cosh\left(m\sinh\beta\right) - m\sinh m \sinh\beta]$.

In the vicinity of the phase transition for small enough a, such that $\rho_0 \gg |\delta\rho|$, we can reduce this model to the cubic order model with additive noise presented in the Methods. We use the cubic reduction for the dynamical RG analysis in Sec. VII.

To show that the qualitative conclusions of this model are independent of the precise form of the local interactions, in Section VI we also consider the situation where particles interact with others on neighboring sites a, which leads to a transition rate $r = \gamma \exp\left(-\beta \sum_{\langle i,j\rangle} m_{i,j}s\right)$, where $\sum_{\langle i,j\rangle}$ denotes the sum over nearest-neighbor spins (not including the site i). In the limit $\rho_0 \gamma a^2/D \ll 1$, we find that the resulting macroscopic (hydrodynamic) model is unchanged from the standard same-site DIM, up to some small modifications in the relationship between microscopic parameters and hydrodynamic coefficients, allowing us to focus on the case of same-site interactions in the main text.

II. INFORMATION THEORY FOR SELF-ORGANIZATION

In this section, we define and compare measures of the robustness and self-organization for systems with externally broken symmetry [7, 8], and analyze the positional information in spatially-extended systems with discrete-valued fields. We provide some general analyzes before analyzing specific Ising-type models and establishing that discrete valued systems with exponentially-decaying correlations are subject to a fundamental bound on their positional information

A. Information-theoretic measures of robust self-organization

We consider a similar formalism as in Ref. [8]: We consider the state of a self-organized system of N cells, or more generally components, to be described by the state vector $\mathbf{z} = (z_1, ..., z_N)$ where $z_i \in \{1, ..., Z\}$ is the state of cell i chosen among Z possible states. We consider that the cells are fixed in space: thus the index i reflects spatial position. Given a stochastic patterning process, we obtain or estimate from experiments the probability of observing a given pattern of cell states $P(\mathbf{z})$.

As a first way to assess the reproducibility of the patterns, we can consider the entropy of this distribution

$$S_{\text{rep}} = \frac{1}{N} S[P(\mathbf{z})] = -\frac{1}{N} \sum_{\mathbf{z}} P(\mathbf{z}) \log_2 P(\mathbf{z}) \tag{S4}$$

which following Ref. [8] we term reproducibility entropy. S_{rep} ranges between 0, achieved for a perfectly reproducible system where every replicate is identical, and $\log_2 Z$ for a system where every one of the Z^N possible states is equiprobable.

S_{rep} alone cannot be a perfect measure of robust patterning: for instance, a perfectly uniform system has no spatially-varying pattern but is perfectly reproducible.

To account for these spatial correlations the positional information (PI) is defined as the mutual information between position and state, which can be understood as the information one gains on the cell state by knowing the position of the cell [7]. To compute the PI, we need to assign a probability of picking the cell at position i, which we take as uniform $P(i) = 1/N$.

$$\text{PI} = \sum_{i=1}^{N} \sum_{z=1}^{Z} P(z,i) \log_2 \left(\frac{P(z,i)}{P_z(z)P(i)} \right) = \frac{1}{N} \sum_{i=1}^{N} \sum_{z=1}^{Z} P_i(z_i) \log_2 \left(\frac{P_i(z_i)}{P_z(z)} \right) \tag{S5}$$

with $P(z,i) = P_i(z_i)P(i)$ the joint distribution of states and positions and

$$P_z(z) = \frac{1}{N} \sum_{i=1}^{N} \sum_{z_i=1}^{Z} P(\mathbf{z}) \delta_{z_i,z} \tag{S6}$$

is the pooled distribution of cell states, giving the probability of finding a cell in state z across all positions.

To quantify the diversity of the cell population, Ref. [8] defines the patterning entropy

$$S_{\text{pat}} = -\sum_{z=1}^{Z} P_z(z) \log_2 P_z(z). \tag{S7}$$

If all cells have identical states, then $S_{\text{pat}} = 0$ while if all states are identical $S_{\text{pat}} = \log_2 Z$. For all distributions, $0 \le S_{\text{pat}} \le \log_2 Z$. We can then rewrite the PI as

$$\text{PI} = S_{\text{pat}} - \frac{1}{N} \sum_{i=1}^{N} S[p_i(z_i)] \equiv S_{\text{pat}} - S_{\text{cf}} \tag{S8}$$

where we have defined the correlation-free entropy $S_{\text{cf}} = \frac{1}{N} \sum_{i=1}^{N} S[p_i(z_i)]$. S_{cf} can be understood as the (normalized) entropy of the product of the marginals, ignoring the correlations between states at different sites.

In the main text, we consider symmetric systems for which both states are equally likely across replicates and this patterning entropy is always $S_{\text{pat}} = 1$ bit. More generally, S_{pat} is maximized in a symmetric system where, averaged over all positions, particles are equally likely to be in every state. In such symmetric systems, we have

$$\text{PI} = \log_2 Z - \frac{1}{N} \sum_{i} S[p_i(z_i)] \tag{S9}$$

Additionally, Ref. [8] defines the correlational information $\text{CI} = S_{\text{cf}} - S_{\text{rep}}$ to measure the reduction in entropy due to the information contained in the spatial correlations. We show these quantities in Fig. S1a-b.

An alternative way to measure the robustness of the patterns comes from considering the defined deterministic pattern of the system. We can then define the robustness of the pattern distribution by defining probabilistic distances between the observed distributions and the target distribution $Q(\mathbf{z})$ corresponding to the deterministic pattern. Here we explore two such measures, the Wasserstein and Jensen-Shannon distances.
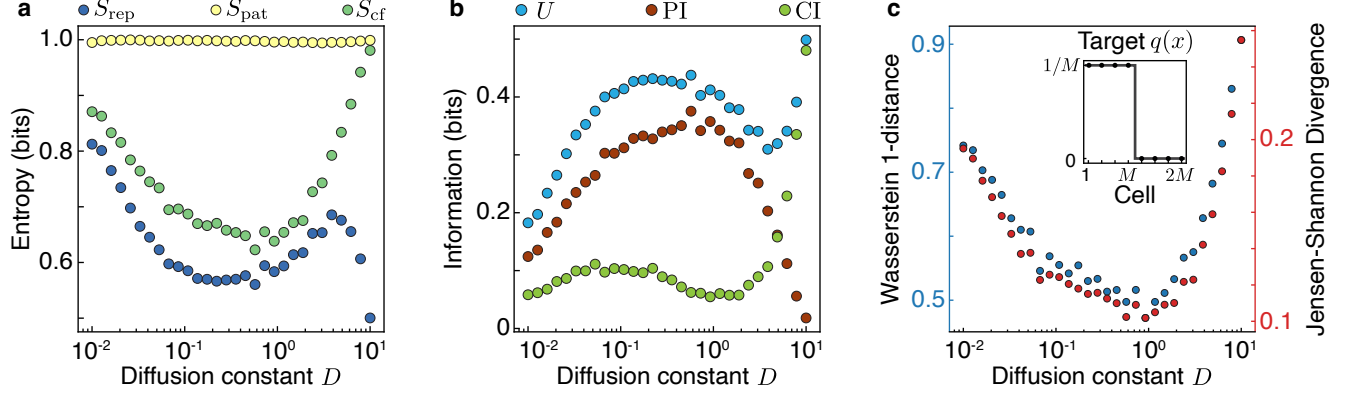
FIG. S1. Information-theoretic measures of self-organization. *(a)* Reproducibility, Patterning and Correlation-free entropies for the DIM system. *(b)* Utility, Positional Information and Correlation Information for the DIM system. *(c)* Wasserstein 1-distance and Jensen-Shannon Divergence for the observed probability distributions, with target distribution $q(x)$ plotted in inset. Simulation parameters: $N = 2M = 8$, $L = 4$, $a = L/48$, $\beta = 2\beta_c$, $h = 3\beta$.

The Wasserstein-1 metric between the distributions $p(x)$ and $q(y)$ is defined in terms of a transport plan $\gamma(x, y)$ associated with the cost function $c(x, y) = |d(x - y)|$, where the difference $d(x - y)$ accounts for the periodicity of the domain. The metric is defined as the solution to a constrained optimization problem [9]

$$W_1(p, q) = \min_{\gamma} \int \gamma(x, y) c(x, y) \, \mathrm{d}x\mathrm{d}y \qquad (S10)$$

with $\int \gamma(x, y)\mathrm{d}x = p(x)$ and $\int \gamma(x, y)\mathrm{d}y = q(x)$. Computing this distance requires solving a linear program to obtain the optimal transport plan $\gamma^*(x, y)$.

The (squared) Jensen-Shannon distance between distributions p and q is defined in terms of the symmetrized Kullback-Leibler divergence between p, q and their mixture distribution $m = (p + q)/2$ [10]

$$\mathrm{JSD}(p||q) = \frac{1}{2} D(p||m) + \frac{1}{2} D(q||m). \qquad (S11)$$

For both of these approaches, we use as $p(x)$ the normalized marginal probability $p_i/(\sum_i p_i)$ and define the target q as the step pattern associated with the deterministic bipartite solution (Fig. S1c, inset).

The positional information has the advantage over these two measures that it is agnostic to a target pattern. Since we find qualitative agreement between PI and both the JSD and W_1 distances (Fig. S1b-c), in the main text we report only the positional information.

B. Positional information in the 1D Ising model

We consider an Ising model with a site varying magnetic field h_i, such that the Hamiltonian is given by

$$H(\{s_i\}_{i=1,...,N}) = -\sum_{i=1}^{N} J s_i s_{i+1} + h_i s_i \qquad (S12)$$

with periodic boundary conditions such that $s_{N+1} = s_N$. The 1D Ising model can be solved exactly using transfer matrices [11], with the transfer matrix at the i-th bond given by

$$T_i = \begin{pmatrix} e^{J+h_i} & e^{-J} \\ e^{-J} & e^{J-h_i} \end{pmatrix}. \qquad (S13)$$

The partition function is given by

$$\mathcal{Z} = \mathrm{tr} \prod_{i=1}^{N} T_i \qquad (S14)$$

from which the probability of a particular spin configuration $\{s_i\}$ is given by

$$p(\{s_i\}) = \frac{e^{-H(\{s_i\})}}{\mathcal{Z}}. \tag{S15}$$

From the probability distribution, some transfer matrix manipulations allow to write the marginal probability of finding a positive spin at site i. and its mean value are given by

$$p_i \equiv p_i(s_i = +) = \frac{1}{\mathcal{Z}} \text{tr}\left[\left(\prod_{j=1}^{i-1} T_j\right) P \left(\prod_{j=i}^{N} T_j\right)\right], \quad \langle s_i \rangle = \frac{1}{\mathcal{Z}} \text{tr}\left[\left(\prod_{j=1}^{i-1} T_j\right) \sigma_Z \left(\prod_{j=i}^{N} T_j\right)\right] \tag{S16}$$

with the matrices

$$P = \begin{pmatrix} 1 & 0 \\ 0 & 0 \end{pmatrix}, \qquad \sigma_z = \begin{pmatrix} 1 & 0 \\ 0 & -1 \end{pmatrix} \tag{S17}$$

These marginal probabilities can be numerically evaluated, allowing us to compute the positional information in the Ising model for a given set of h_i and J. To do so, we define the pooled probability of finding a spin in the $+$ state

$$P_+ = \frac{1}{N} \sum_i p_+(i) \tag{S18}$$

which allows us to compute the positional information exactly as

$$\text{PI} = \frac{1}{N} \sum_i p_i \log\left(\frac{p_i}{P_+}\right) + (1 - p_i) \log\left(\frac{1 - p_i}{1 - P_+}\right). \tag{S19}$$

We show results of the numerical evaluation of the marginals in Fig. E2. We find that as the effective temperature T defined by $J = \tilde{J}/T$, $h = \tilde{h}/T$ is reduced, the PI saturates to a value Π_N dependent on the number of sites N. We calculate the value of Π_N in the Methods, which is in agreement with numerical results to high accuracy.

C. Accounting for conserved noise

In the theorem presented in the main text, correlations are assumed to decay exponentially, which generically happen with local interactions and no coupling to conserved fields. In the diffusive Ising model, the presence of conserved noise leads to a non-exponential correlation function. The measured marginal probabilities p_i thus do not exactly satisfy the convexity requirements for the bound to hold. Unfortunately, the correlation functions in the presence of conserved noise are singular, limiting our analytical reach. To model these non-exponential marginal probabilities, we thus turn to the limiting case of diffusive dynamics for which after a finite time $\sim 1/\gamma$, the particles released at source points lose memory of their past. This leads to marginals of the form

$$p_\sigma(x) = \frac{1}{2}\left(1 + e^{-\frac{x^2}{2\sigma^2}} - e^{-\frac{(1-x)^2}{2\sigma^2}}\right) \tag{S20}$$

where $0 \le p_\sigma(x) \le 1$ and there is no normalization requirement on p_σ. To optimize the positional information, we seek σ such that $\partial_x p_\sigma(x = 1/2)$ is largest in magnitude by solving $\partial_\sigma \partial_x p_\sigma = 0$. We find an optimum for $\sigma = 1/\sqrt{8} = 1/(2\sqrt{2})$, leading to a different system-size dependent bound on PI for diffusive dynamics (Fig. S2a,c).

D. Extending to multiple species: Potts model and bound extension

We consider the Potts model with Z states on a periodic 1D lattice, which has a Hamiltonian

$$H(\{s_i\}_{i=1,...,N}) = -J \sum_{i=1}^{N} \delta_{s_i, s_{i+1}} - \sum_{q=1}^{Z} \sum_{i=1}^{N} h_{q,i} \delta_{s_i, q}. \tag{S21}$$

where again we use the convention $s_{N+1} = s_1$. The $Z \times Z$ transfer matrix at position i is then given by its components

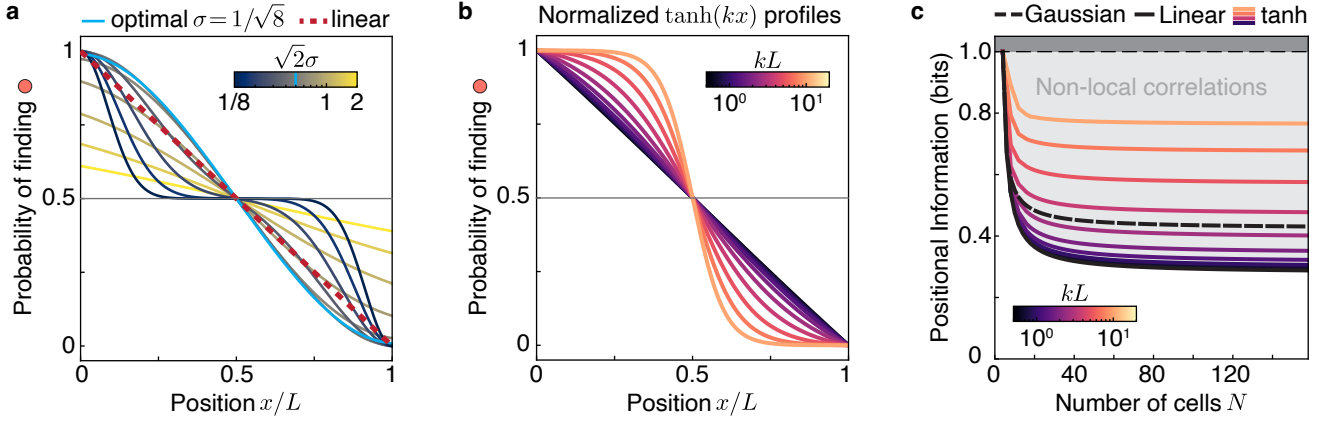$$T_i^{k,q} = e^{J\delta_{kq}} e^{h_{k,i}/2 + h_{q,i}/2} \tag{S22}$$

FIG. S2. Positional information and convexity of the marginals. **a.** Marginal probabilities for a Gaussian profile described by Eq. (S20). There is an optimal profile for $\sigma = 1/\sqrt{8} = 1/(2\sqrt{2})$. **b.** Hyperbolic tangent profiles $\tanh(kx)$ linearly scaled such that $p(0) = 1$ and $p(1) = 0$. **c.** Corresponding bound on the positional information for the optimal Gaussian profile (rescaled as done for hyperbolic profiles), the sawtooth linear profile for exponentially-correlated systems and for the hyperbolic profile with varying k.

where $k, q \in \{1, \ldots, Z\}$. The partition function is again $\mathcal{Z} = \mathrm{tr}\left(\prod_{i=1}^{N} T_i\right)$, allowing us to obtain the steady-state probability distribution. Defining the projection matrix on the q-th species $[\mathcal{P}_q]_{ij} = \delta_{iq}\delta_{jq}$, we can again obtain the marginal probability for the q-th species at site i by

$$p_{q,i} \equiv p_i(s_i = q) = \frac{1}{\mathcal{Z}}\mathrm{tr}\left[\left(\prod_{j=1}^{i-1} T_j\right)\mathcal{P}_q\left(\prod_{j=i}^{N} T_j\right)\right]. \tag{S23}$$

We can then compute PI from the probabilities $p_{q,i}$ as

$$\mathrm{PI} = \frac{1}{N}\sum_{i=1}^{N}\sum_{q=1}^{Z} p_i^q \log_2\left(\frac{p_i^q}{P_q}\right) \tag{S24}$$

where P_q is the expected fraction of cells in state q. We compute these probabilities for symmetric systems with $h_{q,i} = h\delta_{i,qM}$, with h a prescribed intensity. In Fig S3b-d we show the steady-state probabilities and the PI as a function of J and h. In particular, we again find that for a given system size $N = ZM$, the PI is bounded below its maximal value of $\log_2 Z$.

Examining the marginals p_i^q, we find again an optimal sawtooth profile (Fig. S3c). We now prove the optimality of the sawtooth profile for the systems with $Z > 2$ and compute the corresponding optimal value of the PI by an extension of the previous argument.

If there are $Z > 2$ possible fates (outcomes) for each cell, then the maximum PI is achieved for a symmetric system with $N = ZM$ sites, with sources of different species at $i = qM$, $q = 1, \ldots, Z$. By symmetry, we focus on the source at $i = 1$ and the interval $i \in \{1, \ldots, M\}$. Then to be as deterministic as possible and satisfy the exponential correlation decay, each source leads to an exponentially-decaying probability profile p_i^1 of finding species 1, while p_i^2 correspondingly rises as $p_i^2 = 1 - p_i^1$ and all other $p_i^q = 0$ for $2 < q \leq Z$. We are thus reduced to the $Z = 2$ case on this interval $i \in \{1, \ldots, M\}$, which leads to a contribution to the PI bounded by the sawtooth profile

$$\frac{1}{N}\sum_{i}^{M}\left[p_i^1 \log_2 p_i^1 + (1 - p_i^1)\log_2(1 - p_i^1)\right] \leq \frac{2}{N}\sum_{i=0}^{M-1}\frac{i}{M}\log_2\left(\frac{i}{M}\right) \tag{S25}$$

By symmetry, all intervals $i \in \{(q-1)M + 1, qM\}$ with $q \in \{1, \ldots, Z\}$ add an identical contribution, which sum up to

$$\mathrm{PI} \leq \log_2 Z + \frac{2Z}{N}\sum_{i=1}^{M}\frac{i-1}{M}\log_2\left(\frac{i-1}{M}\right) \tag{S26}$$

$$= \log_2 Z + \frac{2}{M}\sum_{i=1}^{M}\frac{i-1}{M}\log_2\left(\frac{i-1}{M}\right) = \Pi_N^Z \tag{S27}$$
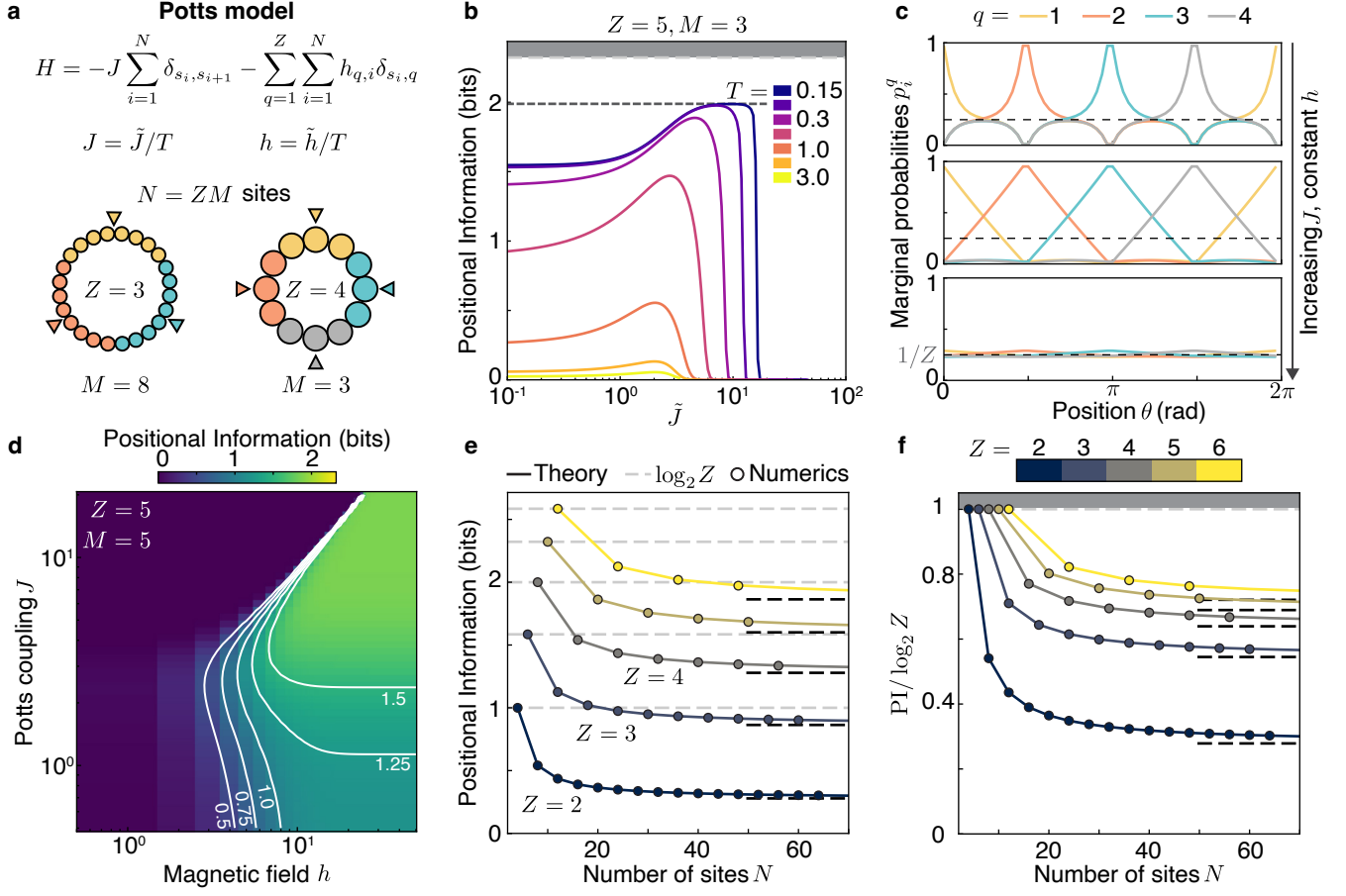
FIG. S3. Positional information saturation in the Potts model. (a) The Potts model with symmetric sources (triangles) as described in the main text. (b) Similarly as the Ising model, the Potts model shows a saturation of the PI with decreasing temperature at constant temperature-scaled magnetic field $\tilde{h}$. Greyed region indicates maximal PI for $Z = 5$, while dashed line indicates the theoretical bound of Eq. S27 for local coupling. (c) Marginal probabilities again display a sawtooth profile at optimal J. Here, $Z = 4, M = 16, h = 6, J \in \{2, 5, 8\}$ with J increasing from top to bottom rows. (d) The PI as a function of J, h saturates around 1.6 bits for $Z = 5, M = 5$. (e-f) The maximal PI from numerics is in excellent agreement with the theoretical bound. Light dash lines indicate absolute maximum $\log_2 Z$, while black dash lines indicate asymptotic value $\Pi_\infty^Z = \log_2 Z - 1/(2 \ln 2)$. (f) The maximum PI as Z increases becomes closer to $\log_2 Z$, as the limit imposed by the sawtooth profile becomes relatively less important as $\sim 1/\ln Z$.

Again, recognizing a Riemann sum, we find the asymptotic bound

$$\Pi_N^Z \to \Pi_\infty^Z = \log_2 Z - \frac{1}{2 \ln 2}. \tag{S28}$$

with $\Pi_N^Z \geq \Pi_\infty^Z$. The predicted curves Π_N^Z match accurately our numerically determined values, and the bound becomes relatively less constraining as Z increases (Fig. S3ef).

III. INTERPRETATION IN TERMS OF DOMAIN WALL DYNAMICS

We show in Sec. II, Fig. E2 that we can justify the existence of an optimal diffusion constant as a consequence of Ising physics. Intuitively, information from the boundaries can only penetrate a distance of the order of the correlation length, and systems that have too large correlations lengths are homogeneous. Here, we present an alternative view of this result as a consequence of domain wall dynamics, which helps us generalize our results to other front-sustaining systems [12]. In particular, while we consider in the main text $\mathbb{Z}_2$-symmetric systems, in experimentally relevant settings there might be imperfections that break the symmetry in rates between $\oplus$ and $\ominus$ states. After presenting

general results on the dynamics of asymmetric fronts, we compute the front diffusion constant in asymmetric systems and derive the confinement force acting on the front in the presence of boundaries. Finally, we derive a quantitative criterion under which we can safely ignore asymmetries in rates between $\oplus$ and $\ominus$ states by comparing the velocity due to the relative stability of states to the noise amplitude.

A. Domain wall dynamics in bistable systems

We will consider simplified cubic order dynamics and neglect density fluctuations $\rho = \rho_0$, but extend to the general cubic 1D reaction-diffusion system [13–15]

$$\partial_t m = D\partial_x^2 m + f(m) = D\partial_x^2 m + r(m - m^*)(1 - m^2) \tag{S29}$$

where $f(m)$ denotes the reaction term. We note that by using the transformation $m \leftarrow 2\rho - 1$, $m^* \leftarrow 2\rho^* - 1$, $r \leftarrow 8r$ we recover the model studied in Ref. [14, 15]. To derive the effects of noise and external sources on front dynamics, we here present and extend relevant results of the theory of wave propagation in metastable states in infinite domains [14, 16–18]. If $m^* = 0$, we recover the symmetric case, which admits stable domain-wall solutions connecting stable domains at $m = \pm 1$ with characteristic width $\ell = \sqrt{D/r}$. If $m^* \neq 0$, the two stable solutions at $m_- = -1$ to $m_+ = 1$ are no longer equivalent, and the domain walls of width ℓ_f can have a non-zero front velocity c. To find c, we consider solutions of the form $m(\xi) = m(x - ct)$ which must satisfy

$$Dm'' + cm' + f(m) = 0. \tag{S30}$$

For fronts connecting the stable states $m_- = -1$ to $m_+ = 1$, we can multiply Eq. (S30) by $m'(\xi)$ and integrate from $\xi = -\infty$ to $+\infty$. Multiplying by m' and integrating over the domain, we thus find the relationship

$$c = -\frac{\int_{m_-}^{m_+} f(m)\mathrm{d}m}{\int_{-\infty}^{+\infty} (m')^2 \mathrm{d}\xi} \tag{S31}$$

where we assume $m' \to 0$ at infinities. The front profile is given by

$$m(\xi) = -\tanh\left(\frac{x}{\sqrt{2}\ell}\right) = \frac{e^{-\frac{x}{\sqrt{2}\ell}} - e^{\frac{x}{\sqrt{2}\ell}}}{e^{-\frac{x}{\sqrt{2}\ell}} + e^{\frac{x}{\sqrt{2}\ell}}} \tag{S32}$$

where $\ell = \sqrt{D/r}$. By changing variables and using that $m' = (1 - m^2)/(\sqrt{2}\ell)$, the denominator above can be computed as

$$\int_{-\infty}^{+\infty} (m')^2 \mathrm{d}\xi = \int_{-1}^{1} \frac{1}{\sqrt{2}\ell}(1 - m^2)\mathrm{d}m = \frac{2\sqrt{2}}{3\ell}. \tag{S33}$$

For the cubic reaction term considered here, the numerator is equal to

$$-\int_{m_-}^{m_+} f(m)\mathrm{d}m = \frac{4r}{3}m^* \tag{S34}$$

indicating that c is proportional to m^* as

$$c = \sqrt{2rD}m^*. \tag{S35}$$

If $m^* > 0$, the wave travels forward ($c > 0$), while $m^* < 0$ leads to backward propagating waves ($c < 0$). The direction of travel can be understood by interpreting the numerator as a difference in potential $\int_{m_-}^{m_+} f(m)\mathrm{d}m = V(m_+) - V(m_-)$, with $f(m) = -\mathrm{d}V/\mathrm{d}m$: the more stable steady state (deeper potential) invades the less stable state (shallower potential) [12, 14].

The motility of the domain walls can destroy bistable patterns, by sending the fronts all the way to the edges of the domain. However, as we we detail below, in the presence of noise the front position fluctuates about its average position $x = ct$ with a diffusion constant D_f scaling with $\sqrt{D}$ [15, 17].

B. Front diffusivity

We now present the calculation of the front diffusivity D_f by perturbative methods, which will lay out the strategy we use later for the derivation of the confinement force [15–17, 19]. Counterintuitively, the front diffusivity D_f scales as $\sqrt{D}$. This can be understood as $D_f \sim D/N_{\rm int}$, where $N_{\rm int} \sim \sqrt{D}$ is the number of particles within interaction range between reactions. In the presence of non-conserved noise, the dynamics of the system are given by

$$\partial_t m = D\partial_x^2 m + f(m) + \eta(x,t) \tag{S36}$$

where $\langle \eta(t_1,x_1)\eta(t_2,x_2)\rangle = \Gamma(\phi(t_1,x_1))^2\delta(t_1-t_2)\delta(x_1-x_2)$. For conciseness, we refer to Ref. [15] for the derivation in the presence of conserved noise. In the co-moving frame $\xi = x - ct$, the profile now satisfies

$$Dm'' + cm' + f(m) + \eta(t,\xi) = 0. \tag{S37}$$

Note that in the co-moving frame the noise is still explicitly time-dependent and satisfies $\langle \eta(t_1,\xi_1)\eta(t_2,\xi_2)\rangle = \Gamma(\phi(\xi_1))^2\delta(t_1-t_2)\delta(\xi_1-\xi_2)$. The effect of noise is twofold: noise shifts the position of the front $\xi = x - ct$ by a time-dependent term $\mu(t)$, and changes the shape of the front away from its unperturbed shape ρ. To solve Eq. (S37) perturbatively, we thus write the solution in terms of the shifted unperturbed solution ρ and the first-order perturbation of the front profile ϕ (Fig. S4a)

$$m(t,\xi) = \rho(\xi - \mu(t)) + \phi(t, \xi - \mu(t)). \tag{S38}$$

Note, again, that $\phi(t,\xi)$ is explicitly time-dependent. Introducing the decomposition of Eq. (S38) into Eq. (S37), we have

$$\partial_t \phi - \mathcal{L}\phi = \rho'\dot{\mu} + \eta(t,\xi) \tag{S39}$$

where $\dot{\mu} = \mathrm{d}\mu/\mathrm{d}t$ and we introduced the differential operator $\mathcal{L} = \frac{\mathrm{d}^2}{\mathrm{d}\xi^2} + c\frac{\mathrm{d}}{\mathrm{d}\xi} + f'(m)$. Reflecting the translational invariance of the dynamics, we have $\mathcal{L}\rho' = 0$. The adjoint $\mathcal{L}^\dagger = \frac{\mathrm{d}^2}{\mathrm{d}\xi^2} - c\frac{\mathrm{d}}{\mathrm{d}\xi} + f'(m)$ thus has a zero eigenvector $\mathcal{L}^\dagger\psi = 0$, with $\psi = e^{c\xi}\rho'(\xi)$. To exclude translations of the profiles from being included in ϕ, as they should only be incorporated through $\mu(t)$, we require the solvability condition (which implicitly defines $\mu(t)$)

$$\int_{-\infty}^{+\infty} \mathrm{d}\xi\, \psi(\xi)\phi(\xi) = 0. \tag{S40}$$

Multiplying Eq. (S39) by ψ and integrating over ξ, we find by using the solvability condition

$$\dot{\mu}(t) = -\frac{\int_{-\infty}^{+\infty} \mathrm{d}\xi\, \psi(\xi)\eta(t,\xi)}{\int_{-\infty}^{+\infty} \mathrm{d}\xi\, \psi(\xi)\rho'(\xi)}. \tag{S41}$$

Since $\langle \eta(t,\xi)\rangle = 0$, we remark that $\langle \dot{\mu}(t)\rangle = 0$. Integrating $\dot{\mu}(t)$ in time, we now have an expression for the shift in position $\mu(t)$ as a function of the noise dynamics

$$\mu(t) = X(t) - ct = -\int_0^t \frac{\int_{-\infty}^{+\infty} \mathrm{d}\xi\, \psi(\xi)\eta(t',\xi)}{\int_{-\infty}^{+\infty} \mathrm{d}\xi\, \psi(\xi)\rho'(\xi)}\mathrm{d}t'. \tag{S42}$$

The diffusivity can now be obtained by computing the mean squared displacement at a time t

$$D_f^{\rm nc} = \frac{\langle X_f^2(t)\rangle - \langle X_f\rangle^2}{2t} = \frac{\langle \mu^2(t)\rangle}{2t}. \tag{S43}$$

Inserting the expression of $\mu(t)$ in Eq. (S42) to compute the variance, we have

$$D_f^{\rm nc} = \frac{1}{2t}\left\langle \int_0^t \frac{\int_{-\infty}^{+\infty} \mathrm{d}\xi\, \psi(\xi)\eta(t_1,\xi)}{\int_{-\infty}^{+\infty} \mathrm{d}\xi\, \psi(\xi)\rho'(\xi)}\mathrm{d}t_1 \int_0^t \frac{\int_{-\infty}^{+\infty} \mathrm{d}\xi\, \psi(\xi)\eta(t_2,\xi)}{\int_{-\infty}^{+\infty} \mathrm{d}\xi\, \psi(\xi)\rho'(\xi)}\mathrm{d}t_2 \right\rangle \tag{S44}$$

$$= \frac{1}{2t}\frac{\int_0^t \mathrm{d}t_1 \int_0^t \mathrm{d}t_2 \int_{-\infty}^{+\infty} \mathrm{d}\xi_1 \int_{-\infty}^{+\infty} \mathrm{d}\xi_2\, \psi(\xi_1)\psi(\xi_2)\langle \eta(t_1,\xi_1)\eta(t_2,\xi_2)\rangle}{\left(\int_{-\infty}^{+\infty} \mathrm{d}\xi\, \psi(\xi)\rho'(\xi)\right)^2} \tag{S45}$$

$$= \frac{1}{2}\frac{\int_{-\infty}^{+\infty} \mathrm{d}\xi\, \psi(\xi)^2\Gamma(\phi(\xi))^2}{\left(\int_{-\infty}^{+\infty} \mathrm{d}\xi\, \psi(\xi)\rho'(\xi)\right)^2} \tag{S46}$$
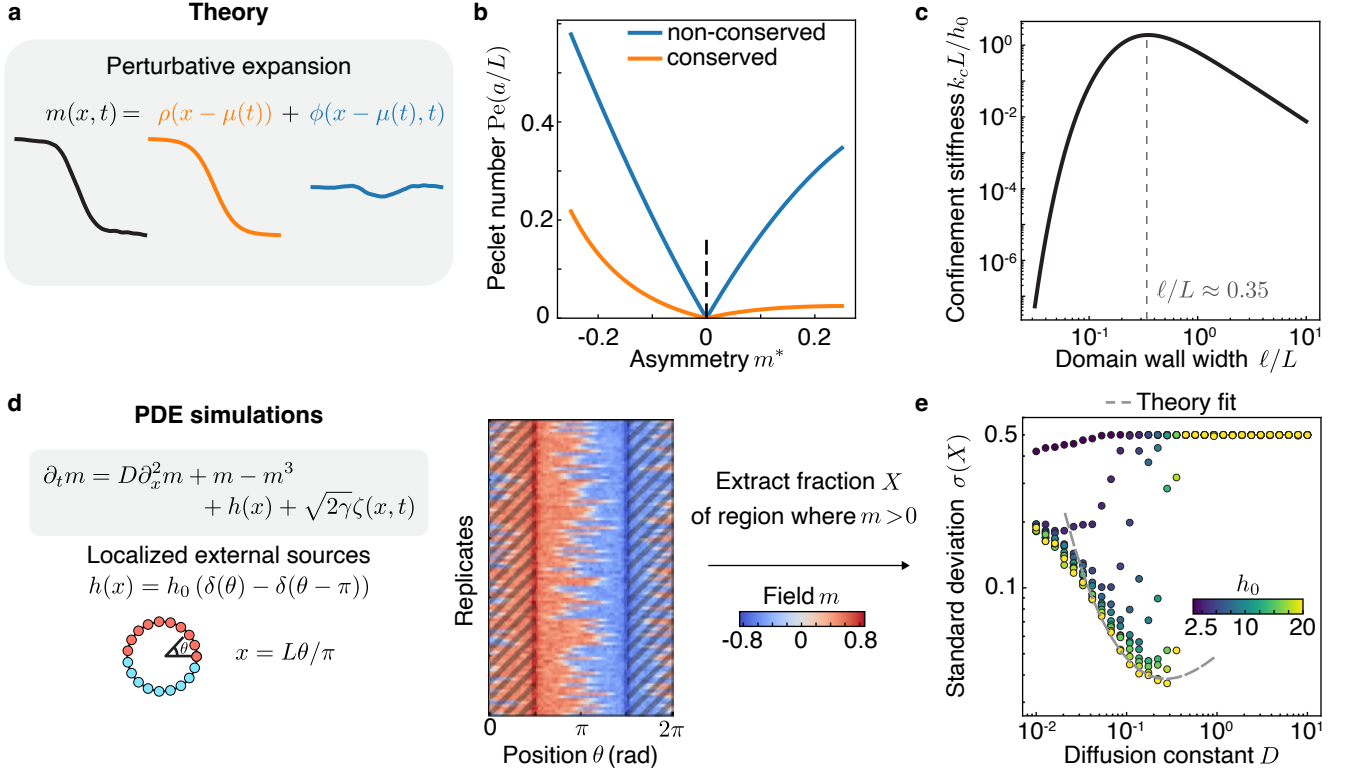
FIG. S4. Results from nonlinear front propagation theory, and comparison to simulations. **a.** Perturbative expansion used to compute the front diffusivity D_f and the confinement stiffness k_c. **b.** Péclet number (rescaled by a/L) as a function of the asymmetry parameter m^*, for non-conserved and conserved noise considered separately. Here $\rho_0 = \chi = 1$. **c.** Calculated confinement stiffness at first order, showing a rapid exponential decay as $\ell/L \to 0$. **d.** We simulate the cubic polynomial reaction-diffusion system, and measure the fraction of positive region for $\theta \in [\pi/2, 3\pi/2]$ (excluding the hashed region). **e.** We find that while the confinement stiffness computed perturbatively gives the correct trend, other effects effectively stiffen the confinement. Results computed using 500 replicates, $\gamma = 0.1$.

For additive noise $\Gamma^2 = a\rho_0\hat\gamma$ as we find in the DIM, we then have

$$D_f^{\mathrm{nc}} = \frac{3a\rho_0\hat\gamma}{4\pi}\sqrt{\frac{D}{r}}\frac{(4(m^*)^2 - 1)}{m^*(1+m^*)(m^* - 1)^2}\tan\pi m^* = \frac{3a\rho_0}{4\chi}\sqrt{rD} + O(m^*) \tag{S47}$$

where we define $\chi = r/\hat\gamma$.

In the presence of conserved noise $\partial_x(\Gamma(\phi)\eta)$, one finds that D_f is given by [15]

$$D_f^{\mathrm{c}} = \frac{a\rho_0}{5\pi}\sqrt{rD}\frac{(3 + m^*)(4(m^*)^2 - 1)(1 + 2m^*)(9 + 7m^*)}{m^*(1 + m)(1 - m)^2}\tan\pi m^* = \frac{27a\rho_0}{5}\sqrt{rD} + O(m^*) \tag{S48}$$

when $\Gamma^2 = a\rho_0 D$ as in the (simplified) Diffusive Ising model. If both conserved and non-conserved noises are present and uncorrelated, then those contributions are additive

$$D_f = D_f^{\mathrm{nc}} + D_f^{\mathrm{c}}. \tag{S49}$$

and we see that D_f overall scales with $a\rho_0\sqrt{rD}$.

To compute the relative importance of the state asymmetry compared to the diffusion of the front, we can compute the Péclet number $\mathrm{Pe} = cL/D_f$ where L is the size of the domain. In both conserved and non-conserved cases, Pe scales as $L/(\rho_0 a)$ with a m^* dependent scaling factor, with an additional scaling $\mathrm{Pe} \propto \chi$ in the non-conserved case: as the system gets closer to criticality ($\chi = 0$), the effect of the noise is amplified (Fig. S4b).

C.   Front confinement by external sources

Now we consider an external symmetry-breaking field $h(x) = h_0 [\delta(x - L/2) - \delta(x + L/2)]$, and we restrict ourselves for simplicity to the case $c = 0$. Now that translational symmetry is broken, we stay in (x, t) coordinates. The stationary front solution now satisfies

$$D\rho''(x) + f(\rho(x)) = -h(x) \tag{S50}$$

where we emphasize the functional dependence on the position. We now look for the restoring force on the front when the front is perturbed and shifted away from its equilibrium position. Decomposing again $m(x, t) = \rho(x - \mu(t)) + \phi(x - \mu(t), t)$, at first order

$$\partial_t \phi(x - \mu(t)) - \mathcal{L}\phi(x - \mu(t)) = D\rho''(x - \mu(t)) + f(\rho(x - \mu(t)) + h(x) + \rho'(x - \mu(t))\dot{\mu}(t). \tag{S51}$$

By introducing $h(x - \mu(t))$ in Eq. S51, we can use Eq. (S50) and the operator $\mathcal{L}$ defined previously to write

$$\partial_t \phi - \mathcal{L}\phi = \rho'\dot{\mu} + (h(x) - h(x - \mu)) \approx \rho'\dot{\mu} + h'(x)\mu \tag{S52}$$

where we now suppress the position dependence except on the source field and use that $\mu(t)$ is assumed small. Since $c = 0$, the operator $\mathcal{L} = \mathcal{L}^\dagger$ is now self-adjoint and has a zero-mode given by ρ_0', where $\rho_0(x) = -\tanh(x/\sqrt{2}\ell)$ is the steady profile in the absence of sources. After projecting onto this zero mode by multiplying Eq. S52 by $\rho_0'(x)$ and integrating over x and using the solvability condition $\int \mathrm{d}x \rho_0(x)\phi(x - \mu(t), t) = 0$, we find the first-order differential equation for $\mu(t)$

$$\dot{\mu}(t) = -\frac{\int_{-\infty}^{+\infty} \mathrm{d}x\, \rho_0' h'}{\int_{-\infty}^{+\infty} \mathrm{d}x\, \rho_0'\rho'}\mu(t) \equiv -k_c\mu(t). \tag{S53}$$

The solvability condition effectively defines $\mu(t)$ so that ϕ has no overlap with ρ_0. If we assume that the source field strength h_0 is small enough so that the solution of Eq. S50 is close to the solution of the homogeneous problem, we can approximate $\rho \approx \rho_0$. We then find a confinement stiffness

$$k_c = \frac{\int_{-\infty}^{+\infty} \mathrm{d}x\, \rho_0' h'}{\int_{-\infty}^{+\infty} \mathrm{d}x\, \rho_0'\rho_0'} = \frac{2\rho_0''(L/2)h_0}{\int \mathrm{d}x\, (\rho_0')^2}. \tag{S54}$$

where the last equality follows from the oddness of the unperturbed profile $\rho(-L/2) = -\rho(L/2)$. With $\rho_0(x) = -\tanh(x/\sqrt{2}\ell)$, we thus find

$$k_c = \frac{3h_0}{\sqrt{2}\ell} \frac{\sinh\left(L/(2\sqrt{2}\ell)\right)}{\cosh\left(L/(2\sqrt{2}\ell)\right)^3} \tag{S55}$$

which has a maximum at $\ell \approx 0.35L$, tends to zero for both $\ell \to 0$ and $\ell \to +\infty$ and asymptotically scales as

$$k_c L \sim \begin{cases} 6\sqrt{2}h_0 \left(\frac{L}{\ell}\right) e^{-L/(\sqrt{2}\ell)} & \text{if } \ell \ll L \\ \frac{3h_0}{4\sqrt{2}} \left(\frac{L}{\ell}\right)^2 & \text{if } \ell \gg L \end{cases} \tag{S56}$$

This exponential decay as $\ell/L \ll 1$ is very strong, and we expect other effects such as front deformation at the edges will dominate the confinement effects. In direct simulations of the noisy reaction-diffusion system with non-conserved noise, we fit the position and amplitude of the confinement force to the observed variance, which relates to the confinement stiffness as $\sigma = \sqrt{D_f/k_c}$. (Fig. S4d-e). More precisely, to allow some margin for deviations of the front profile from the hyperbolic tangent shape, we fit the constants α and β where $\ell = \alpha\sqrt{D}$ and $\sigma = \beta/\sqrt{k_c[\ell]}$ such that the minimum coincides with the observed one. We find that while there is a clear minimum variance (maximum confinement stiffness) with varying $D \propto \ell^2$, the variance does not grow as fast as predicted as $D \to 0$. We also remark that while the source strength h_0 sets the width of the region where the front solutions exist, the front variance only weakly varies with h_0 in this existence region. In conclusion, while the confinement force derived above seems to capture some of the observed phenomenology, it is not quantitative, perhaps because it fails to account for the stability of the homogeneous solutions.

Landau-Ginzburg fluctuating PDE $\partial_t m = D\partial_x^2 m + m - m^3 + h(x) + \sqrt{2\gamma}\zeta(x,t)$

Unscaled source $h(x) = h_0\left(\delta(x - L/4) - \delta(x - 3L/4)\right)$

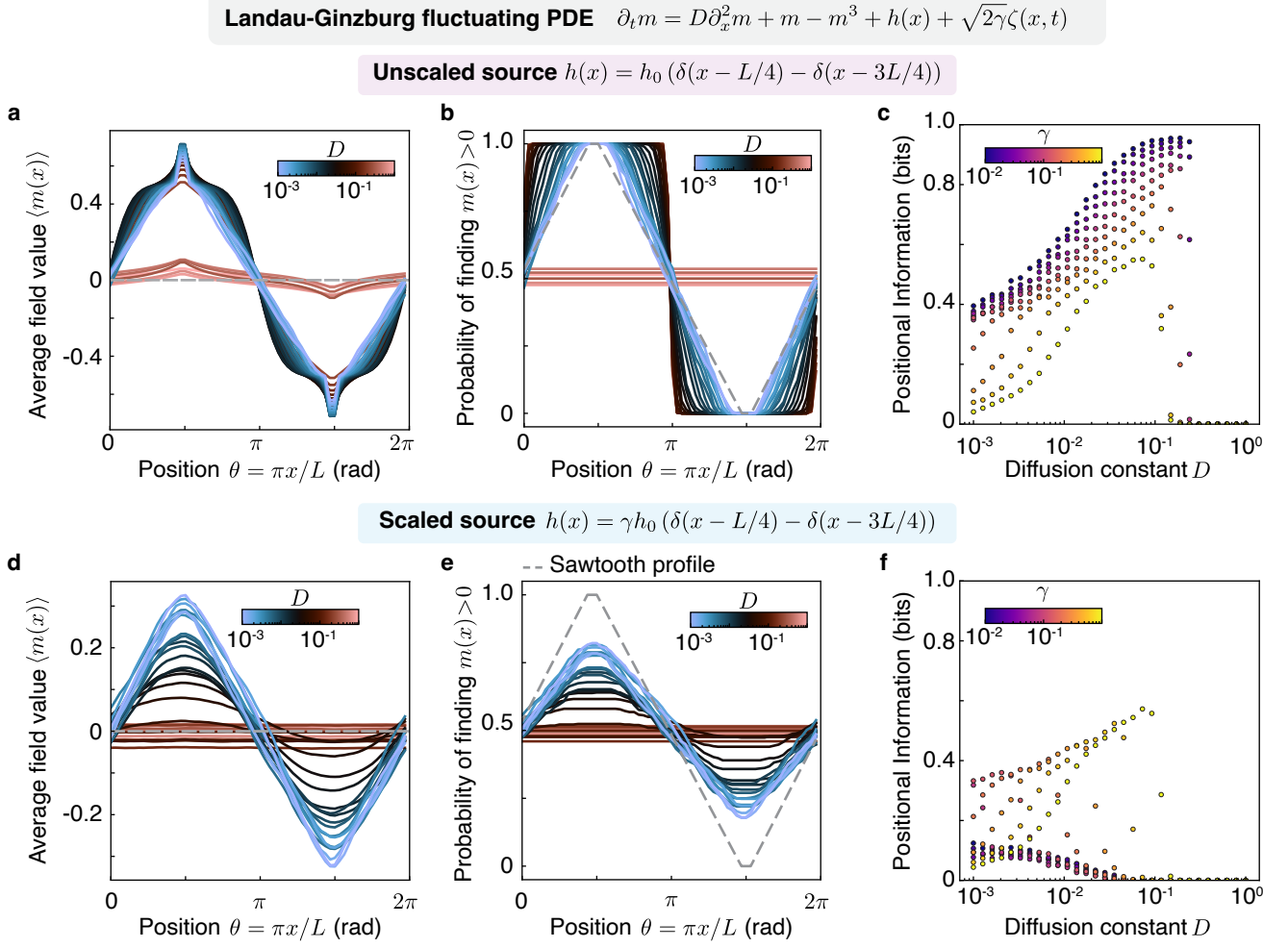**Scaled source** $h(x) = \gamma h_0\left(\delta(x - L/4) - \delta(x - 3L/4)\right)$

FIG. S5. Landau-Ginzburg theory recapitulates results from lattice simulations when constrained by microscopic rules. Without any microscopic constraint, **a-b.** The average field value $\langle m(x)\rangle$ peaks at sources, and the marginal probability can now become step-like **c.** The positional information now increases with decreasing noise, still showing a sharp optimum for intermediate D. **d-e.** With the relationship between noise and source strength imposed by microscopic dynamics, positional information is limited Average field value $\langle m(x)\rangle$ shows a sawtooth-like profile, which is reflected in the marginal probability. **f.** Positional information saturates to a low value as noise is decreased. In **a,b,d,e**, $\gamma = 10^{-3}$. All simulations have $h_0 = 10$, $L = 4$, are integrated over a duration $T = 100/D$ in dimensionless units and are discretized in space in time using finite differences $\Delta x = L/128$, $\Delta t = 0.03(\Delta x)^2/D$.

IV. COMPARISON BETWEEN DIFFUSIVE ISING AND LANDAU-GINZBURG PHENOMENOLOGY

To understand the reach of our results, we simulate the Landau-Ginzburg theory to which our microscopic models reduce to in the limit of large particle numbers and infinite site density. The numerical implementation uses a Euler-Mayurama scheme with standard second-order finite-difference discretization of the Laplacian. We find that these models, unconstrained to be discrete-valued, are generally not subject to the information-theoretic bounds we derived in Sec. II (Fig. S5a-c). However, when the model coefficients are constrained by the microscopic dynamics, the model reproduces the information saturation phenomenon even at low noise (Fig. S5d-f). Indeed, since the variance of the noise in the DIM is proportional to the lattice length scale a and the effective macroscopic source intensity is also proportional to a, the noise and the source strengths are intrinsically linked in the microscopic model.

V. WAVE-PINNING AS INTEGRAL FEEDBACK

A. The wave-pinning Ising system

We consider a diffusive Ising system with coupling to a finite reservoir. In this model, particles of type $\oplus$ and $\ominus$ can diffuse along a 1D membrane with diffusion coefficient D. Instead of 'color switching' dynamics, particles unbind from the membrane into a reservoir with a rate dependent on the concentration of the other species $R_+ = r + kn_-(n_- - 1)$ and $R_- = r + kn_+(n_+ - 1)$. The particles in the reservoir can bind anywhere on the membrane at rate r. Thus, the influx of particles onto the membrane is proportional to the number of particles in the reservoir, which is equal to the total number of particles minus those bound to the membrane. These systems with global feedback are known as wave-pinning systems [20, 21]; such a reservoir-coupling mechanism is frequently encountered in biology.

The coarse-grained equations corresponding to this system with global concentration coupling are given by (Calculations in Sec. VI A 3)

$$\partial_t n_+ = D\partial_x^2 n_+ - rn_+ - kn_-^2 n_+ + rn_+^c \tag{S57a}$$

$$\partial_t n_- = D\partial_x^2 n_- - rn_- - kn_+^2 n_- + rn_-^c \tag{S57b}$$

$$n_\pm^c = n_\pm^0 - \frac{1}{a}\int \mathrm{d}x\, n_\pm \tag{S57c}$$

Here, a is the lattice spacing, proxies for the interaction range. Defining the total density $\rho = n_+ + n_-$ and magnetization $m = n_+ - n_-$,

$$\partial_t m = D\partial_x^2 m + (\frac{k}{4}\rho^2 - r)m - \frac{k}{4}m^3 + rm^c \tag{S58a}$$

$$\partial_t \rho = D\partial_x^2 \rho - r\rho - \frac{k}{4}\rho(\rho^2 - m^2) + r\rho^c \tag{S58b}$$

$$m^c = m^0 - \frac{1}{a}\int \mathrm{d}x\, m \tag{S58c}$$

$$\rho^c = \rho^0 - \frac{1}{a}\int \mathrm{d}x\, \rho \tag{S58d}$$

When D is sufficiently small so that domain walls and density fluctuations around its steady-state value $\bar{\rho}$ can be safely ignored, the magnetization dynamics then obey the reduced Ising-like dynamics

$$\partial_t m = D\partial_x^2 m + r_2 m - u_2 m^3 + h \tag{S59}$$

$$h = rm^0 - \frac{r}{a}\int \mathrm{d}x\, m \tag{S60}$$

with $\alpha > 0$, and where the flux from the reservoir can be understood as a uniform, self-organized magnetic field.

Its effect can be understood in the following sense: if the average magnetization $\langle m \rangle_x = \frac{1}{L}\int \mathrm{d}x\, m$ is greater than m^0, then $h < 0$, biasing the effective reaction free energy towards the negative state. If the system contains domain walls, this asymmetry then leads to the domain walls drifting until $\langle m \rangle_x = m^0$, imposing a set ratio of positive and negative domains. If $m^0 = 0$, this dynamical balance is achieved when $\langle m \rangle_x = 0$, which happens when the positive and negative domains are the same size.

The coupling to the reservoir can therefore be understood as a form of spatial integral feedback, whose effects can also be seen in the wave-propagation picture [18, 20]. In this picture, the position of the front at position $X(t)$ propagating at velocity c evolves under the dynamics

$$\frac{\mathrm{d}X}{\mathrm{d}t} = c. \tag{S61}$$

We can use Eq. S31 to calculate the front velocity c as a function of the profile $m(x,t)$: assuming that the domain size L is large enough compared to the domain wall width $\ell = \sqrt{D/r_2}$ such that the profile is given by a hyperbolic

tangent $m(x,t) = \tanh\left[(x - X(t))/\sqrt{2}\ell\right]$, then we have

$$c = -\frac{\int_{m_-}^{m_+} dm \left(r_2 m - u_2 m^3 + h\right)}{\int_{-\infty}^{\infty} dx (\partial_x m)^2} \tag{S62}$$

$$= -\frac{3h\sqrt{r_2/u_2}}{\sqrt{2}\ell} \tag{S63}$$

$$= -3r\sqrt{\frac{r_2 D}{2u_2^2}} \left(\frac{m^0}{m_+} + \frac{1}{a}(2X(t) - L)\right) \tag{S64}$$

with $m_\pm = \pm\sqrt{r_2/u_2}$, and where we used $\int dx\, m(x,t) \approx m_+ X(t) + m_-(L - X(t))$ by approximating the solution as constant on either side of the wall. When $m^0 = 0$, we thus have a restoring force

$$\frac{dX}{dt} = f_{\rm wp}(X) = -\frac{3}{\sqrt{2}}\frac{r}{u_2}\sqrt{r_2 D}\left(X(t) - \frac{L}{2}\right) \equiv -k_{\rm wp}(X(t) - X_0) \tag{S65}$$

with wave-pinning-induced confinement stiffness $k_{\rm wp} \propto \sqrt{D}$.

To compute the coefficients r_2, u_2 and choose simulation parameters, we examine steady homogeneous solutions for which $\rho = \bar{rho}$, $m = \bar{m}$. For a system in dynamical balance, in the homogeneous domains $m^c = 0$ and $\rho^c = \rho^0 - \bar{\rho}/a$. The steady state values thus satisfy

$$\bar{m}\left(\frac{k}{4r}\bar{\rho}^2 - 1 - \frac{k}{4r}\bar{m}^2\right) = 0 \tag{S66a}$$

$$\bar{\rho}\left(2 + \frac{k}{4r}(\bar{\rho}^2 - \bar{m}^2)\right) = \rho^0 \tag{S66b}$$

To impose $\bar{m} \neq 0$, this imposes

$$\bar{\rho} = \frac{\rho^0}{2 + 1/a}, \quad \bar{m} = \pm\sqrt{\bar{\rho}^2 - \frac{4r}{k}}. \tag{S67}$$

The steady state density in the WPI model is $\bar{\rho} = \rho^0/(2 + 1/a)$. For simulations, we want the bistable solutions $\bar{m} \neq 0$ to exist. For ρ^0 large enough, $k = (4/3)r$ satisfies the requirement.

B. Two-point correlations in the Wave-Pinning Ising model

Here we compute the two-point correlation function for the Wave-pinning model, confirming that this model has non-vanishing long-range correlations. To proceed, we consider the linearization of the dynamics around a steady-state front solution $m_0(x) = \text{sgn}(x - L/2)M_0$ with $M_0 = \sqrt{u_2/r_2}$ on a periodic domain of length L. We take $m^0 = 0$ We write the magnetization $m(x,t) = m_0(x) + \phi(x,t)$, which leads to the dynamics

$$\partial_t \phi = D\partial_{xx}^2\phi - 2r_2\phi - \frac{r}{a}\int_0^L dx\,\phi + f(x,t) \tag{S68}$$

To compute the two-point correlation function, we can write the Fourier transform of ϕ in time and space

$$\phi(x,t) = \sum_q \int_{-\infty}^{+\infty}\frac{d\omega}{2\pi}\phi_{q,\omega}e^{-i(qx-\omega t)} \tag{S69a}$$

$$\phi_{q,\omega} = \frac{1}{L}\int_0^L dx \int_{-\infty}^{+\infty} dt\,\phi(x,t)e^{i(qx-\omega t)} \tag{S69b}$$

where we note that the sum over the wavenumber $q = 2\pi n/L, n \in \mathbb{Z}$ is discrete due to the periodicity of the domain.

In Fourier space, the equations for $q = 0$ and $q \neq 0$ modes read

$$i\omega\phi_{0,\omega} = -\left(2r_2 + \frac{Lr}{a}\right)\phi_{0,\omega} + f_{0,\omega}, \tag{S70a}$$

$$i\omega\phi_{q,\omega} = -(Dq^2 + 2r_2)\phi_{q,\omega} + f_{q,\omega}, \tag{S70b}$$

For Gaussian driving noise $\langle f_{q,\omega} f_{q',\omega'} \rangle = \theta \delta(q+q')\delta(\omega+\omega')$, we thus find that the correlation function in Fourier space is given by

$$\langle \phi_{q,\omega} \phi_{q',\omega'} \rangle = \delta(q+q')\delta(\omega+\omega') \left(\frac{\delta_{q,0}}{\omega^2 + (2r_2 + Lr/a)^2} + \frac{1 - \delta_{q,0}}{\omega^2 + (Dq^2 + 2r_2)^2} \right) \tag{S71a}$$

As $t \to \infty$, we can find the steady-state correlation function

$$\langle \phi(x)\phi(x') \rangle = \sum_q \langle \phi_{q,0} \phi_{-q,0} \rangle \approx \frac{\theta}{2r_2 + Lr/a} + \theta \int_{-\infty}^{+\infty} \frac{\mathrm{d}q}{2\pi} \frac{e^{-iq(x-x')}}{Dq^2 + 2r_2} = \frac{\theta}{2r_2 + Lr/a} + \frac{\theta}{2\sqrt{2Dr_2}} e^{-|x-x'|/\ell} \tag{S72}$$

with $\ell = \sqrt{D/(2r_2)}$ and the approximation comes from approximating the finite sum by an integral. The coupling to the spatially uniform ($q = 0$) mode thus leads to long-range coupling by preventing the vanishing of correlations in fluctuations as $|x - x'| \to +\infty$.

C. Experimental example: *C. elegans* antero-posterior patterning

Wave-pinning models have found important use in explaining *C. elegans* antero-posterior patterning. In this section, we develop a microscopically-plausible lattice model that coarse-grains to the continuum model introduced by Goehrings et al [22]. In this model, the embryo is modeled as a prolate spheroid with radii $27 \times 15 \times 15$ μm and by axisymmetry the system is reduced to one-dimensional dynamics. We here use the notation from that reference.

In the lattice version model, the binding and unbinding reactions for the anterior PARs A (aPARs: PAR-3, PAR-6, and atypical protein kinase C) A and posterior PARs P (pPARs: PAR-1, PAR-2, and LGL)

$$A \rightleftharpoons A_{\text{cyto}} \tag{S73a}$$
$$P \rightleftharpoons P_{\text{cyto}} \tag{S73b}$$

have reaction rates in lattice units given by $k_{\text{off}}^A + \tilde{k}_{AP}P$, $k_{\text{off}}^A + \tilde{k}_{PA}A(A-1)$. The challenge here is to relate the lattice units to the measured experimental values.

From these reactions, the coarse-graining procedure performed on the wave-pinning Ising (Sec. VI A 3) can be readily adapted, with the Poissonian ansatz giving

$$\partial_t N_A = D_A \partial_x^2 N_A - k_{\text{off}}^A N_A - \tilde{k}_{AP} N_P N_A + \tilde{k}_{\text{on}}^A N_{A,\text{cyto}}$$
$$+ \partial_x \left[\sqrt{2D_A N_A \Delta x} \zeta_1 \right] + \sqrt{(k_{\text{off}}^A N_A + \tilde{k}_{AP} N_P N_A + \tilde{k}_{\text{on}}^A N_{A,\text{cyto}})\Delta x} \zeta_2 \tag{S74a}$$
$$\partial_t N_P = D_P \partial_x^2 N_P - k_{\text{off}}^P N_P - \tilde{k}_{PA} N_A^2 N_P + \tilde{k}_{\text{on}}^P N_{P,\text{cyto}}$$
$$+ \partial_x \left[\sqrt{2D_P N_P \Delta x} \zeta_3 \right] + \sqrt{(k_{\text{off}}^P N_P + \tilde{k}_{PA} N_A^2 N_P + \tilde{k}_{\text{on}}^P N_{P,\text{cyto}})\Delta x} \zeta_4 \tag{S74b}$$

Where N_A and and N_P the number of a- and p-PARs on a given lattice site, and $N_{X,cyto}$ their number in the cytoplasm of the embryo. How do we relate this model to the experimental concentration units? To find the appropriate conversion factors, we seek the conversion factor Ω (which has units of surface) such that $A = N_A/\Omega$, $P = N_P/\Omega$. To find Ω, we use the number conservation laws written in lattice and continuum units.

Number conservation in the continuum model reads

$$A_{\text{cyto}} V = \rho_{\text{tot}}^A V - S\langle A \rangle \tag{S75}$$

or

$$A_{\text{cyto}} = \rho_{\text{tot}}^A - \psi \langle A \rangle \tag{S76}$$

where $\psi = S/V = 0.174$ μm^{-1} for the prolate spheroid representing the embryo, and $\langle A \rangle = L^{-1} \int_0^L \mathrm{d}x A(x)$ is the average membrane-bound density, with $L = 135$ μm. Written as is, this conservation law neglects the curvature of the embryo, which according to Ref. [22] does not significantly contribute. In terms of molecule numbers, we have

$$N_{\text{cyto}}^A = N_{\text{tot}}^A - S\langle A \rangle \tag{S77}$$

In the microscopic lattice model, we have

$$N_{\text{cyto}}^A = N_{\text{tot}}^A - \left(\frac{L}{\Delta x}\right)\langle N_A\rangle \tag{S78}$$

For number conservation to be consistent between Eqs. (S77) and (S78), we thus find that

$$\Omega = \left(\frac{\Delta x}{L}\right)S. \tag{S79}$$

We thus get the fluctuating continuum equations in the experimental units of [22],

$$
\begin{aligned}
\partial_t A =& D_A \nabla^2 A - k_{\text{off}}^A A - k_{AP} P A + k_{\text{on}}^A A_{\text{cyto}} \\
&+ \partial_x\left[\sqrt{2D_A A\left(\frac{\Delta x}{\Omega}\right)}\zeta_1\right] + \sqrt{\frac{\Delta x}{\Omega}(k_{\text{off}}^A A + k_{AP} A P + k_{\text{on}}^A A_{\text{cyto}})}\zeta_2
\end{aligned} \tag{S80a}
$$

$$
\begin{aligned}
\partial_t P =& D_P \nabla^2 P - k_{\text{off}}^P P - k_{PA} A^2 P + k_{\text{on}}^P P_{\text{cyto}} \\
&+ \partial_x\left[\sqrt{2D_P P\left(\frac{\Delta x}{\Omega}\right)}\zeta_3\right] + \sqrt{\frac{\Delta x}{\Omega}(k_{\text{off}}^P P + k_{PA} A^2 P + k_{\text{on}}^P P_{\text{cyto}})}\zeta_4
\end{aligned} \tag{S80b}
$$

with $\tilde{k}_{AP} = (k_{AP}/S)(L/a)$, $\tilde{k}_{PA} = (k_{PA}/S^2)(L/a)^2$, $\tilde{k}_{\text{on}}^A = k_{\text{on}}^A(a/L)\psi$, $\tilde{k}_{\text{on}}^P = k_{\text{on}}^P(a/L)\psi$.

If we wanted to simulate these dynamics at full scale, how many particles do we need to include in our microscopic dynamics?

For our simulations to be faithful, we need our simulations to be in a regime where there exists homogeneous steady states with positive concentrations. Let ϕ^A and ϕ^P be the average number of particles per site of type A or P. Then in steady state, in homogeneous domains, we have

$$\phi^A = \frac{k_{\text{on}}^A}{k_{\text{off}}^A}\left(\frac{a}{L}\right)\psi N_{\text{cyto}}^A, \tag{S81}$$

$$\phi^P = \frac{k_{\text{on}}^P}{k_{\text{off}}^P}\left(\frac{a}{L}\right)\psi N_{\text{cyto}}^P. \tag{S82}$$

Total number conservation implies

$$\frac{N_{\text{cyto}}^A}{N_{\text{tot}}^A} = 1 - \frac{k_{\text{on}}^A}{k_{\text{off}}^A}\psi \tag{S83}$$

and likewise for P

$$\frac{N_{\text{cyto}}^P}{N_{\text{tot}}^P} = 1 - \frac{k_{\text{on}}^P}{k_{\text{off}}^P}\psi. \tag{S84}$$

For the values of the rate constants tabulated in Ref. [22], $k_{\text{off}}^A = 5.4 \cdot 10^{-3}\ s^{-1}$, $k_{\text{off}}^P = 7.3 \cdot 10^{-3}\ s^{-1}$, $k_{\text{on}}^A = 8.58 \cdot 10^{-3}\ \mu m/s$, $k_{\text{on}}^P = 4.74 \cdot 10^{-2}\ \mu m/s$, $k_{AP} = 0.19\ \mu m^2/s$, $k_{PA} = 2.0\ \mu m^4/s$ and geometric factor ψ and ratio $N_{\text{tot}}^A/N_{\text{tot}}^P = 1.56 \approx 3/2$, we have $\psi k_{\text{on}}^A/k_{\text{off}}^A \approx 1/3$, $\psi k_{\text{on}}^P/k_{\text{off}}^P \approx 1/10$, and thus that to obtain $\phi^P \approx 1$, we need $\phi^A \approx 5\phi^P = 5$, which requires

$$N_{\text{tot}}^A = 15\left(\frac{L}{a}\right)\phi^P, \quad N_{\text{tot}}^P = 10\left(\frac{L}{a}\right)\phi^P. \tag{S85}$$

where L/a is the number of lattice sites. To get the experimental number of particles $N_{\text{tot}}^A = 4.0 \cdot 10^4$, $N_{\text{tot}}^P = 2.5 \cdot 10^4$, we thus need $a = 4 \cdot 10^{-4}L$, or $a = 5 \cdot 10^{-2}\ \mu m$. Such a simulation would require $\approx 2.7 \cdot 10^3$ lattice sites, which while computationally expensive is within reach of tau-leaping schemes used in this article.

VI. COARSE-GRAINING DIFFUSIVE LATTICE MODELS

We follow the method outlined in [3] to obtain a fluctuating hydrodynamics description of our microscopic lattice dynamical models. Briefly, the method consists of deriving a field-theoretic form of the chemical master equation,

and then leverage a Poissonian ansatz (when diffusion dominates as $a \to 0$) to compute higher-order correlations and derive a closed hydrodynamic equation.

In what follows, we consider particles of type $+$ and $-$ which can hop to a neighboring site with probability rate D/a^2 and change type at site i with rate $g_i^{\pm}(\{n_+, n_-\})$ which can depend on the populations at the same site or neighboring sites. For the DIM, the case considered in [3], the flip rate from $+$ to flip to $-$ is $g_i^+ = \gamma e^{-\beta(n_+ - n_-)}$ while the flip rate from $-$ to $+$ is $g_i^- = \gamma e^{+\beta(n_+ - n_-)}$.

We also consider the case of nearest-neighbor interactions in the DIM, where the flip rate for particles at site i is $g_{\pm}(\{n_+, n_-\}) = \gamma \prod_{\langle i,k \rangle} e^{\mp\beta(n_+^k - n_-^k)}$ where the product is taken over the sites k which are nearest-neighbors of i (not including i itself). We find that this case recovers, up to a rescaling of the reaction timescale, the coarse-graining of the same-site DIM.

Finally, we coarse-grain the lattice version of the wave-pinning system, in which particles diffuse and bind or unbind from the lattice into a reservoir, which rates varying depending on the local environment.

A. From master equation to mean-field hydrodynamics

To construct the master equation, we consider the random variables $n_i^{\pm}(t_j)$ counting the number of particles of type $\pm$ at site i at time t_j for $(i,j) \in \{1, \ldots, L\} \times \{1, \ldots, M\}$. The probability of observing any configuration $\{n\} \equiv \{n_i^{\pm}(t_j), (i,j) \in \{1, \ldots, L\} \times \{1, \ldots, M\}\}$ is given by

$$P[\{n\}] = \left\langle \prod_{i=i}^{L} \prod_{j=1}^{M} \prod_{\sigma=\pm} \delta \left(n_i^{\sigma}(t_{j+1}) - n_i^{\sigma}(t_j) - J_i^{\sigma}(t_j) \right) \right\rangle_{\{J\}} \tag{S86}$$

where $J_i^{\pm}(t_j) \in \{-1, 0, 1\}$ is the change in particle number of type $\pm$ at site i in the infinitesimal time $t_{j+1} - t_j = dt$, and the average is taken over all possible such changes in configuration. For our set of reactions, there are four cases:

(i) A particle hops from site i to site $i+1$: $J_i^{\pm}(t_j) = -1$, $J_{i+1}^{\pm}(t_j) = 1$.

(ii) A particle hops from site i to site $i-1$: $J_i^{\pm}(t_j) = -1$, $J_{i-1}^{\pm}(t_j) = 1$.

(iii) A $+$ particle flips at site i: $J_i^+(t_j) = +1 = -J_i^-(t_j)$.

(iv) A $-$ particle flips at site i: $J_i^-(t_j) = +1 = -J_i^+(t_j)$.

For each of these events, all others $J_{k \neq i}^{\pm}(t_j) = 0$.

To proceed, we use the integral expression of the Dirac function $\delta(s) = \int (2\pi)^{-1} d\hat{s} \, e^{is\hat{s}}$, which allows us to rewrite the probability as

$$P[\{n^{\pm}\}] = \int \prod_{j=1}^{M} \prod_{i=i}^{L} d\hat{n}_i^+(t_j) d\hat{n}_i^-(t_j) e^{\hat{n}_i^+(t_j)\left[n_i^+(t_{j+1}) - n_i(t_j)^+\right]} e^{\hat{n}_i^-(t_j)\left[n_i^-(t_{j+1}) - n_i(t_j)^-\right]} \left\langle e^{-\hat{n}_i^+(t_j)J_i^+(t_j) - \hat{n}_i^-(t_j)J_i^-(t_j)} \right\rangle_{\{J^j\}} \tag{S87}$$

where the imaginary unit is absorbed into the (now imaginary-valued) fields $\hat{n}_i^{\pm}(t_j)$, and the average is taken over the possible changes in particle states $\{J^j\} \equiv \{J_i^{\pm}(t_j), i \in \{1, \ldots, L\}\}$.

To evaluate this average, we denote $f(C) = \prod_{i=1}^{L} e^{-\hat{n}_i^+(t_j)J_i^+(t_j) - \hat{n}_i^-(t_j)J_i^-(t_j)}$ for a given particle configuration C, and write out

$$\langle f \rangle_{\{J^j\}} = \sum_{C \in \{J^j\}} f(C) P(C|\{n^j\}). \tag{S88}$$

To proceed, we decompose this sum into the terms corresponding to different types of moves:

1. C_0: all $J_i(t_j) = 0$, there are no moves during dt. $f(C_0) = 1$.

2. $\mathcal{N}_d^j$ Diffusive move: for $i \to i \pm 1$, $J_i^{\sigma}(t_j) = -1$, $J_{i\pm 1}^{\sigma}(t_j) = +1$, $P(C|\{n^j\}) = \frac{D}{a^2} n_i^{\sigma}(t_j) dt$

3. $\mathcal{N}_{f,+}^j$ Particle at site i flips from $+$ to $-$: $J_i^+(t_j) = -1, J_i^-(t_j) = +1$, and

$$P(C|\{n^j\}) = n_i^+(t_j) g_i^+(\{n_+(t_j), n_-(t_j)\}) dt \tag{S89}$$

4. $\mathcal{N}_{f,-}^j$ Particle at site i flips from $-$ to $+$: $J_i^+(t_j) = +1, J_i^-(t_j) = -1$, and

$$P(C|\{n^j\}) = n_i^-(t_j)g_i^-(\{n_+(t_j), n_-(t_j)\})\mathrm{d}t \tag{S90}$$

$$\langle f \rangle_{\{J^j\}} = f(C_0)P(C_0|\{n^j\}) + \sum_{C \in \mathcal{N}_d^j} f(C)P(C|\{n^j\})$$
$$+ \sum_{C \in \mathcal{N}_c^j} f(C)P(C|\{n^j\})$$
$$+ \sum_{C \in \mathcal{N}_a^j} f(C)P(C|\{n^j\}) \tag{S91}$$

Since $P(C_0|\{n^j\}) = 1 - \sum_{C \in \mathcal{N}_d^j} P(C|\{n^j\}) - \sum_{C \in \mathcal{N}_c^j} P(C|\{n^j\}) - \sum_{C \in \mathcal{N}_a^j} P(C|\{n^j\})$, we have

$$\langle f \rangle_{\{J^j\}} = 1 + T_d + T_{f,+} + T_{f,-} \tag{S92}$$

with $T_x = \sum_{C \in \mathcal{N}_x^j}(f(C) - 1)P(C|\{n^j\})$, $x \in \{d, f+, f-\}$. Since $T_x \propto \mathrm{d}t$ since the probabilities are themselves proportional to $\mathrm{d}t$, we can re-exponentiate to find

$$\langle f \rangle_{\{J^j\}} = \exp(T_d + T_{f,+} + T_{f,-}) + O(\mathrm{d}t^2) \tag{S93}$$

We can now write down each term in the sum:

$$T_d = \sum_i \frac{D}{a^2}\mathrm{d}t \left(\left[e^{\hat{n}_i^+(t_j) - \hat{n}_{i+1}^+(t_j)} - 1 \right] n_i^+(t_j) + \left[e^{\hat{n}_{i+1}^+(t_j) - \hat{n}_i^+(t_j)} - 1 \right] n_{i+1}^+(t_j) \right)$$
$$+ \frac{D}{a^2}\mathrm{d}t \left(\left[e^{\hat{n}_i^-(t_j) - \hat{n}_{i+1}^-(t_j)} - 1 \right] n_i^-(t_j) + \left[e^{\hat{n}_{i+1}^-(t_j) - \hat{n}_i^-(t_j)} - 1 \right] n_{i+1}^-(t_j) \right) \tag{S94a}$$
$$T_{f,+} + T_{f,-} = \sum_i \mathrm{d}t \left(e^{\hat{n}_i^+(t_j) - \hat{n}_i^-(t_j)} - 1 \right) g_i^+(\{n_+, n_-\})n_i^+(t_j)$$
$$+ \mathrm{d}t \left(e^{-\hat{n}_i^+(t_j) + \hat{n}_i^-(t_j)} - 1 \right) g_i^-(\{n_+, n_-\})n_i^-(t_j) \tag{S94b}$$

Putting everything together, we now have

$$P[\{n\}] = \int \prod_{j=1}^M \prod_{i=i}^L \mathrm{d}\hat{n}_i(t_j)e^S \tag{S95}$$

With the exact microscopic action S given by

$$S = \sum_{i,j} \hat{n}_i^+(t_j) \left(n_i^+(t_{j+1}) - n_i^+(t_j) \right) + \hat{n}_i^-(t_j) \left(n_i^-(t_{j+1}) - n_i^-(t_j) \right)$$
$$+ \frac{D\mathrm{d}t}{a^2} \left[n_i^+(t_j) \left(e^{\hat{n}_i^+(t_j) - \hat{n}_{i+1}^+(t_j)} - 1 \right) + n_{i+1}^+(t_j) \left(e^{-\hat{n}_i^+(t_j) + \hat{n}_{i+1}^+(t_j)} - 1 \right) \right]$$
$$+ \frac{D\mathrm{d}t}{a^2} \left[n_i^-(t_j) \left(e^{\hat{n}_i^-(t_j) - \hat{n}_{i+1}^-(t_j)} - 1 \right) + n_{i+1}^-(t_j) \left(e^{-\hat{n}_i^-(t_j) + \hat{n}_{i+1}^-(t_j)} - 1 \right) \right]$$
$$+ \mathrm{d}t \left(e^{\hat{n}_i^+(t_j) - \hat{n}_i^-(t_j)} - 1 \right) g_i^+(\{n_+, n_-\})n_i^+(t_j)$$
$$+ \mathrm{d}t \left(e^{-\hat{n}_i^+(t_j) + \hat{n}_i^-(t_j)} - 1 \right) g_i^-(\{n_+, n_-\})n_i^-(t_j) \tag{S96}$$

To obtain a continuum (in space) model, we have to switch from a discrete number representation to a continuum parametrization. To this end, we first replace the integer-valued $n_i^\pm$ by real-valued averages. We remark that as $a \to 0$ and the system is dominated by diffusion, the random variables $n_i(t_j)^\pm$ are Poisson-distributed: we denote the parameters of these distribution $\rho_i^\pm(t_j)$, such that, for instance,

$$\langle n_i(t_j)^\pm \rangle = \rho_i^\pm(t_j) \tag{S97a}$$
$$\langle n_i^+(t_j)(n_i^+(t_j) - 1) \rangle = \sum_{l=0}^\infty \frac{[\rho_i(t_j)]^l}{l!}l(l-1)e^{-\rho_i(t_j)} = \rho_i(t_j)^2 \tag{S97b}$$

and we denote the averaged reaction term by

$$\langle g_\pm(\{n_+, n_-\})n_i(t_j)^\pm\rangle = f_\pm(\{\rho_+, \rho_-\}) \tag{S98}$$

This implies that the average action, taken over this factorized Poisson distribution is given by

$$\langle S\rangle = \sum_{i,j} \hat{n}_i^+(t_j)(\rho_i^+(t_{j+1}) - \rho_i^+(t_j)) + \hat{n}_i^-(t_j)(\rho_i^-(t_{j+1}) - \rho_i^-(t_j))$$
$$+ \frac{D\mathrm{d}t}{a^2}\left[\rho_i^+(t_j)\left(e^{\hat{n}_i^+(t_j)-\hat{n}_{i+1}^+(t_j)} - 1\right) + \rho_{i+1}^+(t_j)\left(e^{-\hat{n}_i^+(t_j)+\hat{n}_{i+1}^+(t_j)} - 1\right)\right]$$
$$+ \frac{D\mathrm{d}t}{a^2}\left[\rho_i^-(t_j)\left(e^{\hat{n}_i^-(t_j)-\hat{n}_{i+1}^-(t_j)} - 1\right) + \rho_{i+1}^-(t_j)\left(e^{-\hat{n}_i^-(t_j)+\hat{n}_{i+1}^-(t_j)} - 1\right)\right]$$
$$+ \mathrm{d}t\left(e^{\hat{n}_i^+(t_j)-\hat{n}_i^-(t_j)} - 1\right)f_+(\{\rho_+, \rho_-\})$$
$$+ \mathrm{d}t\left(e^{-\hat{n}_i^+(t_j)+\hat{n}_i^-(t_j)} - 1\right)f_-(\{\rho_+, \rho_-\}) \tag{S99}$$

Since the $\rho_i(t_j)$ are real-valued, we can now Taylor-expand in time $\rho_i(t_{j+1}) = \rho_i(t_j) + \dot{\rho}_i\mathrm{d}t + O(\mathrm{d}t^2)$ to find

$$\langle S\rangle = \int \mathrm{d}t \sum_i \left[\hat{n}_i^+(t_j)\dot{\rho}_i^+ + \hat{n}_i^-(t_j)\dot{\rho}_i^- + \frac{D}{a^2}\left[\rho_i^+(t_j)\left(e^{\hat{n}_i^+(t_j)-\hat{n}_{i+1}^+(t_j)} - 1\right) + \rho_{i+1}^+(t_j)\left(e^{-\hat{n}_i^+(t_j)+\hat{n}_{i+1}^+(t_j)} - 1\right)\right]\right.$$
$$+ \frac{D}{a^2}\left[\rho_i^-(t_j)\left(e^{\hat{n}_i^-(t_j)-\hat{n}_{i+1}^-(t_j)} - 1\right) + \rho_{i+1}^-(t_j)\left(e^{-\hat{n}_i^-(t_j)+\hat{n}_{i+1}^-(t_j)} - 1\right)\right]$$
$$\left.+ \left(e^{\hat{n}_i^+(t_j)-\hat{n}_i^-(t_j)} - 1\right)f_+(\{\rho_+, \rho_-\}) + \left(e^{-\hat{n}_i^+(t_j)+\hat{n}_i^-(t_j)} - 1\right)f_-(\{\rho_+, \rho_-\})\right]$$

To simplify the action, we can change variables to the density ρ and magnetization m and their corresponding response fields $\hat{\rho}, \hat{m}$

$$\rho_i = \rho_i^+ + \rho_i^-, \quad m_i = \rho_i^+ - \rho_i^-, \quad \hat{\rho}_i = \frac{\hat{n}_i^+ + \hat{n}_i^-}{2}, \quad \hat{m}_i = \frac{\hat{n}_i^+ - \hat{n}_i^-}{2}. \tag{S100}$$

With those new variables, we can Taylor-expand the particle and response fields as

$$\rho_{i+1} = \rho_i + a\partial_x\rho_i + \frac{a^2}{2}\partial_x^2\rho_i + o(a^2) \tag{S101a}$$

$$\hat{\rho}_{i+1} = \hat{\rho}_i + a\partial_x\hat{\rho}_i + \frac{a^2}{2}\partial_x^2\hat{\rho}_i + o(a^2) \tag{S101b}$$

and likewise for $m, \hat{m}$. Neglecting terms of order ∇^3 and above, we have an effective continuum action

$$\langle S\rangle = \int \mathrm{d}t\frac{\mathrm{d}x}{a}S[\rho, m, \hat{\rho}, \hat{m}] + o(a) \tag{S102}$$

with

$$S = \hat{\rho}\partial_t\rho + \hat{m}\partial_t m + D(\partial_x\hat{\rho})(\partial_x\rho) + D(\partial_x\hat{m})(\partial_x m)$$
$$+ \frac{D}{2}[(\partial_x\hat{\rho} + \partial_x\hat{m})^2 + (\partial_x\hat{\rho} - \partial_x\hat{m})^2]\rho + \frac{D}{2}[(\partial_x\hat{\rho} + \partial_x\hat{m})^2 - (\partial_x\hat{\rho} - \partial_x\hat{m})^2]m$$
$$+ \left(e^{2\hat{m}} - 1\right)f_+\left(\frac{\rho+m}{2}, \frac{\rho-m}{2}\right) + \left(e^{-2\hat{m}} - 1\right)f_-\left(\frac{\rho+m}{2}, \frac{\rho-m}{2}\right)$$

For higher-dimensional settings, the same construction leads to the same action with all derivatives replaced by gradients $(\partial_x\hat{\rho})(\partial_x\rho) \to (\nabla\hat{\rho})^T(\nabla\rho)$, $\partial_{xx} \to \nabla^2$.

In the presence of external sources localized at single sites, the contributions from a single term $\langle S\rangle = \sum_i \delta_{ij}$ in the average action become $S_{\text{source}} = a\delta(x)$ in the continuum action, leading to a source strength scaled by the lattice width a. In the microscopic rules used in main text where the reaction rate term at site i is $g_i^\pm = \gamma e^{\mp\beta(n_+-n_-)+h_0\delta_{ij}}$, we thus have contributions to the action $f_\pm\left(\frac{\rho+m+h(x)}{2}, \frac{\rho-m-h(x)}{2}\right)$ with $h(x) = a(h_0/\beta)\delta(x)$.

To find the equations of motion, we look for saddle-point solutions of

$$\frac{\delta\langle S\rangle}{\delta\rho} = \frac{\delta\langle S\rangle}{\delta m} = \frac{\delta\langle S\rangle}{\delta\hat{\rho}} = \frac{\delta\langle S\rangle}{\delta\hat{m}} = 0 \tag{S103}$$

The conditions a$\frac{\delta\langle S\rangle}{\delta\rho} = \frac{\delta\langle S\rangle}{\delta m} = 0$ are satisfied for $\hat{\rho} = \hat{m} = 0$, and the remaining conditions give $\partial_t\rho, \partial_t m$.

1. Same-site interactions

With same-site interactions, as studied in Ref. [2, 3], we find

$$\partial_t \rho = D\partial_{xx}^2 \rho \tag{S104a}$$

$$\partial_t m = D\partial_{xx}^2 m - g(\delta\rho, m + h(x)) \tag{S104b}$$

with the functions

$$g(\rho, m) = 2\gamma e^{-\beta + (\cosh\beta - 1)\rho} \left(\cosh\left(\sinh(\beta)m\right)m - \sinh\left(\sinh(\beta)m\right)\rho\right) \tag{S105a}$$

$$\bar{g}(\rho, m) = 2\gamma e^{-\beta + (\cosh\beta - 1)\rho} \tag{S105b}$$

Decomposing $\rho = \rho_0 + \delta\rho$, we recover the deterministic part of Eq. S1.

2. Nearest-neighbor interactions

To investigate the effect of nearest-neighbor interactions, we consider a reaction term where the flip rate at site i from $+$ to $-$ is $g_+^i = \gamma e^{\beta \sum_{\langle ij \rangle}(n_j^+ - n_j^-)}$ where $\sum_{\langle i,j \rangle}$ denotes the sum over neighboring sites (not including i itself, which does not change the results qualitatively).

In this case, the reaction rate averaged over the factorized Poisson measure reads

$$\langle n_i(t_j)^+ e^{-\beta \sum_{\langle i,k \rangle}[n_k^+(t_j) - n_k^-(t_j)]} \rangle = \rho_i^+(t_j) \prod_{\langle i,k \rangle} \sum_{m=0}^{\infty} \sum_{l=0}^{\infty} \frac{(\rho_k^+(t_j))^m}{m!} \frac{(\rho_k^-(t_j))^l}{l!} e^{-\rho_k^+(t_j) - \rho_k^-(t_j) - \beta(m-l)}$$

$$= \rho_i^+(t_j) \prod_{\langle i,k \rangle} e^{-\rho_k^+(t_j) - \rho_k^-(t_j) + e^{-\beta}\rho_k^+(t_j) + e^{\beta}\rho_k^-(t_j)} \tag{S106}$$

which lead to a continuum action

$$S = \hat{\rho}\partial_t\rho + \hat{m}\partial_t m + D(\partial_x\hat{\rho})(\partial_x\rho) + D(\partial_x\hat{m})(\partial_x m)$$

$$+ \frac{D}{2}[(\partial_x\hat{\rho} + \partial_x\hat{m})^2 + (\partial_x\hat{\rho} - \partial_x\hat{m})^2]\rho + \frac{D}{2}[(\partial_x\hat{\rho} + \partial_x\hat{m})^2 - (\partial_x\hat{\rho} - \partial_x\hat{m})^2]m$$

$$+ \gamma\left(e^{2\hat{m}} - 1\right)\left(\frac{\rho + m}{2}\right)e^{(\cosh\beta - 1)z\rho - z\sinh\beta m}f(\nabla^2\rho, \nabla^2 m)$$

$$+ \gamma\left(e^{-2\hat{m}} - 1\right)\left(\frac{\rho - m}{2}\right)e^{(\cosh\beta - 1)z\rho + z\sinh\beta m}f(\nabla^2\rho, -\nabla^2 m). \tag{S107}$$

where z is the coordination number of the square lattice ($z = 2^d$ in d-dimensions) with the shorthand $f(\nabla^2\rho, \nabla^2 m) = 1 + a^2 z(\cosh\beta - 1)\nabla^2\rho + a^2 z\sinh\beta\nabla^2 m$. The corresponding dynamical equations are then given by

$$\partial_t\rho = D\nabla^2\rho \tag{S108a}$$

$$\partial_t m = D\nabla^2 m + 2\gamma e^{(\cosh\beta - 1)z\rho}\left[m\cosh(zm\sinh\beta) - \sinh(zm\sinh\beta)\rho\right]$$

$$+ a^2 D_{\rho\rho}\rho\nabla^2\rho + a^2 D_{\rho m}\rho\nabla^2 m + a^2 D_{m\rho}m\nabla^2\rho + a^2 D_{mm}m\nabla^2 m \tag{S108b}$$

with the nonlinear diffusion coefficients

$$D_{\rho\rho} = 2\gamma z e^{(\cosh\beta - 1)z\rho}\sinh(zm\sinh\beta)(1 - \cosh\beta) \tag{S109a}$$

$$D_{\rho m} = 2\gamma z e^{(\cosh\beta - 1)z\rho}\cosh(zm\sinh\beta)\sinh\beta \tag{S109b}$$

$$D_{m\rho} = 2\gamma z e^{(\cosh\beta - 1)z\rho}\cosh(zm\sinh\beta)(1 - \cosh\beta) \tag{S109c}$$

$$D_{mm} = -2\gamma z e^{(\cosh\beta - 1)z\rho}\sinh(zm\sinh\beta)\sinh\beta \tag{S109d}$$

At the deterministic level if $a \to 0$, we recover the result of Eq. (S104) with a slightly different reaction term: In the limit $m \to 0$, $\delta\rho - \rho_0 \to 0$ and introducing $\bar{\gamma} = 2\gamma e^{(\cosh\beta - 1)z\rho_0}$ we now have at cubic order

$$\partial_t\delta\rho = D\nabla^2\delta\rho \tag{S110a}$$

$$\partial_t m = D\nabla^2 m + \bar{\gamma}(1 - z\rho_0\sinh\beta)m - \mu m\delta\rho - um^3 \tag{S110b}$$

If density fluctuations can be ignored (if $D \sim a^2 \gamma z$), the dynamics of the magnetization are given by

$$\partial_t m = (D + a^2 \bar{\gamma} \rho_0 z \sinh \beta) \nabla^2 m + \bar{\gamma}(1 - z\rho_0 \sinh \beta) m - u m^3 \tag{S111}$$

We recover a Landau-Ginzburg-type theory with a diffusion term that accounts for both hopping and spin dynamics.

3.   Wave-Pinning Ising

We here extend this coarse-graining approach to our lattice model of wave-pinning systems introduced in the Methods. We now have a different set of moves, with a reservoir with n_+^r, n_-^r particles. For our set of reactions, there are now six cases:

(i) A particle hops from site i to site $i + 1$: $J_i^{\pm}(t_j) = -1$, $J_{i+1}^{\pm}(t_j) = 1$.

(ii) A particle hops from site i to site $i - 1$: $J_i^{\pm}(t_j) = -1$, $J_{i-1}^{\pm}(t_j) = 1$.

(iii) A + particle unbinds at i and goes into the reservoir: $J_r^+(t_j) = +1 = -J_i^+(t_j)$.

(iv) A − particle unbinds at i and goes into the reservoir: $J_r^-(t_j) = +1 = -J_i^-(t_j)$.

(v) A + particle from the reservoir binds at site i: $J_i^+(t_j) = +1 = -J_r^+(t_j)$.

(vi) A − particle from the reservoir binds at site i: $J_i^-(t_j) = +1 = -J_r^-(t_j)$.

The time-dependent and diffusion terms in the action are unchanged, but the reaction terms now read as

$$S_{wp} = \left(e^{\hat{n}_r^+(t_j) - \hat{n}_i^+(t_j)} - 1 \right) r n_r^-(t_j) \mathrm{dt} + \left(e^{\hat{n}_r^-(t_j) - \hat{n}_i^-(t_j)} - 1 \right) r n_r^-(t_j) \mathrm{dt}$$
$$+ \left(e^{\hat{n}_i^+(t_j) - \hat{n}_r^+(t_j)} - 1 \right) R_+^{i,j} n_i^+(t_j) \mathrm{dt} + \left(e^{\hat{n}_i^-(t_j) - \hat{n}_r^-(t_j)} - 1 \right) R_-^{i,j} n_i^-(t_j) \mathrm{dt} \tag{S112}$$

where the reaction rates are $R_\pm^{i,j} = r + k n_i^{\mp}(t_j)(n_i^{\mp} - 1)$. As before, we notice that as $D/a^2 \to +\infty$ diffusion dominates, leading to our Poisson ansatz such that

$$\langle n_i(t_j)^{\pm} \rangle = \rho_i^{\pm}(t_j) \tag{S113a}$$
$$\langle R_\pm^{i,j} n_i^{\pm}(t_j) \rangle = r \rho_i^{\pm}(t_j) - k[\rho_i^{\mp}(t_j)]^2 \rho_i^{\pm}(t_j) \tag{S113b}$$

By number conservation, we also have

$$\langle n_r^{\pm}(t_j) \rangle = \left\langle N_0^{\pm} - \sum_i n_i^{\pm}(t_j) \right\rangle = N_0^{\pm} - \sum_i \rho_i^{\pm}(t_j) \equiv \rho_r^{\pm}(t_j). \tag{S114}$$

After Taylor-expanding the particle and response fields in space and time, by variation of the action we find the dynamics

$$\partial_t \rho_+ = D \nabla^2 \rho_+ - r \rho_+ - k \rho_-^2 \rho_+ + r \rho_r^+ \tag{S115a}$$
$$\partial_t \rho_- = D \nabla^2 \rho_- - r \rho_- - k \rho_+^2 \rho_- + r \rho_r^- \tag{S115b}$$

with $\rho_r^{\pm} = N_0^{\pm} - (1/a) \int \mathrm{dx}\, \rho_{\pm}(x)$.

B.   Fluctuating hydrodynamics

Here we detail the derivation of the fluctuating hydrodynamics for the same-site interacting Diffusive Ising model [3]. To obtain the fluctuating hydrodynamic equations, we Taylor-expand to second order the action $\langle S \rangle$ in the response fields $\hat{\rho}, \hat{m}$ about $\hat{\rho} = \hat{m} = 0$, keeping terms up to order a. We find the action

$$\langle S \rangle = \begin{pmatrix} S_0^\rho & S_0^m \end{pmatrix} \begin{pmatrix} \hat{\rho} \\ \hat{m} \end{pmatrix} + \frac{1}{2} \begin{pmatrix} \partial_x \hat{\rho} & \partial_x \hat{m} & \hat{m} \end{pmatrix} \bar{M} \begin{pmatrix} \partial_x \hat{\rho} \\ \partial_x \hat{m} \\ \hat{m} \end{pmatrix}, \tag{S116}$$

in which we introduced the deviations from the deterministic hydrodynamics

$$S_0^\rho = \partial_t \rho - D\nabla^2 \rho \tag{S117a}$$

$$S_0^m = \partial_t m - D\nabla^2 m + 2\gamma m e^{-\beta+\rho(\cosh\beta-1)}(\cosh[\sinh(\beta)m]m - \sinh[\sinh(\beta)m]\rho) \tag{S117b}$$

with the shorthands $\hat{\gamma} = 2\gamma e^{-\beta+\rho(\cosh\beta-1)}$ and

$$S_f^m = \frac{1}{2}\left(\cosh[\sinh(\beta)m]\rho - \sinh[\sinh(\beta)m]m\right), \tag{S118}$$

and where we define the matrix

$$\bar{M} = \begin{pmatrix} 2D\rho & 2Dm & 0 \\ 2Dm & 2D\rho & 0 \\ 0 & 0 & \hat{\gamma}S_f^m \end{pmatrix}. \tag{S119}$$

We can then rewrite the probability density as

$$P[\rho,m] = \int \mathcal{D}\rho\mathcal{D}\hat{\rho}\mathcal{D}m\mathcal{D}\hat{m} \exp\left(\int \mathrm{d}t\mathrm{d}x \frac{1}{a}\begin{pmatrix} S_0^\rho & S_0^m \end{pmatrix}\begin{pmatrix} \hat{\rho} \\ \hat{m} \end{pmatrix} + \frac{1}{2a}\begin{pmatrix} \partial_x\hat{\rho} & \partial_x\hat{m} & \hat{m} \end{pmatrix}\bar{M}\begin{pmatrix} \partial_x\hat{\rho} \\ \partial_x\hat{m} \\ \hat{m} \end{pmatrix}\right). \tag{S120}$$

Using a Hubbard-Stratonovich transform, we introduce three Gaussian fields η_1, η_2, η_3 such that

$$P[\rho,m] = \int \mathcal{D}\rho\mathcal{D}\hat{\rho}\mathcal{D}m\mathcal{D}\hat{m}\eta_1\mathcal{D}\eta_2\mathcal{D}\eta_3 \exp\left(\int \mathrm{d}t\mathrm{d}x \frac{1}{a}\begin{pmatrix} S_0^\rho & S_0^m \end{pmatrix}\begin{pmatrix} \hat{\rho} \\ \hat{m} \end{pmatrix} + \frac{1}{\sqrt{a}}\begin{pmatrix} \eta_1 & \eta_2 & \eta_3 \end{pmatrix}\begin{pmatrix} \partial_x\hat{\rho} \\ \partial_x\hat{m} \\ \hat{m} \end{pmatrix} - \frac{1}{2}\begin{pmatrix} \eta_1 & \eta_2 & \eta_3 \end{pmatrix}M^{-1}\begin{pmatrix} \eta_1 \\ \eta_2 \\ \eta_3 \end{pmatrix}\right). \tag{S121}$$

By integrating η_1, η_2 by parts, then integrating out the response fields $\hat{\rho}, \hat{m}$, the probability density reads

$$P[\rho,m] = \int \mathcal{D}\rho\mathcal{D}m\mathcal{D}\eta_1\mathcal{D}\eta_2\mathcal{D}\eta_3\, \delta(S_0^\rho - \sqrt{a}\partial_x\eta_1)\delta(S_0^m - \sqrt{a}\partial_x\eta_2 - \sqrt{a}\eta_3)e^{-\int \mathrm{d}x\mathrm{d}t \frac{1}{2}\begin{pmatrix} \eta_1 & \eta_2 & \eta_3 \end{pmatrix}\bar{M}^{-1}\begin{pmatrix} \eta_1 \\ \eta_2 \\ \eta_3 \end{pmatrix}}. \tag{S122}$$

which leads to the final SPDEs

$$\partial_t \rho = D\nabla^2 \rho + \sqrt{a}\partial_x\eta_1 \tag{S123a}$$

$$\partial_t m = D\nabla^2 m - 2\gamma m e^{-\beta+\rho(\cosh\beta-1)}(\cosh[\sinh(\beta)m]m - \sinh[\sinh(\beta)m]\rho) + \sqrt{a}\partial_x\eta_2 + \sqrt{a}\eta_3 \tag{S123b}$$

with $\langle \eta_i(x,t)\eta_j(x',t')\rangle = \bar{M}_{ij}\delta(x-x')\delta(t-t')$, and the noise is to be interpreted in the Itô sense due to the time-discretization employed in the model. For further RG work we will then rewrite this Langevin SPDE into a Martin-Siggia-Rose action (Eq. (S127)).

VII. SELF-CONSISTENCY OF FLUCTUATING HYDRODYNAMICS BY DYNAMICAL RENORMALIZATION GROUP ANALYSIS

In this section, we derive the effective deterministic hydrodynamic equations for the diffusive Ising model in the presence of finite particle numbers by using the dynamical renormalization group (RG) approach. After rewriting our hydrodynamic equation in the Martin-Siggia-Rose formalism, we will derive the renormalization group equations in the absence of noise. We will then compute perturbatively the corrections to the RG flow equations due to finite noise and compute the effective correlation function used in Fig. E1e.

We will work using the cubic order model applicable in the disordered phase and in the vicinity of the phase transition for small enough a. As $\rho_0 = 1$, this implies the condition $\sinh\beta \approx 1$, which implies $\cosh\beta \approx 2 + \sqrt{2}$. The dynamics are then given by

$$\partial_t \delta\rho = D\partial_{xx}^2 \delta\rho + \sqrt{a}\partial_x\eta_1 \tag{S124a}$$

$$\partial_t m = D\partial_{xx}^2 m - rm - um^3 - \mu m\delta\rho + \sqrt{a}\partial_x\eta_2 + \sqrt{a}\eta_3 \tag{S124b}$$

where the coefficients in the equation are related to the microscopic parameters via $\hat{\gamma} = 2\gamma e^{-\beta+(\cosh\beta-1)\rho_0}$, $r = \hat{\gamma}(1-\rho_0\sinh\beta)$ $u = \hat{\gamma}\sinh\beta/3$ and $-\mu = \hat{\gamma}(1-\rho_0\sinh\beta)(1-\cosh\beta)+\hat{\gamma}\sinh\beta \approx \hat{\gamma}\sinh\beta \approx \hat{\gamma}$, with the approximations holding near the phase transition at $\beta = \ln(1 + \sqrt{2})$. Close to the phase transition $m \approx 0$ and we assume that the noise is such that $\delta\rho \ll \rho_0$. The noise correlations are then $\langle\eta_n(x,t)\eta_{n'}(x',t')\rangle = M_{n,n'}\delta(x-x')\delta(t-t')$

$$M_{nn'} = \begin{pmatrix} 2D\rho_0 & 0 & 0 \\ 0 & 2D\rho_0 & 0 \\ 0 & 0 & 2\rho_0\hat{\gamma} \end{pmatrix}. \tag{S125}$$

MSR action   The probability distribution for the fields ρ, m can be written introducing response fields $\hat{\rho}, \hat{m}$ as

$$P[\rho, m] \propto \int \mathcal{D}[i\hat{\rho}]\mathcal{D}[i\hat{m}] \exp\left(-S[\rho, m, \hat{\rho}, \hat{m}]\right) \tag{S126}$$

Breaking down Gaussian, anharmonic and noise contributions, we rewrite the Langevin PDEs Eq. (S124) as the MSR action

$$S[\rho, m, \hat{\rho}, \hat{m}] = \int \mathrm{d}x\mathrm{d}t \left[(S_0^\rho \; S_0^m)\begin{pmatrix}\delta\hat{\rho}\\\hat{m}\end{pmatrix} + \mathcal{A}[\delta\rho, m, \delta\hat{\rho}, \hat{m}] + \mathcal{A}_{\text{ext}} - \frac{a}{2}(\partial_x\delta\hat{\rho} \; \partial_x\hat{m} \; \hat{m})M\begin{pmatrix}\partial_x\delta\hat{\rho}\\\partial_x\hat{m}\\\hat{m}\end{pmatrix} \right] \tag{S127}$$

where the Gaussian action density is given by

$$(S_0^\rho \; S_0^m)\begin{pmatrix}\delta\hat{\rho}\\\hat{m}\end{pmatrix} = \left[\partial_t\delta\rho - D\partial_{xx}^2\delta\rho\right]\hat{\rho} + \left[\partial_t m - D\partial_{xx}^2 m + rm\right]\hat{m} \tag{S128}$$

The anharmonic contribution is given by

$$\mathcal{A}[\delta\rho, m, \delta\hat{\rho}, \hat{m}] = \left[\mu\delta\rho m + um^3\right]\hat{m} \tag{S129}$$

while the noise terms up to first order noise are given by

$$\frac{a}{2}(\partial_x\delta\hat{\rho} \; \partial_x\hat{m} \; \hat{m})M\begin{pmatrix}\partial_x\delta\hat{\rho}\\\partial_x\hat{m}\\\hat{m}\end{pmatrix} = \frac{a}{2}\left[2D\rho_0(\partial_x\delta\hat{\rho})^2 + 2D\rho_0(\partial_x\hat{m})^2 + 2\hat{\gamma}\rho_0\hat{m}^2\right]. \tag{S130}$$

The external field term contributes to the action as

$$\mathcal{A}_{\text{ext}} = -\hat{m}h \tag{S131}$$

The Gaussian propagators of the density and magnetization fields are given by

$$\langle\rho(x,t)\hat{\rho}(x',t')\rangle_0 = G_0^\rho(x-x',t-t') \tag{S132a}$$
$$\langle m(x,t)\hat{m}(x',t')\rangle_0 = G_0^m(x-x',t-t') \tag{S132b}$$

which are given in Fourier space by

$$G_0^\rho(q,\omega) = \frac{1}{-i\omega + Dq^2} \tag{S133a}$$

$$G_0^m(q,\omega) = \frac{1}{-i\omega + Dq^2 + r} \tag{S133b}$$

with $r = \hat{\gamma}(1 - \sinh\beta)$. We will choose the Fourier transform convention

$$\phi(q,\omega) = \int \mathrm{d}^d\mathbf{x}\mathrm{d}t\, e^{i(\mathbf{q}\cdot\mathbf{x}-\omega t)}\phi(\mathbf{x},t), \quad \phi(\mathbf{x},t) = \int \frac{\mathrm{d}^d\mathbf{q}}{(2\pi)^d}\frac{\mathrm{d}\omega}{2\pi} e^{-i(\mathbf{q}\cdot\mathbf{x}-\omega t)}\phi(\mathbf{q},\omega). \tag{S134}$$

Since $m(x,t)$ and $\rho(x,t)$ are unitless, this implies that $m(q,\omega)$ and $\rho(q,\omega)$ have units of L^dT.

A. 0-loop: scaling in the absence of fluctuations

We consider a renormalization group transformation in the absence of fluctuations ($a = 0$) in d dimensions. We introduce the extra parameters λ_m, λ_ρ such that

$$(G_0^m)^{-1} = -i\lambda_m\omega + D_m q^2 + r, \tag{S135}$$

$$(G_0^\rho)^{-1} = -i\lambda_\rho\omega + D_\rho q^2. \tag{S136}$$

while the noise vertices are given by

$$\Gamma_{\hat{m}\hat{m}} = 2\tilde{\gamma} + 2\tilde{D}_m q^2, \tag{S137}$$

$$\Gamma_{\hat{\rho}\hat{\rho}} = 2\tilde{D}_\rho q^2. \tag{S138}$$

In the bare theory $\lambda_m = \lambda_\rho = 1$, $\tilde{D}_m = \tilde{D}_\rho = aD$, $D_m = D_\rho = D$ and $\tilde{\gamma} = a\hat{\gamma}$. Momentum and time are rescaled by $q \to q/b$. As is the case for models C and D of the Hohenberg-Halperin classification [23, 24], we allow for two distinct dynamical scaling exponents z_ρ, z_m with $\omega \to b^{z_m}\omega$ in each integrand. The fields are renormalized in Fourier space (momentum and frequency) as

$$m \to \zeta_m m, \quad \hat{m} \to \hat{\zeta}_m \hat{m}, \quad \rho \to \zeta_\rho \rho, \quad \hat{\rho} \to \hat{\zeta}_\rho \hat{\rho}. \tag{S139}$$

We thus find, denoting by u the coefficient of the cubic term

$$\lambda_m' = b^{-d}\zeta_m\hat{\zeta}_m\lambda_m \tag{S140a}$$

$$\lambda_\rho' = b^{-d}\zeta_\rho\hat{\zeta}_\rho\lambda_m \tag{S140b}$$

$$D_m' = b^{-d+z_m-2}\zeta_m\hat{\zeta}_m D_m \tag{S140c}$$

$$D_\rho' = b^{-d+z_m-2}\zeta_\rho\hat{\zeta}_\rho D_\rho \tag{S140d}$$

$$r' = b^{-d+z_m}\zeta_m\hat{\zeta}_m r \tag{S140e}$$

$$\mu' = b^{-2d+z_m}\zeta_m\zeta_\rho\hat{\zeta}_m\mu \tag{S140f}$$

$$u' = b^{-3d+z_m}\zeta_m^3\hat{\zeta}_m u \tag{S140g}$$

$$\tilde{D}_\rho' = b^{-d+z_m-2}\hat{\zeta}_\rho^2\tilde{D}_\rho \tag{S140h}$$

$$\tilde{\gamma}' = b^{-d+z_m}\hat{\zeta}_m^2\tilde{\gamma} \tag{S140i}$$

$$\tilde{D}_m' = b^{-d+z_m-2}\hat{\zeta}_m^2\tilde{D}_m \tag{S140j}$$

We choose for the λ's to stay constant such that

$$\zeta_m\hat{\zeta}_m = \zeta_\rho\hat{\zeta}_\rho = b^d \tag{S141}$$

Choosing z_m such that the diffusion constants stay finite, we have $z_m = 2$. We now have

$$r' = b^{z_m}r \tag{S142a}$$

$$\mu' = b^{-d+z_m}\zeta_\rho\mu \tag{S142b}$$

$$u' = b^{-2d+z_m}\zeta_m^2 u \tag{S142c}$$

$$\tilde{D}_\rho' = b^{-d+z_m-2}\hat{\zeta}_\rho^2\tilde{D}_\rho \tag{S142d}$$

$$\tilde{\gamma}' = b^{-d+z_m}\hat{\zeta}_m^2\tilde{\gamma} \tag{S142e}$$

$$\tilde{D}_m' = b^{-d+z_m-2}\hat{\zeta}_m^2\tilde{D}_m \tag{S142f}$$

To proceed, we need to find the scaling dimensions of the Gaussian fields. For the linear correlator to stay finite, we choose ζ_m, ζ_ρ so that the conservative noises stay finite, which implies $\hat{\zeta}_m = b^{(d-z_m)/2+1}$ and $\hat{\zeta}_\rho = b^{(d-z_m)/2+1}$. This leads to

$$\zeta_m = b^{(d+z_m)/2-1} \tag{S143a}$$

$$\zeta_\rho = b^{(d+z_m)/2-1} \tag{S143b}$$

$$\tag{S143c}$$

Without the noise, we thus find the recursion relations

$$r' = b^z r = b^2 r \tag{S144a}$$

$$\mu' = b^{3z/2-1-d/2}\mu = b^{2-d/2}\mu \tag{S144b}$$

$$u' = b^{2z-2-d}u = b^{2-d}u \tag{S144c}$$

$$\tilde{D}'_m = b^2 \tilde{D}_m \tag{S144d}$$

B. Perturbative calculations

In what follows, we will set $\rho_0 = 1$ and use the notation $\rho, \hat{\rho}$ for $\delta\rho, \delta\hat{\rho}$. We use the MSR action to compute perturbed propagator and two-point correlation functions [24]. The Gaussian propagators of the density and magnetization fields are given by

$$\langle \rho(x,t)\hat{\rho}(x',t')\rangle_0 = G_0^\rho(x-x', t-t') \tag{S145a}$$

$$\langle m(x,t)\hat{m}(x',t')\rangle_0 = G_0^m(x-x', t-t') \tag{S145b}$$

which are given in Fourier space by

$$G_0^\rho(q,\omega) = \frac{1}{-i\omega + D_\rho q^2} \tag{S146a}$$

$$G_0^m(q,\omega) = \frac{1}{-i\omega + D_m q^2 + r} \tag{S146b}$$

with $r = \hat{\gamma}(1 - \sinh\beta)$. The 2-pt (additive) noise vertices lead to Gaussian correlators

$$\langle m(q,\omega)m(q',\omega')\rangle_0 = \delta(q+q')\delta(\omega+\omega')|G_0^m(q,\omega)|^2 2\tilde{\gamma} \tag{S147a}$$

$$\langle \rho(q,\omega)\rho(q',\omega')\rangle_0 = \delta(q+q')\delta(\omega+\omega')|G_0^\rho(q,\omega)|^2 2\tilde{D}_\rho q^2 \tag{S147b}$$

We will now proceed to do a perturbative treatment of the corrections induced by a small but finite value of $a = \tilde{D}_\rho/D_\rho$ (or in terms of dimensionless number $a^2\gamma/D \ll 1$). At the first order in a, multiplicative noise corrections are negligible and the first order corrections are given by the two diagrams in Fig. S6.

1. Self-energy

To 1-loop order, the effective magnetization propagator (vertex function $\Gamma_{\hat{m}m}(q,\omega)$) is given by

$$\Gamma_{\hat{m}m}(q,\omega) = G^m(q,\omega)^{-1} = G_0^m(q,\omega)^{-1} - \Sigma(q,\omega) \tag{S148}$$

$$= -i\omega + r + D_m q^2 - \Sigma(q,\omega) \tag{S149}$$

with $\Sigma(q,\omega)$ the self energy given by

$$\Sigma(q,\omega) = -3u \int \frac{d^d k}{(2\pi)^d} \frac{d\nu}{2\pi} G_0^m(k,\nu)G_0^m(-k,-\nu)(2\tilde{D}_m k^2 + 2\tilde{\gamma})$$

$$+ \mu^2 \int \frac{d^d k}{2\pi}\frac{d\nu}{2\pi} G_0^\rho\left(\frac{q}{2}+k, \frac{\omega}{2}+\nu\right) G_0^\rho\left(-\frac{q}{2}-k, -\frac{\omega}{2}-\nu\right) G_0^m\left(\frac{q}{2}-k, \frac{\omega}{2}-\nu\right) 2\tilde{D}_\rho\left(\frac{q}{2}+k\right)^2 \Bigg] \tag{S150}$$

We will now turn to each diagram in order.

  a. *Phi-4 process*   We denote this contribution

$$I_0 = -3u \int \frac{d^d k}{(2\pi)^d}\frac{d\nu}{2\pi}\frac{2\tilde{D}_m k^2 + 2\tilde{\gamma}}{[D_m k^2 + r]^2 + \nu^2} \tag{S151}$$

We first integrate the frequency integral through elementary means in this one-dimensional system

$$\int_{-\infty}^{\infty} \frac{d\nu}{2\pi}\frac{2\tilde{\gamma}}{[D_m k^2 + r]^2 + \nu^2} = \frac{\tilde{D}_m k^2 + \tilde{\gamma}}{D_m k^2 + r}. \tag{S152}$$

Notice that this integral is singular at the critical point – we will thus need to renormalize the correction in the vicinity of the critical point.
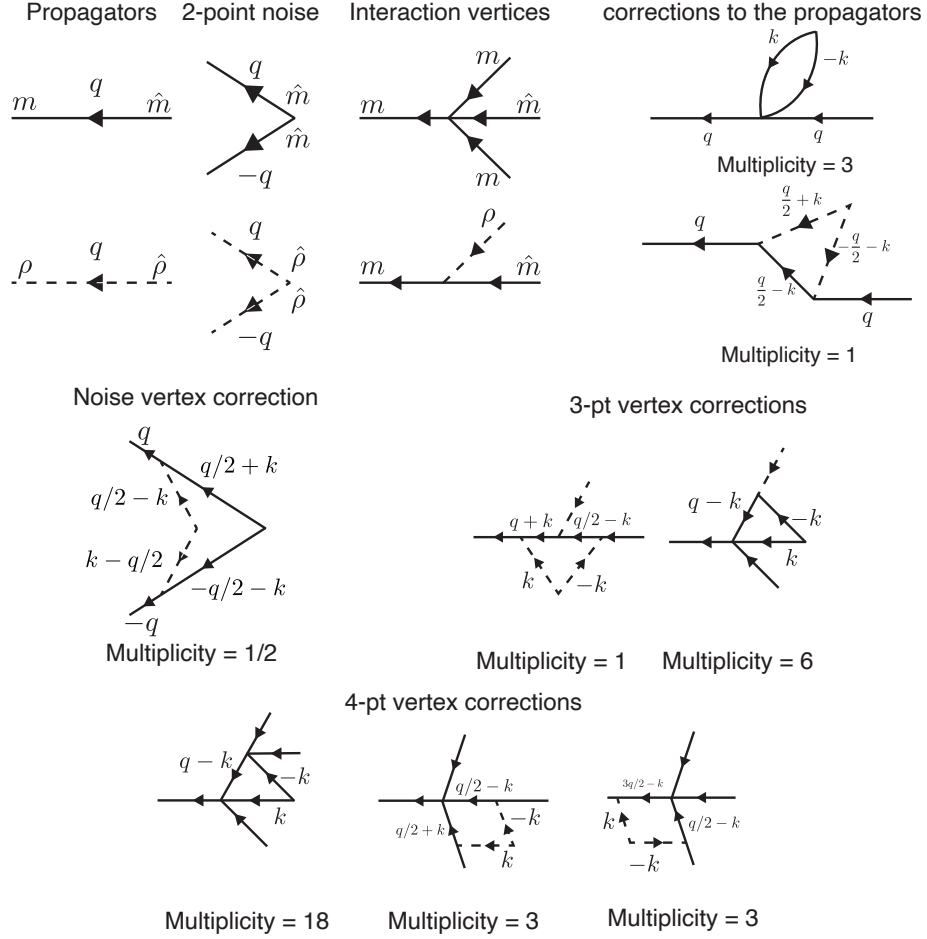
FIG. S6. Elements of diagrammatic perturbation theory and first order diagrams for finite-a effects.

b. *Coupling to density fluctuation*   We have, accounting for the factor $2 \times 1/2!$ from the two interaction vertices,

$$I_1(q,\omega) = \mu^2 \int \frac{\mathrm{d}^d k}{(2\pi)^d} \frac{\mathrm{d}\nu}{2\pi} \frac{2\tilde{D}_\rho \left(\frac{q}{2}+k\right)^2}{D_\rho^2 \left(\frac{q}{2}+k\right)^4 + \left(\frac{\omega}{2}+\nu\right)^2} \frac{1}{D_m \left(\frac{q}{2}-k\right)^2 - i\left(\frac{\omega}{2}-\nu\right) + r} \tag{S153}$$

We evaluate the integral over frequency $\int \mathrm{d}\nu$ using the residue theorem. The integrand has a pole at $\nu = \omega/2 + iD_m(q/2-k)^2 + ir$ which in the disordered phase $(r > 0)$ lies in the upper complex plane, along with 2 other poles at $\nu = -\omega/2 \pm iD_m(q/2+k)^2$. Integrating over the lower complex plane, we find

$$I_1(q,\omega) = \frac{\mu^2 \tilde{D}_\rho}{D_\rho} \int \frac{\mathrm{d}^d k}{(2\pi)^d} \frac{2}{4D_m k^2 + D_m q^2 + 2r - 2i\omega} \tag{S154}$$

We thus have a self energy $\Sigma(q,\omega) = I_0 + I_1(q,\omega)$, which leads to contributions

$$\Gamma_{\hat{m}m}(0,0) = r + 3u \int \frac{\mathrm{d}^d k}{(2\pi)^d} \frac{\tilde{D}_m k^2 + \tilde{\gamma}}{D_m k^2 + r} - \frac{\mu^2 \tilde{D}_\rho}{D_\rho} \int \frac{\mathrm{d}^d k}{(2\pi)^d} \frac{1}{D_m[1+w]k^2 + r} \tag{S155}$$

$$\frac{\partial \Gamma_{\hat{m}m}}{\partial q^2}(0,0) = D_m \left[1 + \frac{\mu^2 \tilde{D}_\rho}{4D_\rho} \int \frac{\mathrm{d}^d k}{(2\pi)^d} \left(\frac{D_m(1+w)}{(D_m(1+w)k^2+r)^2} - \frac{4}{d} \frac{D_m^2[1-w]^2 k^2}{(D_m[1+w]k^2+r)^3} \right) \right] \tag{S156}$$

$$\frac{\partial \Gamma_{\hat{m}m}}{\partial(-i\omega)}(0,0) = 1 + \frac{\mu^2 \tilde{D}_\rho}{D_\rho} \int \frac{\mathrm{d}^d k}{(2\pi)^d} \frac{1}{(D_m[1+w]k^2+r)^2} \tag{S157}$$

with $w = D_\rho/D_m$.

2. Noise vertex correction

We are interested in first-order perturbations at order $O(a)$ - since the noise vertex is already $\propto a$, we do not need to consider its 1-loop order correction which contributes at order $O(a^2)$.

3. 3-pt vertex correction

Density coupling: From the diagram pertaining to the coupling to density fluctuation we find

$$I_3^\rho(q,p) = \mu^3 \int \frac{d^d k}{(2\pi)^d} \frac{d\nu}{2\pi} 2\tilde{D}_\rho k^2 G_0^\rho(k,\nu) G_0^\rho(-k,-\nu) G_0^m(p-k,\omega-\nu) G_0^m(p+q-k,\omega+\omega'-\nu) \tag{S158}$$

$$= \mu^3 \frac{\tilde{D}_\rho}{D_\rho} \int \frac{d^d k}{(2\pi)^d} \frac{d\nu}{2\pi} \frac{2D_\rho k^2}{\nu^2 + D_\rho^2 k^4} \frac{1}{D_m(p-k)^2 + r - i(\omega-\nu)} \frac{1}{D_m(p+q-k)^2 + r - i(\omega'-\nu)} \tag{S159}$$

which after integration over the internal frequency ν and Taylor-expanding for $\omega, \omega', p, q \to 0$ gives

$$I_3^\rho(q,p) = \mu^3 \frac{\tilde{D}_\rho}{D_\rho} \int \frac{d^d k}{(2\pi)^d} \frac{1}{(D_m[1+w]k^2 + r)^2}. \tag{S160}$$

Magnetization coupling: This diagram has multiplicity 6: 3 ways to choose which leg of the 4-pt vertex to attach to the external momentum, and then 2 ways each to attach the density external leg. Thus, the second diagram gives for vanishing external legs

$$I_3^m(q,p) = -6\mu u \int \frac{d^d k}{(2\pi)^d} \frac{d\nu}{2\pi} \left(2\tilde{\gamma} + 2\tilde{D}_m k^2\right) G_0^\rho(k,\nu) G_0^\rho(-k,-\nu) G_0^m(-k,-\nu) \tag{S161}$$

$$= -6\mu u \int \frac{d^d k}{(2\pi)^d} \frac{d\nu}{2\pi} \frac{2\tilde{\gamma} + 2\tilde{D}_m k^2}{\nu^2 + (D_m k^2 + r)^2} \frac{1}{D_m(-k)^2 + r - i(-\nu)} \tag{S162}$$

We thus find the 3-pt vertex function

$$\Gamma_{\hat{m}\rho m}(0,0) = \mu \left[1 + \frac{\mu^2 \tilde{D}_\rho}{D_\rho} \int \frac{d^d k}{(2\pi)^d} \frac{1}{(D_m[1+w]k^2 + r)^2} - 3u \int \frac{d^d k}{(2\pi)^d} \frac{\tilde{\gamma} + \tilde{D}_m k^2}{(D_m k^2 + r)^2} \right] \tag{S163}$$

4. 4-pt vertex correction

We have 3 diagrams here, that we will evaluate at symmetrized external momenta. The first one comes from ϕ^4

$$I_4^u = -18u^2 \int \frac{d^d k}{(2\pi)^d} \frac{d\nu}{2\pi} \frac{2\tilde{\gamma} + 2\tilde{D}_m k^2}{(D_m k^2 + r)^2 + \nu^2} \frac{1}{D_m(q-k)^2 + r - i(\omega-\nu)} \tag{S164}$$

Integrating the internal frequency, we find

$$I_4^u = -\frac{18}{2} u^2 \int \frac{d^d k}{(2\pi)^d} \frac{\tilde{D}_m k^2 + \tilde{\gamma}}{(D_m k^2 + r)^2} \tag{S165}$$

Then we have 2 different sets of integrals which differ by the factors of external momenta, which give, at $q, \omega = 0$

$$I_4^{\mu,1} = 3u \frac{\mu^2 \tilde{D}_\rho}{D_\rho} \int \frac{d^d k}{(2\pi)^d} \frac{d\nu}{2\pi} 2D_\rho k^2 G_0^\rho(k,\nu) G_0^\rho(-k,-\nu) G_0^m(+k,\nu) G_0^m(-k,-\nu) \tag{S166}$$

$$= 3u \frac{\mu^2 \tilde{D}_\rho}{D_\rho} \int \frac{d^d k}{(2\pi)^d} \frac{d\nu}{2\pi} \frac{2D_\rho k^2}{D_\rho^2 k^4 + \nu^2} \frac{1}{(D_m k^2 + r)^2 + \nu^2} \tag{S167}$$

and

$$I_4^{\mu,2} = 3u \frac{\mu^2 \tilde{D}_\rho}{D_\rho} \int \frac{d^d k}{(2\pi)^d} \frac{d\nu}{2\pi} \frac{2D_\rho k^2}{D_\rho^2 k^4 \nu^2} \frac{1}{(D_m k^2 + r - i\nu)^2} \tag{S168}$$

which after integration over the internal frequency give

$$I_4(q,p) = I_4^{\mu,1} + I_4^{\mu,2} = 3u\frac{\mu^2 \tilde{D}_\rho}{D_\rho} \int \frac{\mathrm{d}^d k}{(2\pi)^d} \left(\frac{1}{(D_m[1+w]k^2+r)^2} + \frac{1}{(D_m k^2+r)(D_m[1+w]k^2+r)} \right) \tag{S169}$$

We thus find the vertex function

$$\Gamma_{\hat{m}mmm}(0,0) = u\left[1 - \frac{18}{2}u \int \frac{\mathrm{d}^d k}{(2\pi)^d} \frac{\tilde{D}_m k^2 + \tilde{\gamma}}{(D_m k^2+r)^2} \right. $$
$$\left. +3\frac{\mu^2 \tilde{D}_\rho}{D_\rho} \int \frac{\mathrm{d}^d k}{(2\pi)^d} \left(\frac{1}{(D_m[1+w]k^2+r)^2} + \frac{1}{(D_m k^2+r)(D_m[1+w]k^2+r)} \right) \right] \tag{S170}$$

C. Momentum-shell renormalization

Our lattice model provides us with a cutoff momentum $\Lambda = 2\pi/a$. To obtain the effective response at intermediate scales $0 < q < \Lambda$, we compute the corrections to the propagators by using the momentum-shell renormalization group to regularize our singular perturbation theory. We integrate the short-wavelength modes contained in a shell with momentum $\Lambda/b < k < \Lambda$, such that $b = e^s$ with $s \ll 1$. In the regime we consider, the density has linear (Gaussian) dynamics and its propagator thus does not renormalize, which imposes that $z_\rho = 2$.

The self-energy corrections are given to 1-loop order by

$$G^m(q,\omega)^{-1} = -i\omega + D_m q^2 + r - I_0 - I_1 \tag{S171}$$
$$G^\rho(q,\omega)^{-1} = -i\omega + D_\rho q^2 \tag{S172}$$

consistent with the fact that the density propagator does not renormalize. The contributions I_0 and I_1 to the self energy are then

$$I_0 = -3u \int_{\Lambda/b}^{\Lambda} S_d \Lambda^{d-1} \frac{\mathrm{d}k}{(2\pi)^d} \frac{\tilde{\gamma}}{D_m k^2 + r} = -3u K_d \Lambda^d \frac{\tilde{\gamma}}{D_m \Lambda^2 + r} \log b \tag{S173}$$

The regularization of the momentum integrals will lead generically to approximations of the form

$$\int_{\Lambda/b}^{\Lambda} \frac{\mathrm{d}^d k}{(2\pi)^d} f(k) \approx K_d \Lambda^d f(\Lambda) \ln b \tag{S174}$$

as $\log b \ll 1$ with $K_d = (2\pi)^{-d} S_d$, where $S_d = 2\pi^{d/2}/\Gamma(d/2)$ is the d-dimensional solid angle (area of the unit sphere). These contributions lead to renormalized parameters at $r = 0$ (via the vertex functions)

$$-i\omega_R = -i\omega \left[1 + \delta\Omega \ln b \right]$$
$$r_R = r \left[1 + \delta r \ln b \right]$$
$$D_R = D \left[1 + \delta D_m \ln b \right]$$
$$\mu_R = \mu \left[1 + \delta\mu \ln b \right]$$
$$u_R = u \left[1 + \delta u \ln b \right]$$
$$\tilde{\gamma}_R = \tilde{\gamma} \left[1 + \delta\tilde{\gamma} \ln b \right] \tag{S175}$$

1. Rescaling of space and time

We rescale space and time by $k \to bk$ and $\omega \to b^{z_m}\omega$, where z_x are the (yet unknown) dynamical exponents for each fields. Under this rescaling with the same field renormalization as in the Gaussian case, the bare coefficients rescale

Correction	Expression
$\delta\Omega$	$\frac{\mu^2 a^d \rho_0}{(D_m[1+w]\Lambda^2+r)^2} K_d \Lambda^{d-4}$
δr	$\frac{3u a^d \rho_0}{r} \frac{\tilde{\gamma} K_d \Lambda^d}{D_m \Lambda^2+r} - \frac{\mu^2 a}{r} \frac{K_d \Lambda^d}{D_m[1+w]\Lambda^2+r}$
δD_m	$\frac{\mu^2 a^d \rho_0}{4} K_d \Lambda^d \left(\frac{D_m(1+w)}{(D_m[1+w]\Lambda^2+r)^2} - \frac{4}{d} \frac{D_m[1-w]^2\Lambda^2}{(D_m[1+w]\Lambda^2+r)^3} \right)$
$\delta\mu$	$\mu^2 a^d \rho_0 K_d \Lambda^d \frac{1}{(D_m[1+w]\Lambda^2+r)^2} - 3u K_d \Lambda^d \frac{\tilde{\gamma}}{(D_m\Lambda^2+r)^2}$
δu	$-9u a^d \rho_0 K_d \Lambda^d \frac{\tilde{\gamma}}{(D_m\Lambda^2+r)^2} + 3\mu^2 a^d \rho_0 K_d \Lambda^d \left(\frac{1}{(D_m[1+w]\Lambda^2+r)^2} + \frac{1}{(D_m\Lambda^2+r)(D_m[1+w]\Lambda^2+r)} \right)$
$\delta\tilde{\gamma}$	0

TABLE I. Corrections to scaling introduced by fluctuations at 1-loop. Here $w = D_\rho/D_m$

as given by the equations in Eq. (S140) and the renormalization procedure leads to

$$\omega' = b^{-d}\omega\hat{\zeta}_m\zeta_m \left[1 + \delta\Omega \ln b\right] = b^{-d}\omega\hat{\zeta}_\rho\zeta_\rho \tag{S176a}$$

$$r' = b^{-d+z_m}\hat{\zeta}_m\zeta_m r \left[1 + \delta r \ln b\right], \tag{S176b}$$

$$D_m' = b^{-d+z_m-2}D_m\hat{\zeta}_m\zeta_m \left[1 + \delta D_m \ln b\right] \tag{S176c}$$

$$D_\rho' = b^{-d+z_m-2}D_\rho\hat{\zeta}_\rho\zeta_\rho. \tag{S176d}$$

$$\mu' = b^{-2d+z_m}\zeta_\rho\zeta_m\hat{\zeta}_m\mu \left[1 + \delta\mu \ln b\right] \tag{S176e}$$

$$u' = b^{-3d+z_m}\zeta_m^3\hat{\zeta}_m u \left[1 + \delta u \ln b\right] \tag{S176f}$$

$$\tilde{D}_\rho' = b^{-d+z_m-2}\hat{\zeta}_\rho^2\tilde{D}_\rho \tag{S176g}$$

$$\tilde{\gamma} = b^{-d+z_m}\hat{\zeta}_m^2\tilde{\gamma} \left[1 + \delta\tilde{\gamma} \ln b\right] \tag{S176h}$$

$$\tilde{D}_m' = b^{-d+z_m-2}\hat{\zeta}_m^2\tilde{D}_m \left[1 + \delta\tilde{D}_m \ln b\right] \tag{S176i}$$

We choose the ζ's such that the frequency does not renormalize and for both conservative noise amplitudes to remain constant. Since the dynamical action of the density does not renormalize, we find again

$$\zeta_\rho = b^{d/2+z_m/2-1} \tag{S177a}$$

$$\hat{\zeta}_\rho = b^{d/2-z_m/2+1} \tag{S177b}$$

Does the magnetization field picks up an anomalous scaling exponent? The requirement that the conservative noise stays finite gives

$$\hat{\zeta}_m = b^{d/2-z_m/2+1} \left[1 - \frac{1}{2}\delta\tilde{D}_m \ln b\right] \tag{S178}$$

while the time-normalization imposes

$$b^{-d}\hat{\zeta}_m\zeta_m \left[1 + \delta\Omega \ln b\right] = 1 \tag{S179}$$

which leads to

$$\zeta_m = b^{d/2+z_m/2-1} \left[1 - \delta\Omega \ln b + \frac{1}{2}\delta\tilde{D}_m \ln b\right] \tag{S180}$$

where the dynamical exponent z_m is still to be determined by the requirement that D_m stays finite under the renormalization group flow [25]. Inserting the field scaling factors, we find

$$D_m' = b^{z_m-2}D_m \left[1 + \delta D_m \ln b - \delta\Omega \ln b\right] \tag{S181}$$

Which leads to a dynamical exponent

$$z_m = 2 - \delta D_m^* + \delta\Omega^* \tag{S182}$$

where the starred quantities are taken at the RG fixed point values. We can thus rewrite the recursion relations replacing the field scaling functions by their values

$$r' = b^2 r \left[1 + \delta D_m \ln b + \delta r \ln b \right], \tag{S183a}$$

$$\mu' = b^{2-d/2} \mu \left[1 + \frac{1}{2} \delta\Omega \ln b - \frac{3}{2} \delta D_m + \delta\mu \ln b \right] \tag{S183b}$$

$$u' = b^{2-d} u \left[1 - \delta\Omega \ln b - 2\delta D_m \ln b + \delta\tilde{D}_m \ln b + \delta u \ln b \right] \tag{S183c}$$

$$\tilde{\gamma}' = b^2 \tilde{\gamma} \left[1 + \delta\tilde{\gamma} \ln b - \delta\tilde{D}_m \ln b \right] \tag{S183d}$$

The anomalous exponent η such that $\zeta_m = b^{d/2+1-\eta/2}$ is thus given by

$$\eta = \delta D_m^* + \delta\Omega^* - \delta\tilde{\gamma}^* \tag{S184}$$

2. Additive mass renormalization

The critical point is now reached for a value $r = r_c$ where the vertex function $\Gamma_{\hat{m}m}(0,0) = 0$, which is at our 1-loop order given by

$$r_c = -3u K_d \Lambda^d \frac{\tilde{\gamma}}{D\Lambda^2 + r_c} \ln b + \mu^2 a \frac{K_d \Lambda^d}{2D\Lambda^2 + r_c} \ln b = -\frac{3u\tilde{\gamma}}{D} K_d \Lambda^{d-2} \ln b + \frac{\mu^2 a}{2} \frac{K_d \Lambda^{d-2}}{D} \ln b \tag{S185}$$

a. Dimensionless variables We introduce an effective coupling constant and other dimensionless variables in which we will recast our theory

$$g = \frac{\mu^2 a^d \rho_0}{4 D_m^2} K_d \Lambda^{d-4}, \quad f = \frac{3u\tilde{\gamma}}{D_m^2} K_d \Lambda^{d-4}, \quad \alpha = \frac{r}{D_m \Lambda^2}, \quad w = \frac{D_\rho}{D_m} \tag{S186}$$

D. Flow equations

We thus write down our flow equations into differential β-functions with $s = \log b$

$$\frac{\mathrm{d}r}{\mathrm{d}s} = r \left[2 + \delta D_m + \delta r \right] \tag{S187a}$$

$$\frac{\mathrm{d}\mu}{\mathrm{d}s} = \mu \left[2 - \frac{d}{2} + \frac{1}{2}\delta\Omega - \frac{3}{2}\delta D_m + \delta\mu \right] \tag{S187b}$$

$$\frac{\mathrm{d}u}{\mathrm{d}s} = u \left[2 - d - \delta\Omega - 2\delta D_m + \delta\tilde{\gamma} + \delta u \right] \tag{S187c}$$

$$\frac{\mathrm{d}\tilde{D}_m}{\mathrm{d}s} = 0 \tag{S187d}$$

$$\frac{\mathrm{d}\tilde{D}_\rho}{\mathrm{d}s} = (\delta\Omega - \delta D_m) D_m \tag{S187e}$$

$$\frac{\mathrm{d}\tilde{\gamma}}{\mathrm{d}s} = \tilde{\gamma} \left[2 + \delta\tilde{\gamma} \right] \tag{S187f}$$

$$\frac{\mathrm{d}\tilde{D}_\rho}{\mathrm{d}s} = 0 \tag{S187g}$$

$$\frac{\mathrm{d}\tilde{D}_m}{\mathrm{d}s} = 0 \tag{S187h}$$

which we integrate up to a scale $s = \ln(\Lambda/q)$ to obtain scale-dependent parameters $r(s), \mu(s), D_m(s), \tilde{D}_m(s), D_\rho(s), \tilde{D}_\rho(s), \tilde{\gamma}$. With the rescaled momenta $q' = qe^s$, the power spectrum is then given by

$$\langle |m_q|^2 \rangle = a^d \frac{\tilde{D}_m(s)(q'(s))^2 + \tilde{\gamma}(s)}{D_m(s)(q'(s))^2 + r(s)} = a^d \frac{\tilde{D}_m^R(q)q^2 + \tilde{\gamma}_R(q)}{D_m^R(q)q^2 + r_R(q)} \tag{S188}$$

Replacing q' by its expression in terms of q and s, we find the renormalized coefficients $\tilde{D}_m^R = \tilde{D}_m(0), D_m^R = D_m(0), \tilde{\gamma}_R(q) = \tilde{\gamma}(s)e^{-2s}, r_R(q) = r(s)e^{-2s}$ from which we can understand the effective scale-dependent response of the fluctuating hydrodynamic theory.

E. Scaling analysis and interpretation

We can recover the RG result that $g = \rho_0 \left(\hat{\gamma} a^2 / D \right) \ll 1$ controls the convergence to the mean-field reaction-diffusion equations by a simplified scaling analysis. Consider the cubic order version of the model ignoring density fluctuations, which reduces to the Landau-Ginzburg dynamics

$$\partial_t m = D\nabla^2 m + rm - um^3 + \sqrt{\hat{\gamma} a^d}\zeta(x,t) \tag{S189}$$

The goal is to understand the relevance of noise at the smallest available spatial scale, which is $L = a$. Introducing rescaled space, time, and fields by $x = a\bar{x}$, $t = T\bar{t}$ and $m = M\bar{m}$, we have

$$\partial_{\bar{t}}\bar{m} = \frac{DT}{L^2}\bar{\nabla}^2\bar{m} + rT\bar{m} - uM^2T\bar{m}^3 + \sqrt{T\frac{\hat{\gamma}a^d}{L^dM^2}}\bar{\zeta} \tag{S190}$$

by choosing $T = L^2/D = a^2/D$ the corresponding diffusion timescale and $M^2 = D/(a^2u)$, we have

$$\partial_{\bar{t}}\bar{m} = \bar{\nabla}^2\bar{m} + \frac{ra^2}{D}\bar{m} - \bar{m}^3 + \sqrt{\left(\frac{\hat{\gamma}ua^4}{D^2} \right)}\bar{\zeta} \tag{S191}$$

The mass is thus increased at large scales as in the Gaussian RG and, since $u \sim \hat{\gamma}/\rho_0 \sim \hat{\gamma}$, the dimensionless noise amplitude is as expected now $g = \left(\frac{\hat{\gamma}a^2}{D} \right)^2 \rho_0$, where ρ_0 is the average occupation number per site.

In the presence of conserved noise due to transport, the corresponding term has dimensionless amplitude

$$\sqrt{\rho_0 T \frac{Da^d}{M^2L^d}\frac{1}{L}} = \sqrt{\rho_0 \left(\frac{\hat{\gamma}a^2}{D} \right)} \tag{S192}$$

which indicates a slightly different scaling with $f = \rho_0 \left(\frac{\hat{\gamma}a^2}{D} \right)$. Whenever $\left(\frac{\hat{\gamma}a^2}{D} \right) < 1$, which should be common in chemical systems, f is in fact the dominant noise term. In very dilute systems, non-conserved noise dominates.

The situation can be understood as a crossover away from Gaussian universality to a strongly-interacting fixed point [26]: in the same manner as the Ginzburg criterion quantifies the departure away from mean-field behavior as a nonlinearity appears and interacts with fluctuations, here number fluctuations interact with nonlinearities to bring the system away from the Gaussian RG fixed point. In this system, the noise source is due to the finite microscopic scale inducing dimension-dependent fluctuations.

The dimensionless number $\mathrm{Da} = \left(\hat{\gamma}a^2/D_m \right)$ can be understood as a Damköhler number quantifying reaction timescale to residency time: in that picture, it indicates the convergence to local equilibrium within the microscopic-ranged 'box' a. Alternatively, it is the ratio of the microscopic lengthscale a to the typical distance traveled between reaction events. In the limit where $\mathrm{Da} \ll 1$, spins travel far between interactions and the interactions are thus effectively long-ranged: as a long-ranged Ising model, we expect the mean-field behavior to hold. As a final remark, $\hat{\gamma} = \gamma e^{-\beta + \rho_0(\cosh\beta - 1)} \geq \gamma$, with equality when $\sinh\beta = 1/\rho_0$: The effective reaction rate for the validity of the perturbative expansion is smallest at the critical point of the mean-field theory.

---

[1] A. P. Solon and J. Tailleur. Flocking with discrete symmetry: The two-dimensional active Ising model. *Physical Review E*, 92(4):042119, October 2015.

[2] Mattia Scandolo, Johannes Pausch, and Michael E. Cates. Active Ising Models of flocking: a field-theoretic approach. *The European Physical Journal E*, 46(10):103, October 2023.

[3] David Martin, Daniel Seara, Yael Avni, Michel Fruchart, and Vincenzo Vitelli. The transition to collective motion in nonreciprocal active matter: coarse graining agent-based models into fluctuating hydrodynamics, January 2024. arXiv:2307.08251 [cond-mat].

[4] Alexei Andreanov, Giulio Biroli, Jean-Philippe Bouchaud, and Alexandre Lefèvre. Field theories and exact stochastic equations for interacting particle systems. *Physical Review E*, 74(3):030101, September 2006.

[5] Alexandre Lefèvre and Giulio Biroli. Dynamics of interacting particle systems: stochastic process and field theory. *Journal of Statistical Mechanics: Theory and Experiment*, 2007(07):P07024–P07024, July 2007.

[6] Mourtaza Kourbane-Houssene, Clément Erignoux, Thierry Bodineau, and Julien Tailleur. Exact Hydrodynamic Description of Active Lattice Gases. *Physical Review Letters*, 120(26):268003, June 2018.

[7] Julien O. Dubuis, Gašper Tkačik, Eric F. Wieschaus, Thomas Gregor, and William Bialek. Positional information, in bits. *Proceedings of the National Academy of Sciences*, 110(41):16301–16308, October 2013.

[8] David B. Brückner and Gašper Tkačik. Information content and optimization of self-organized developmental systems. *Proceedings of the National Academy of Sciences*, 121(23):e2322326121, June 2024.

[9] Gabriel Peyré and Marco Cuturi. Computational Optimal Transport. 2018.

[10] J. Lin. Divergence measures based on the Shannon entropy. *IEEE Transactions on Information Theory*, 37(1):145–151, January 1991.

[11] Mehran Kardar. *Statistical Physics of Fields*. Cambridge University Press, 1st edition, June 2007.

[12] Stefano Di Talia and Massimo Vergassola. Waves in Embryonic Development. *Annual Review of Biophysics*, 51(1):327–353, May 2022.

[13] W Van Saarloos. Front propagation into unstable states. *Physics Reports*, 386(2-6):29–222, November 2003.

[14] Sergei V. Petrovskii and Bai-Lian Li. *Exactly Solvable Models of Biological Invasion*. Chapman and Hall/CRC, 0 edition, July 2005.

[15] Gabriel Birzu, Oskar Hallatschek, and Kirill S. Korolev. Fluctuations uncover a distinct class of traveling waves. *Proceedings of the National Academy of Sciences*, 115(16), April 2018.

[16] Baruch Meerson, Pavel V. Sasorov, and Yitzhak Kaplan. Velocity fluctuations of population fronts propagating into metastable states. *Physical Review E*, 84(1):011147, July 2011.

[17] Evgeniy Khain and Baruch Meerson. Velocity fluctuations of noisy reaction fronts propagating into a metastable state. *Journal of Physics A: Mathematical and Theoretical*, 46(12):125002, March 2013.

[18] Yoichiro Mori, Alexandra Jilkine, and Leah Edelstein-Keshet. Asymptotic and Bifurcation Analysis of Wave-Pinning in a Reaction-Diffusion Model for Cell Polarization. *SIAM Journal on Applied Mathematics*, 71(4):1401–1427, January 2011.

[19] Andrea Rocco, Jaume Casademunt, Ute Ebert, and Wim Van Saarloos. Diffusion coefficient of propagating fronts with multiplicative noise. *Physical Review E*, 65(1):012102, December 2001.

[20] Yoichiro Mori, Alexandra Jilkine, and Leah Edelstein-Keshet. Wave-Pinning and Cell Polarity from a Bistable Reaction-Diffusion System. *Biophysical Journal*, 94(9):3684–3697, May 2008.

[21] Pearson W. Miller, Daniel Fortunato, Cyrill Muratov, Leslie Greengard, and Stanislav Shvartsman. Forced and spontaneous symmetry breaking in cell polarization. *Nature Computational Science*, 2(8):504–511, August 2022. Publisher: Springer Science and Business Media LLC.

[22] Nathan W. Goehring, Philipp Khuc Trong, Justin S. Bois, Debanjan Chowdhury, Ernesto M. Nicola, Anthony A. Hyman, and Stephan W. Grill. Polarization of PAR Proteins by Advective Triggering of a Pattern-Forming System. *Science*, 334(6059):1137–1141, November 2011.

[23] P. C. Hohenberg and B. I. Halperin. Theory of dynamic critical phenomena. *Reviews of Modern Physics*, 49(3):435–479, July 1977.

[24] Uwe C. Täuber. *Critical Dynamics: A Field Theory Approach to Equilibrium and Non-Equilibrium Scaling Behavior*. Cambridge University Press, 1 edition, March 2014.

[25] Andrea Cavagna, Luca Di Carlo, Irene Giardina, Luca Grandinetti, Tomas S. Grigera, and Giulia Pisegna. Renormalization group crossover in the critical dynamics of field theories with mode coupling terms. *Physical Review E*, 100(6):062130, December 2019.

[26] John L. Cardy. *Scaling and renormalization in statistical physics*. Number 5 in Cambridge lecture notes in physics. Cambridge University Press, Cambridge ; New York, 1996.